Relativistic rapidly differentially rotating hot neutron stars

Miguel Marques

THÈSE DE DOCTORAT

de l'Université de recherche Paris Sciences et Lettres
PSL Research University

Préparée à l'Observatoire de Paris

Relativistic rapidly differentially rotating hot neutron stars

Ecole doctorale n°127

Astronomie et Astrophysique D'Île de France

Spécialité Astrophysique

COMPOSITION DU JURY :

Mme. OERTEL Micaela
Observatoire de Paris, Directrice de Thése

M. PONS José
Universidad de Alicante, Rapporteur

M. RIEUTORD Michel
Observatoire Midi-Pyrénées, Rapporteur

M. NOVAK Jérôme
Observatoire de Paris, Examinateur

M. VILLAIN Loic
Université François Rabelais, Examinateur

M. TUCKEY Philip
Observatoire de Paris, Président

Soutenue par Miguel MARQUES
le 28 Septembre 2016

Dirigée par **Micaela OERTEL**

l'Observatoire de Paris

PSL RESEARCH UNIVERSITY PARIS

To the memory of my mother, Manuela, to whom I owe so much and gave so little.

$\heartsuit\infty$

Acknowledgements

I would like to start by thanking my supervisors Micaela Oertel and Jérôme Novak. When I first arrived in Meudon three years ago, I could barely realize how crude and limited my knowledge about neutron stars was; I now feel that, thanks to my experience with Micaela and Jérôme, I have developed a rather deep understanding of the different aspects of this fascinating topic. Thank you for all the guidance, patience and availability throughout these three years.

As a member of the relativity group of LUTh, I had the opportunity to work in a rather stimulating environment, and to participate in very interesting group meetings where we would discuss about different topics, mostly on relativistic astrophysics and mathematical relativity. I'm very thankful to every person who contributed to create such an inspiring atmosphere, namely Eric Gourgoulhon, Philippe Grandclément, Silvano Bonazzola, Alexandre Le Tiec, Aurélien Sourie, Debarati Chatterjee, Grégoire Martinon, Bruno Péres, Claire Somé, Gyula Fodor, Micaela and Jérôme. I also had the opportunity to meet very interesting visitors of our group, and I would like to thank Loic Villain, Dorota Gondek-Rosińska and Constança Providência, for interesting and stimulating discussions on the physics and technicalities of relativistic stars.

I am very happy to thank my office colleagues, Olivier Hervet and Julien Lefaucheur, for the very friendly environment we shared in our office. And of course, besides the already mentioned PhD students and postdoc members, all other PhD students and postdoc members of LUTh helped making this three years more joyable. I am particularly thankful to Riccardo Musella, Guillaume Voisin, Julian Adamek, Océane Saincir, and Linda Blot, for all the interactions inside and outside the lab.

During these three years living in Paris, I was fortunate enough to meet very interesting people and create friendships which I definitely want to preserve throughout my lifetime. An extensive list of these people feels inappropriate, but without their assistance to guarantee that my "decompression valve" would keep functioning properly throughout these years, this thesis would probably have not been possible. I want nevertheless to send a big hug to every amazing musician who plays, or did play at some point in the "quais de la seine" jam sessions (or wherever those jams happened/will happen). I'm sure that in the future, I'll remember every weekend spent playing with you guys not only as part of my experience in Paris, but as part of my experience as a PhD student.

In the last years I had to endure some very tough moments, and I need to thank some people who with small gestures, helped me maintaining my emotional stability, probably far more than what they can even understand. I want to thank Myriam Rodrigues, for being there and knowing exactly what to do when I most needed, Marie Nontanovanh, who could precisely guess when I just needed to be taken out for a drink and forced to put my mind

somewhere else, and my flatmates Ana Delcia and Maud Bonbayl, for all their understanding and support (especially during the last month of thesis writing).

Finally, I am infinitely indebted to my family, for their absolute unconditional support. Without them, in way too many senses, this thesis would have never happened. A big big thank you to my brother and my dad, for all the countless hours in the phone, for all the motivational talks, for all the unbelievable support when they had so much to worry about and to deal with.

Sadly, my mother passed away before I could finish this thesis. She always encouraged me, and supported me in every way she could, to seek my dream career, to work on something I would really enjoy, instead of simply searching for whatever job regardless of my desires. Even though she could barely understand what my thesis was really about, she was always very proud to tell everybody that I was working on a thesis in which I was "explaining the stars with maths". Albeit this is too late, I want to take this opportunity to express my infinite love for her. I will never forget what you taught me, what you wished for me, what you most liked in me, and all the unconditional love I've received from you.

Résumé

Les étoiles à neutrons sont parmi les objets les plus extrêmes dans l'univers. Elles sont des étoiles compactes, nées à la suite d'une explosion de supernova gravitationnelle, au point final de l'évolution stellaire. Le champ gravitationnel y est très fort, et la matière à l'intérieur atteint des densités extrêmement élevées. Elles sont donc des "laboratoires" prometteurs, non seulement pour tester le régime de champ fort en relativité générale, mais aussi pour en apprendre davantage sur la physique nucléaire à haute densité, qui actuellement ne peut pas être reproduit avec des expériences terrestres. Ainsi, les étoiles à neutrons nous permettent d'adresser des questions telles que l'existence éventuelle de particules autres que nucléons à haute-densité. À cause de la naissance violente de ces objets, les étoiles à neutrons très jeunes, que l'on appelle proto-étoiles à neutrons, sont également très chaudes, et souvent en rotation différentielle rapide. Dans cette thèse nous avons pour but de développer un modèle stationnaire d'une telle proto-étoile à neutrons.

Ainsi, nous présentons une nouvelle méthode pour calculer numériquement les équations d'équilibre d'un fluide parfait relativiste, axisymétrique et stationnaire, en rotation différentielle et à température finie, valable pour une équation d'état réaliste. Nous présentons en détail le code (accessible au public) développé. Nous avons appliqué ce code avec des nouvelles équations d'état réalistes à température finie, basée sur une théorie relativiste du champ moyen, en incluant tous les degrés de liberté hyperoniques. Nous avons calculé des modèles relativistes stationnaires de proto-étoiles à neutrons en rotation différentielle rapide. Nous allons discuter les applications de nos modèles pour explorer plus en détail la physique de ces objets.

Mot-clés: Étoiles relativistes, Étoiles à neutrons, Température finie, Supernovae gravitationnelle, Hypérons dans les étoiles compact

Abstract

Neutron stars are among the most extreme objects in the universe. They are compact stars born as the aftermath of a core-collapse supernova explosion, at the endpoint of stellar evolution, with a strong gravitational field, and extremely high densities. They are therefore promising 'laboratories', not only to test the strong-field regime of general relativity, but also to learn about nuclear physics in the high density regime, which presently is not accessible in earth based experiments. This allows to address questions such as the possible existence of particles other than nucleons at high-densities. As a consequence of the violent birth of these objects, new-born (proto-)neutron stars are extremely hot and, in general, rapidly rotating, which raises interesting problems in the task of developing a stationary model of such objects.

In this thesis, we present a new self-consistent method to numerically compute the equilibrium equations of stationary axisymmetric relativistic (differentially) rotating perfect fluids at finite temperature, with a realistic equation of state. We introduce in detail the (publicly available) code in which we implemented the described numerical scheme. We use newly developed realistic equations of state with finite temperature, which are based on density dependent relativistic mean field theory, and in which all hyperonic degrees of freedom are included, to compute realistic stationary relativistic models of rapidly differentially rotating proto-neutron stars. We discuss future applications of our code for further exploring the physics of proto-neutron stars.

Keywords: Relativistic stars, Neutron stars, Finite temperature, Core-collapse, Hyperon puzzle

Contents

List of Tables

List of Figures

Part I

Introduction

Chapter 1

From star formation to their death: the birth of compact objects

Neutron stars are among the most extreme objects in the universe. Essentially composed of neutrons, they can be thought of as gigantic atomic nucleus, with several kilometers of radius, bounded not by the strong force, but rather by the gravitational force. Its matter is compressed past supra-nuclear densities, and it can spin at frequencies up to several hundred times per second. While born in a violent explosion, these stars are initially considerably hot, and yet, in a few minutes, they will cool down to such temperatures that, given the extreme densities, they become negligible for the microphysical description of its matter. How can such a violent object even exist?

Stars are born as the consequence of the gravitational collapse of molecular clouds. Through a lifetime which spans from a few million years to trillion years, they will support their hydrostatic equilibrium by producing energy via the nuclear fusion of their elements. The smaller the star mass is, the longer it will take to burn its fuel, the longer it will live. Throughout their lifetime, while undergoing different evolutionary phases, they will synthesize most of the nuclei lighter than iron existing in the universe, due to the undergoing nuclear fusion reactions. Eventually, they will run out of fuel to burn, and that's when a compact object is born. Compact objects are rather different from normal stars: they have rather small radii compared to their masses, therefore, they have a much stronger gravitational field, such that Newtonian gravity is not good enough as an approximation[1]; also, they do not burn nuclear fuel like normal stars do, they support themselves against gravity by rather different mechanisms. If the progenitor star's mass is smaller than $8 \sim 10\, M_\odot$, the time will come when the star forms a core with such composition (depending on its progenitors mass,

[1]**Remark:** one can quantify how strong a gravitational field is for an object to be described without relativistic gravity in a rather simple way, by looking at the compactness parameter $\eta = 2G_N M/Rc^2$, i.e. the ratio between the object's mass and its radius - if η is on the order of magnitude of $\sim 10^{-2}$, the gravitational potential of general relativity will be considerably deeper than that of Newtonian gravity. For a black hole, the most compact object existing, its value is $\eta = 1$.

either an ^4He core, or a $^{12}C-^{16}O$ core) that it will never become hot enough to proceed with nuclear fusion reactions. It will then form a white dwarf: these are compact stars, composed of a degenerate gas of electrons, typically with cores composed of oxygen and carbon, or, in case the progenitor star had a mass at the order of $\sim 8M_\odot$, composed of neon, magnesium and oxygen. While there are no fusion reactions inside these stars, they support themselves against gravity by electron degeneracy pressure. The nature of its equilibrium is also the reason why it is so dense and compact. There is a mass limit for which this equilibrium state is possible, known as the Chandrasekhar mass limit, which for a white dwarf is $M_{Ch} \sim 1.4\,M_\odot$. What happens if the star is too massive to produce a stable core below this mass limit?

1.1 Core-collapse Supernovae

Back in 1934, Zwicky and Baade [124] recognized a class of astronomical objects, consisting in sudden powerful bursts in luminosity, sometimes capable of outshining the luminosity of an entire galaxy. They coined these objects as supernovae. In a remarkably spectacular vision, they hypothesized that supernovae would actually represent the transition of an ordinary star to a neutron star, just two years after the experimental discovery of neutrons.

The oldest known registered observation of a supernova explosion, now known as SN185, dates back to 185, observed by Chinese astronomers. In 1054, the famous supernova SN1054 was observed at several locations on earth, being registered by astronomers from China, the Arab world and from ancient civilizations in Central America. The remnant left by this supernova explosion is the well known Crab Nebula, known to have a neutron star in its center.

From an observational perspective, these explosions can be classified in four different categories, according to spectral characteristics:

- Type IA - Absence of hydrogen spectral lines; strong absorption lines from Si II.
- Type IB - Absence of hydrogen spectral lines; weak absorption lines from Si II; strong absorption lines from He I.
- Type IC - Absence of hydrogen spectral lines; weak absorption lines from Si II; weak absorption lines from He I.
- Type II - Prominence of hydrogen spectral lines.

Except for Type IA supernovae, all other types share essentially the same explosion mechanism. Type IA supernovae are the aftermath of a thermonuclear explosion, somewhat similar to that of a nuclear bomb, in a rather epic scale.

All other types happen due to a violent gravitational collapse of their core, the death of a star which was too massive to become a stable white dwarf. Massive stars develop an onion-like structure throughout their lifetime, as exemplified in figure 1.1, where within each shell, different nuclei are undergoing fusion processes, distributed according to their weight, from hydrogen in the outermost shell, to silicon, just outside the iron core. Now, the ^{56}Fe is one of the most tightly bound of all nuclei. Therefore, no further energy will be released by nuclear fusion, removing the main source of pressure for hydrostatic equilibrium. The iron

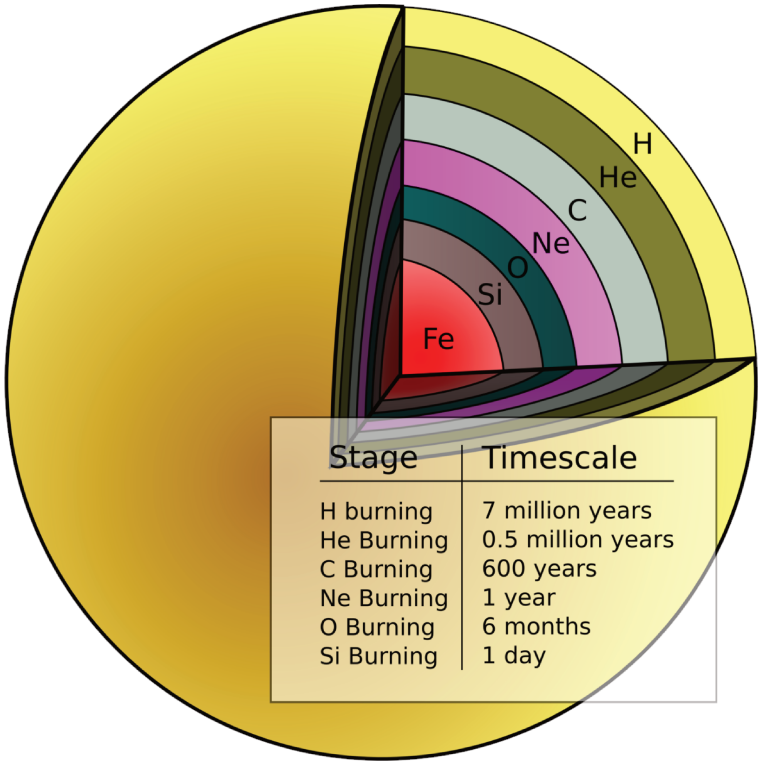

Figure 1.1: The onion-like structure of a massive star at the end of it's life (shells are not to scale), with the burning timescale of each nuclear species. Adapted from [36].

core will exceed the Chandrasekhar mass limit, and for that reason it will undergo a violent gravitational collapse. In hydrodynamical simulations (see e.g. [6] and references therein), it is observed that the outer part of the core can reach velocities up to a quarter of the speed of light. The sudden compression of matter, will lead to an incredible rise in temperature, triggering the production of γ-rays, able to photodisintegrate the iron nuclei

$$\begin{aligned} {}^{56}Fe + \gamma &\rightarrow 13\,{}^{4}He + 4n\,, \\ {}^{4}He + \gamma &\rightarrow 2p + 2n\,. \end{aligned} \tag{1.1}$$

In a naive view, one can think of this as a process in which the collapse smashes atomic matter into its basic elements. Because this are highly endothermic reactions, they'll lead to the loss of thermal pressure, further accelerating the collapse. While under normal conditions, free neutrons will undergo β-decay

$$n \rightarrow p + e^{-} + \bar{\nu}_e\,, \tag{1.2}$$

at this stage of the collapse, the mass density is already so high that such a reaction is not energetically viable. Instead, inverse β-decay will be triggered

$$p + e^{-} \rightarrow n + \nu_e\,, \tag{1.3}$$

transforming most protons and electrons into more neutrons, and electron neutrinos. As the densities increase, they will achieve a value ($\rho_{trap} \sim 10^{12} g/cm^3$) above which neutrinos

become essentially trapped, as their diffusion time becomes larger than the collapse time. At some point, already beyond nuclear saturation density ($\rho_0 \sim 3 \times 10^{14} g/cm^3$), neutrons become degenerate. At this point the collapse is halted, due to repulsive nuclear interaction between nucleons at short distances, with the help of thermal pressure, being the temperature of the order of $T \sim 50 MeV$ (in the Kelvin scale, $1 MeV \sim 1.16 \times 10^{11} K$). A proto-neutron star is born, with a mass larger than the sun, thousands of times warmer than the sun, and with a diameter of the order of $\sim 30\, km$. As the core's outer layers continue to crash down, they will generate a shock wave from matter bouncing back from the star's surface. Intuitively, one would expect this bounce to be the origin of the supernova explosion. It is, however, observed in core-collapse simulations that this shock stalls a few milliseconds after the bounce (see e.g. [6] and references therein). As the shock front has conditions which greatly enhance the cross-section of iron photodisintegration, which by turn leave more protons free to trigger inverse β-decay, the interaction between the shock wave and the free falling matter will lead to a significant fraction of kinetic energy of the shock being absorbed by dissociation of iron nuclei and electron capture processes. The shock wave turns into an accretion shock. If the proto-neutron star keeps accreting the free-falling matter, it

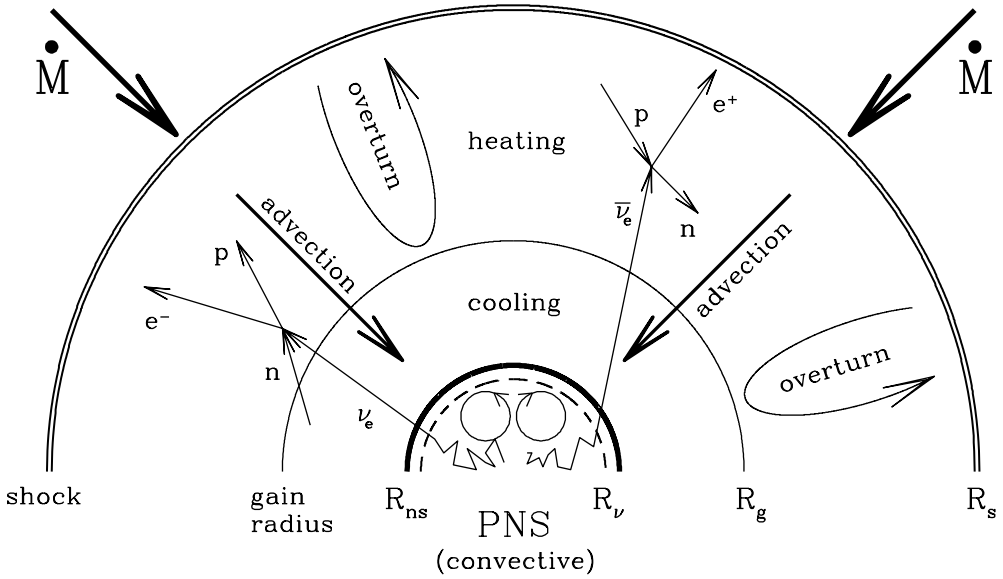

Figure 1.2: A sketch of the ongoing processes prior to the re-ignition of a supernova shock. $\dot{M}$ stands for the accreting mass, PNS stands for proto-neutron star, R_{ns} is the PNS radius, R_ν is the neutrinosphere radius, R_s is the shock position, and R_g (the gain radius) is the location where the temperature is low enough to allow the absorption of neutrinos and antineutrinos to start exceeding the neutrino emission. Adapted from [7].

will collapse to form a black hole, and no supernova would ever be observed. What is then the source of energy that triggers the observed explosions? The most favored scenario is the so-called neutrino heating mechanism. Born hot and lepton reach, proto-neutron stars will cool down by radiating their neutrinos away; the conditions of the proto-neutron star at birth favor the creation of neutrino-pairs of all flavors, further carrying more thermal energy away from the proto-neutron star. In fact, the neutrino luminosity of a core-collapse

supernova has magnitudes of the order of $\sim 10^{51} erg\, s^{-1}$ - fleeing neutrinos will carry away almost all of the gravitational energy released by the collapse [5], the remaining small fraction being released either mechanically by the explosion, or by emission of gravitational waves. As the trapped neutrinos diffuse out, a fraction of them will interact with the top layers of the atmosphere, heating the accreting matter, and eventually depositing enough energy to reignite the shock and successfully drive the explosion, with the help of hydrodynamical instabilities, e.g. convective instabilities and the standing accretion shock instability. This theory is yet to be verified in numerical simulations, but in fact, neutrino heating of supernova matter is unavoidable. Even if it turns out that it is not enough to successfully drive the explosion, it will be a key element for the supernovae physics.

1.2 Neutron Stars

Neutron stars are remarkably compact objects, with diameters ranging between 20 to 30 km, and masses as large as twice that of the sun. Their mean mass density is about two to three times larger than the nuclear saturation density (the mass density of nucleons in heavy atomic nuclei). The equation of state (EoS)[2] describing their interior composition is still unknown, and perhaps the main mystery of neutron stars. An unfamiliar reader might be tempted to guess from their name that these stars are composed solely by neutrons, which would indeed fulfill charge neutrality, but that is not the lowest energy state of dense neutral matter. Protons and electrons (and corresponding anti-particles) will also be present, in a fraction of about $\sim 10\%$. At the high densities of a neutron star, the appearance of other non-nucleonic particles is also expected as their formation becomes energetically favored, such as hyperons (these are baryons with strangeness), condensed states of mesons, in particular pions and kaons, and even a phase transition to deconfined quark matter is a possibility. The composition of matter is considerably different at the star's birth, when neutrinos are trapped in the neutrinosphere, and the star has a lepton fraction[3] of order ~ 0.4, and an entropy per baryon of order ~ 2 (in units of Boltzmann constant), both values significantly larger than what is found in old neutron stars. We show, in figure 1.3, a sketch of the composition of an old (cold) neutron star.

How can we observe neutron stars? Which observable quantities can be used to constraint our theoretical models? As mentioned before, neutron stars will emit a large quantity of neutrinos when born. In 1987, in the advent of a galactic type II supernova, SN 1987A, the Japanese neutrino observatory Kamiokande-II detected a burst of 11 neutrinos originated an SN 1987A. Together with two other observatories located at the USA and the former USSR, a total of 24 events were detected. The total number of events was consistent with the theoretical predictions for the neutrino luminosity of this supernova, strengthening the current theoretical picture of a core-collapse. Supernova neutrinos are an important mean to observe proto-neutron stars.

[2]This acronym will be used throughout this thesis, both for singular and plural forms.

[3]The lepton fraction Y_L is the ratio between the lepton number density $n_L = n_{e^-} - n_{e^+} + n_{\nu_e} - n_{\bar{\nu}_e}$ (where n_{e^-}, n_{e^+} are, respectively, the electron and positron number densities, and n_{ν_e}, $n_{\bar{\nu}_e}$ are, respectively, the electron neutrino and electron anti-neutrino number densities) and the baryon number density: $Y_L = \frac{n_L}{n_b}$.

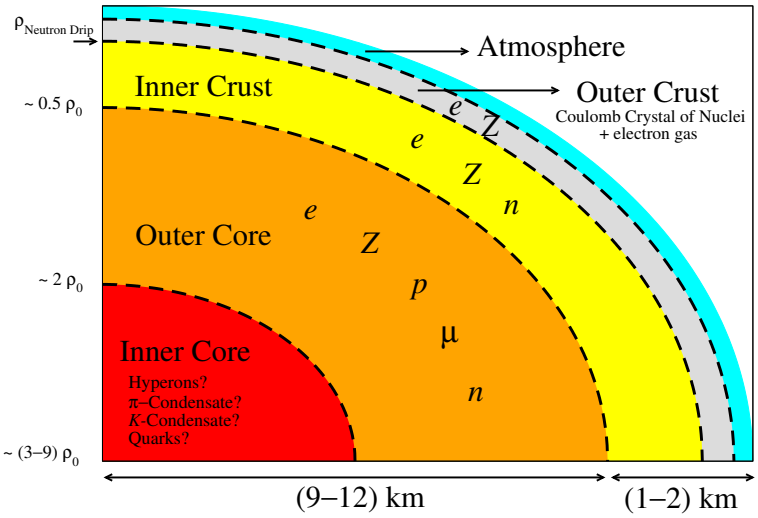

Figure 1.3: A sketch of the interior of a cold neutron star. Adapted from [8]

Furthermore, a core-collapse supernova will also produce gravitational radiation. So far, no direct observation of gravitational waves related to an event involving neutron stars has been published, but such observations should be possible in an earth based observatory, such as LIGO or VIRGO, for a galactic core-collapse supernova. What else can we observe?

1.2.1 Pulsar observations

Pulsars are highly magnetized rotating neutron stars, which convert their rotational energy into electromagnetic radiation (as charged particles are accelerated along the spinning magnetic field lines), as shown in the sketch of figure 1.4, pulsating pretty much like a cosmic lighthouse. When they were first observed in 1967, by Jocelyn Bell Burnell and Antony Hewish, due to the fact that the pulsation period was so short that it would invalidate most of the known astrophysical sources of radiation, the idea came to their mind that this could be a signal from an alien civilization. They therefore named the signal as LGM-1 (for "little green man"). When one month later the same group found a second pulsar in a different location of the sky, this hypothesis was abandoned for good. That first observation is now known as PSR J1921+2153. There were several speculative ideas proposed back then, but the most natural theoretical explanation for pulsars was to identify them with rotating neutron stars. Simple arguments allow astronomers to find a lower limit for the mean density of star matter as a function of its rotation period (see e.g. [4]); for pulsars, the obtained minimum mean densities were about the density of nuclear matter. Neutron stars had however never been observed by then, despite their strong theoretical motivation. It was one year later, with the observation of PSR B0531+21, also known as Crab Pulsar (for being located inside the Crab Nebula, the remnant of the earlier mentioned supernova SN 1054), that this theoretical model was confirmed, as well as the existence of neutron stars themselves.

In 1974, the first binary pulsar system, PSR B1913+16, was discovered by Russell Hulse and Joseph Taylor. This discovery was of major importance, as it consisted in the first indirect

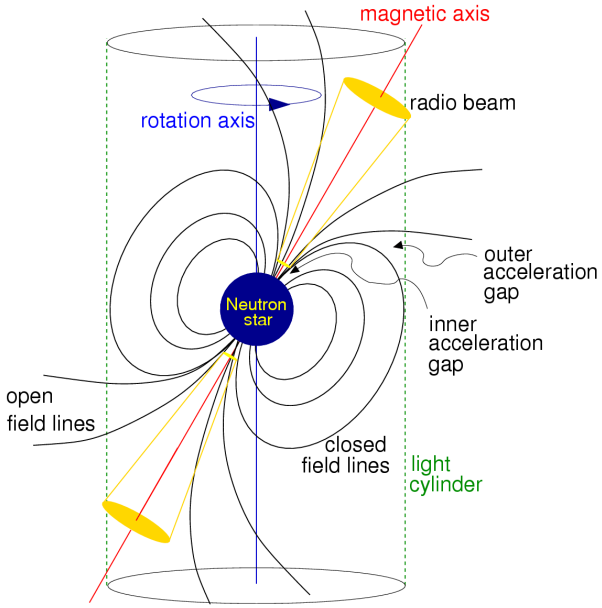

Figure 1.4: A sketch of a pulsar and its magnetic field. Adapted from [4]

observation of gravitational radiation [12]: the observed orbital decay has a precise agreement (as illustrated in figure 1.5) with the prediction from general relativity, that orbital energy would be lost to gravitational waves emission. We now have access to direct observations of these waves from LIGO [53] (from collisions of black holes), further confirming the nature of this observation.

Albeit the large majority of observed pulsars are isolated pulsars, observations of pulsars in binary systems are of major importance as a tool to constrain theoretical models of neutron stars: to measure the mass of a pulsar, all current methods rely on tracking its orbital motion. A review of neutron star mass measurements and the used methods can be found in [13]. We show, in figure 1.6, an up to date list of measured neutron star masses. Double pulsars systems will also allow astronomers to measure the moment of inertia, which might impose strong constraints on the internal structure of neutron stars.

Radii measurements, unfortunately, represent a rather difficult task. The currently available methods rely on observations of thermal emission from the stellar surface.

One approach is to perform spectroscopic measurements, in order to measure its apparent angular size, much like what is done to measure the radii of normal stars. This, of course, imply measuring the neutron star distance, which is already by itself a difficult task, in general yielding results with large uncertainties, which dominate the uncertainties on the radius measurement. Because of their compactness, neutron stars gravitational field will cause gravitational lensing effects on their own surface emission, introducing therefore mass and spin dependent corrections on the observed angular sizes. Also, the pulsar magnetic field might be strong enough to lead to a non-uniform temperature at the stellar surface; and emissions due to a magnetosphere might contaminate the surface thermal emission.

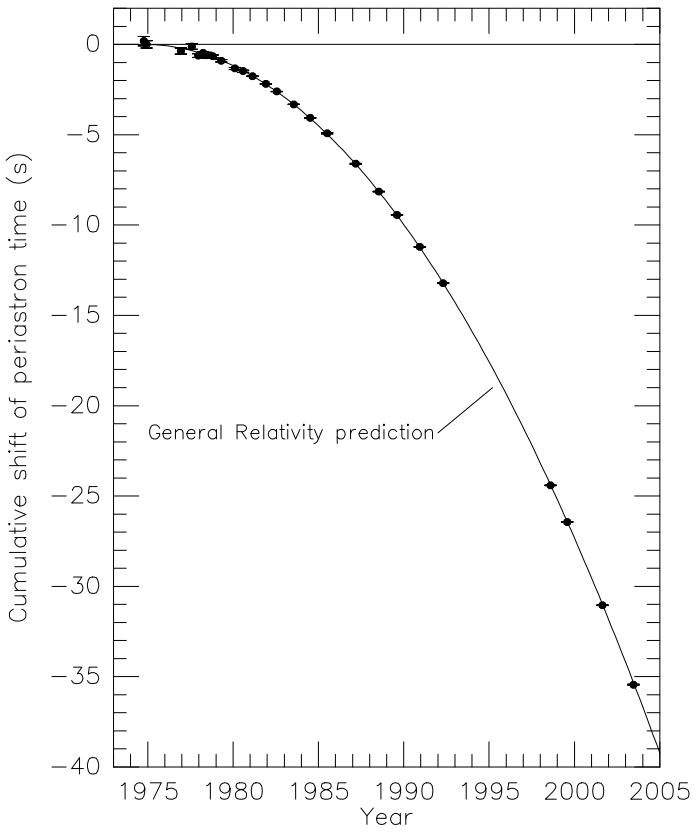

Figure 1.5: Orbital decay of binary pulsar system. Figure from [12].

Another approach is to study the amplitude and spectra of periodic brightness oscillations, originated from temperature anisotropies on the pulsar surface. Such quantities depend not only on the temperature profile at the stellar surface, but also on the gravitational field of the neutron star (therefore its model), and a number of other parameters, leaving room for large uncertainties.

In short, pulsar observations allow us (among other things) to do very precise measurements of rotation rates, precise measurements of their masses, and (unfortunately less reliable as of today) measurements of their radii. A large discussion of how currently available neutron star observation techniques (excluding gravitational wave emission, which only recently became available) could be used to understand their interiors can be found in [9].

1.3 Neutron Star Mergers

As we saw in figure 1.5, the orbit of a neutron star binary system will decay due to gravitational waves emission. What happens when the neutron stars finally collide? A new, hot and massive neutron star (HMNS) is born. Assuming that the total mass of the binary system is greater than the maximum mass limit, the resulting HMNS will always collapse to form a stellar-mass black hole in a relatively short timescale [10]; at birth, the HMNS will support itself against gravity due to its entropy pressure, which will dissipate as the neutron star cools down by radiating its neutrinos. Neutron star mergers are thought to be responsible for the production of short gamma-ray bursts (SGRB) [10]: a short-lived (lifetime of about $\gtrsim 2\,s$) spectacularly powerful burst of γ-rays, the most luminous electromagnetic event in the universe. The mechanism for production of SGRBs is still not understood, and a hot research topic in relativistic astrophysics. They are also thought to be a preferred site for r-process (rapid neutron capture by heavy seed nuclei) nucleosynthesis (which will also occur in core-collapse supernovae), at the origin of some of the heaviest (and rarest) elements of the universe, such as gold and platinum [11].

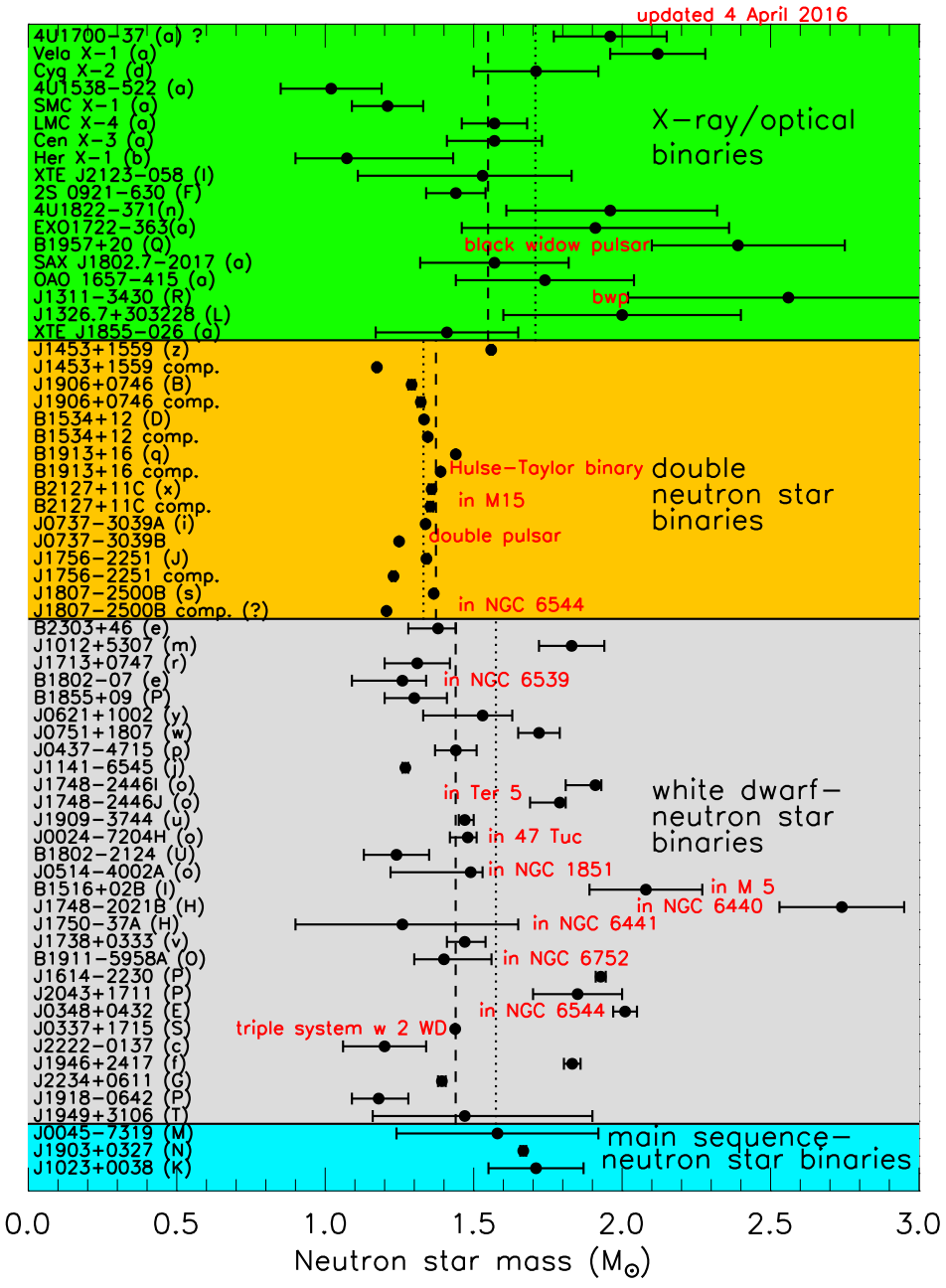

Figure 1.6: Measured neutron star masses with $1-\sigma$ errors. Figure adapted from [16, 17].

Chapter 2

State of the Art

The first studies of relativistic stars date back to the 30's of the twentieth century, when the equations for a static, stationary spacetime of a spherically symmetric perfect fluid were independently derived by Tolman [55], and by Oppehneimer and Volkoff [56]. These equations are still widely used in the literature of relativistic stars, for studies for which the star rotation is not relevant. It was, however, not before the late 60's that the first studies of rotating relativistic stars appeared. The first approach was proposed by Hartle and Thorne [18, 19], who developed an approximation for the spacetime of a slowly rigidly rotating, stationary and axisymmetric body, based on a perturbation of the spherically symmetric body up to second order. The first numerical solutions appeared shortly after [46, 47]. Since then several codes have been developed to solve the structure of stationary rotating relativistic stars, and much interest has been devoted to the study of these solutions, e.g. among other things, to study oscillation modes and stability (of relevance to the analysis of gravitational waves emitted by compact stars), the construction of initial data for general relativistic dynamical simulations, and more recently, to the approximately EoS independent relations between compact stars multipole moments, recently discovered by Yagi and Yunes [114] (see [39] for a comprehensive review on the literature of rotating compact stars, and [115] for a review of the approximate no-hair relations of compact stars).

In this thesis, we are interested in studying stars for which thermal effects are not negligible. Finite temperature effects play an important role in astrophysical extreme events, such as core-collapse supernovae, and compact binary mergers, namely neutron star mergers and black hole - neutron star mergers. As mentioned before, in these events, matter can reach temperatures as high as 100 MeV. It therefore has an important impact in its composition, as it favors the production of non-nucleonic degrees of freedom, such as hyperons (baryons with at least one strange quark), nuclear resonances, or mesons. Even a transition to the quark-gluon plasma could take place, which could facilitate the supernova explosion, as well as explain some gamma-ray bursts, or – within the scenario of "quark-novae" – some unusual supernova lightcurves [75]. The impact of such additional particles on the evolution of proto-neutron stars has received great attention since long time (see e.g. [58, 59, 60, 62, 64, 65, 66, 67, 68, 63]). Several models for proto-neutron stars employ

an EoS taking into account only homogeneous matter, neglecting nuclear clustering in the outer layers and the formation of a crust. The reason might be that the inhomogeneities in the EoS have only a minor impact on global PNS properties. In addition, until recently only a few EoS were available [101, 112, 77], treating the full temperature, baryon density and electron fraction dependence needed for the description of these hot objects, including nuclear clustering. In particular, those models neglected any possibility of non-nucleonic degrees of freedom at high density and temperature, probably more important for PNS than nuclear cluster. The situation changed in recent years, since, triggered by the study of black hole formation, a number of new EoS models has been developed, including as well nuclear clustering as hyperons [70, 73, 74, 75] or quark degrees of freedom [71, 72].

Finite temperature EoS have been used since long time in the studies of core-collapse dynamical simulations; more recently, they have also started to be used for neutron star mergers simulations (see e.g.[109, 110]). A complete hydrodynamical relativistic simulation of a proto-neutron star, is a rather complicated task, which was performed by Fischer et al [57], including a Boltzmann neutrino transport code and consistently taking into account finite temperature effects, but excluding rotation (the simulation was performed in one dimension). As for stationary models of compact stars, the inclusion of finite temperature effects has, for most of the literature, been taken into account neglecting the star's rotation. The first evolutionary relativistic studies of non-rotating proto-neutron stars date back to the mid 80's, by Burrows and Lattimer [122]. Improvements to this study came with Pons et al. [123], including non-nucleonic degrees of freedom such as kaon condensates [59], and quarks [61]. Ferrari et al. [25] used the same models to study the quasi-normal modes evolution of proto-neutron stars. The literature of rotating compact stars at finite temperature is however smaller. In fact, is is difficult to find self-consistent solutions for the equilibrium configuration of relativistic stars with non-trivial entropy gradients.

The earliest stationary models of generally rotating[1] proto-neutron stars have been carried by Goussard et al [1, 2]. The authors restricted their analysis to the case of barotropic fluids, by either considering an isentropic fluid with constant entropy per baryon, or by considering an isothermal fluid with constant redshifted temperature, in which both cases it is possible to solve an analytical first integral of the equilibrium equations. Similar approaches have been used by other authors, e.g. to construct evolutionary sequences of rotating proto-neutron stars [118, 119, 120], and more recently to study the influence of strong magnetic fields in proto-neutron stars with constant lepton fractions [48]. An alternative approach, less constraining with respect to the thermodynamical profiles, is to build an effectively barotropic EoS, by parameterizing temperature (and eventually lepton fraction) as functions of baryon number density, implying assumptions specific to the chosen parameterization. Such an approach was employed, for instance, by Villain et al. [86], to build evolutionary sequences of generally rotating proto-neutron stars by extrapolating results from spherically symmetric simulations [123], and by Kaplan et al. [85], to study quasi-equilibrium configurations of hot hypermassive neutron stars, born in the aftermath of a neutron star merger. The Hartle-Thorne slow rotation expansion has also been considered in the literature of axisymmetric proto-neutron stars, with the earlier study by Romero et al. [121], considering isothermal fluids. Albeit only valid in the regime of slow rotation velocities as compared to the Kepler

[1]Here, generally rotating means rigidly and differentially rotating stars up to Kepler frequency.

frequency, the Hartle-Thorne approximation has the advantage that the equilibrium equations, being a system of ordinary differential equations, can be integrated for a general EoS, without requiring effective barotropicity, as is the case for finding analytical first integrals of generally rotating relativistic stars. In recent studies, the Hartle-Thorne approximation was employed using non-barotropic EoS, by Martinon et al. [50] and Camelio et al. [49], to build evolutionary models of proto-neutron stars (the latter including Boltzmann neutrino transport).

In this thesis, we will introduce a new solution for generally rotating relativistic stars, employing a numerical scheme to find solutions of the equilibrium equations of axisymmetric stationary perfect fluid bodies, which does not require the EoS to be barotropic. We will test the code with an analytical temperature dependent EoS, and with a realistic finite temperature EoS including hyperonic degrees of freedom. Finally, we will discuss the relevance of this solution for further evolutionary studies of proto-neutron stars, deepening our understanding of rapid and differential rotation in their cooling, the quasi-normal modes of radiated gravitational waves, their spin-evolution, proto-neutron star winds, etc.

Part II

Modeling Hot Neutron Stars

Throughout this thesis, unless stated otherwise, we will use natural unites, such that constants will be omitted from equations

$$G_N = c = \hbar = k_b = 1\,,$$

where G_N is the Newton gravitational constant, c is the speed of light, $\hbar$ is the reduced Planck constant, and k_b is the Boltzmann constant.

Unless stated otherwise, ***bold*** letters and symbols stand for tensors of any order superior to zero (all but scalars). Whenever appropriate, the tensor order will be explicitly mentioned, either referring to it as vectors or matrices. Einstein summation convention will be used. As usual in the literature, upper indices stand for contravariant indices, and lower indices stand for covariant indices. Whenever dealing with 4-dimensional spacetimes, tensor indices will be written with the greek alphabet, while when dealing with 3-dimensional spaces, they shall be written with the latin alphabet. If an index does not stand for a tensor component, its meaning shall be explicitly given in the text, except if the symbol does not stand for any non scalar tensor, in which case its meaning shall be made implicit in its definition.

We will use the metric signature (-1,1,1,1).

Chapter 3

Theory of Relativistic Stars

In Newtonian physics, one can fully describe the structure of a stationary star by solving the Euler equations (providing a suitable EoS) along with the Poisson equation for the gravitational field

$$\Delta\phi = 4\pi\rho, \tag{3.1}$$

where Δ is the Laplacian operator, ϕ is the gravitational potential, and ρ is the density of the matter sources of the gravitational field. Relativistic physics taught us that all forms of energy are equivalent to mass. Therefore, the energy of the gravitational field should itself play a role as a source for the equations of a relativistic theory of gravity, rendering these equations non-linear. Such a theory has been proposed by Einstein, the theory of general relativity, which so far has passed all astrophysical tests performed to date [52, 53, 54].

3.1 The Einstein equations

Einstein realized that in a relativistic framework, the gravitational force is better described as a curvature of a spacetime $(\mathcal{M}, \boldsymbol{g})$ (i.e. a metric space, composed by the manifold $\mathcal{M}$, equipped with a distance function which is characterized by the metric tensor $\boldsymbol{g}$) in the presence of energy sources. As posed by Wheeler, matter tells spacetime how to curve, spacetime tells matter how to move. The problem becomes therefore a geometrical one, such that the metric field $\boldsymbol{g} := \boldsymbol{g}(\boldsymbol{\partial}_\mu, \boldsymbol{\partial}_\nu)$ (where $\boldsymbol{\partial}_\beta$ form the canonical basis which span the metric space) can be computed by the Einstein equations

$$R_{\mu\nu} - \frac{1}{2} g_{\mu\nu} R = 8\pi T_{\mu\nu}, \tag{3.2}$$

where $R_{\mu\nu} := R^{\beta}_{\mu\beta\nu}$ is the Ricci tensor (the contraction of the Riemann curvature tensor [1]), $R := R^{\mu}_{\mu}$ is the Ricci scalar, and $T_{\mu\nu}$ is the energy-momentum tensor, given by

$$T_{\mu\nu} = \frac{1}{\sqrt{|g|}} \frac{\delta S_m}{\delta g^{\mu\nu}}, \tag{3.3}$$

where S_m is the action for all non-gravitational sources of energy, and g is the determinant of the metric tensor. Furthermore, contracting twice the Bianchi identities[2], one finds

$$\nabla_\mu \left(R^{\mu\nu} - \frac{1}{2} g^{\mu\nu} R \right) = 0, \tag{3.4}$$

or equivalently

$$\nabla_\mu T^{\mu\nu} = 0, \tag{3.5}$$

which gives us the local conservation of energy and momentum. The simplest non-trivial solution one can find for this set of equations is the Schwarzschild solution: a spherically symmetric spacetime in vacuum (i.e. $T_{\mu\nu} = 0$). In Schwarzschild coordinates, its line element reads

$$ds^2 = -\left(1 - \frac{2M}{r}\right) dt^2 + \left(1 - \frac{2M}{r}\right)^{-1} dr^2 + r^2 d\Omega^2, \tag{3.6}$$

where M is the mass of the curvature source, and $d\Omega^2$ is the two-dimensional line element of a sphere. This solution is most famous for introducing the concept of black hole - a fascinating compact object composed uniquely by space and time. It does however also describe the spacetime outside a non-rotating spherical star. What would then be the solution for the interior of such a star? Let us assume its matter to be described by a perfect fluid. The energy momentum tensor is therefore

$$T^{\mu\nu} = (\varepsilon + p) u^\mu u^\nu + p\, g^{\mu\nu}, \tag{3.7}$$

where ε is the energy density, p stands for pressure, and $\boldsymbol{u}$ is the fluid's 4-velocity, normalized by the relation $u_\mu u^\mu = -1$. Working out the Einstein equations (3.2) for this energy-momentum tensor, employing the Schwarzschild gauge, such that the line element is

$$ds^2 = -e^{2\nu(r)} dt^2 + \left(1 - \frac{2m(r)}{r}\right)^{-1} dr^2 + r^2 d\Omega^2, \tag{3.8}$$

we obtain the so called TOV system (after Tolman-Oppenheimer-Volkof [55, 56]):

$$\partial_r m = 4\pi r^2 \varepsilon\,, \tag{3.9}$$

$$\partial_r p = -(\varepsilon + p) \frac{m + 4\pi r^3 p}{r(r - 2m)}\,, \tag{3.10}$$

$$\partial_r \nu = -\frac{1}{\varepsilon + p} \partial_r p\,, \tag{3.11}$$

[1] The Riemann tensor describes the intrinsic curvature of a manifold equipped with an affine connection; given any vector field $\boldsymbol{A}$, it is defined as $R^{\alpha}_{\beta\lambda\sigma} A^\beta = (\nabla_\lambda \nabla_\sigma - \nabla_\sigma \nabla_\lambda) A^\alpha$.

[2] The following symmetries of the Riemann tensor are called the Bianchi identities: $\nabla_\mu R_{\alpha\beta\nu\lambda} + \nabla_\lambda R_{\alpha\beta\mu\nu} + \nabla_\nu R_{\alpha\beta\lambda\mu} = 0$

where m is the enclosed mass, and ν is a gravitational potential (notice that in the Newtonian limit, ν reduces to the Newtonian gravitational potential in (3.1)). It is easy to see that the matching conditions for the interior and exterior spacetimes (3.6) and (3.8) are trivially fulfilled at the star surface, where $m = M$ and $p = 0$. Providing an EoS relating at least pressure with energy density to close this system, one can find a solution for these equations and fully describe a non-rotating star. What about rotating stars? One approach would be to use the Hartle-Thorne perturbation theory [18, 19], providing an approximate solution for slowly rotating stars. For a complete solution of a rotating star up to the Kepler frequency (i.e. the limit at which the fluid particles travel at Keplerian orbital velocity at the stellar equator, supported against gravity by the centrifugal force), one needs to solve the Einstein equations fully numerically.

3.2 3+1 formulation of Einstein equations

In order to numerically solve the Einstein equations, one needs to recast them in a suitable form. In general, the majority of the used approaches rely on a $D+1$ decomposition of these equations. In layman's words, we want to study a $D-$dimensional space evolving along time. In this section, we will give a brief, but hopefully self-contained overview of the so called 3+1 formalism. throughout this section, we will use a tensorial notation in which Greek indices run for all spacetime coordinates, and Latin indices run only for space coordinates.

Consider a foliation of the spacetime $(\mathcal{M}, \boldsymbol{g})$ by a continuous set of spacelike hypersurfaces Σ_t, as exemplified in figure 3.1. Let us introduce the scalar field $t := t(x^\alpha)$ (representing some

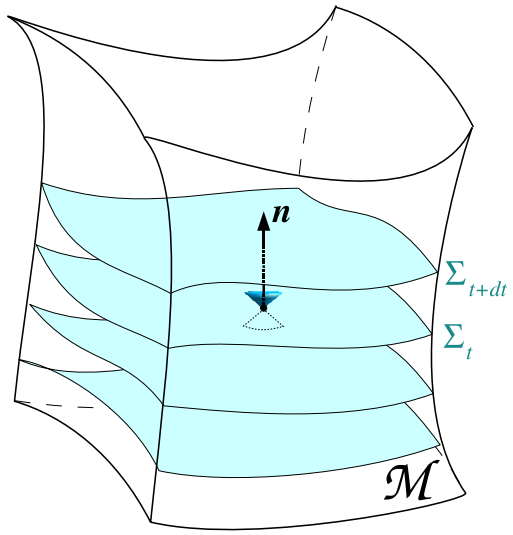

Figure 3.1: Foliation of $(\mathcal{M}, \boldsymbol{g})$ by a continuous set of Σ_t. Figure from [26].

'time function', on some arbitrary coordinates x^α), such that $t =$ constant describes a family of nonintersecting spacelike hypersurfaces Σ_t. Each of those hypersurfaces has a unit timelike

normal 4-vector $\boldsymbol{n}$, such that

$$\boldsymbol{n} = -N\nabla t\,. \tag{3.12}$$

The normalization factor N is called the lapse function. Notice that t can be any arbitrary single-valued function of x^α, as long as $\boldsymbol{n}$ is a future-directed timelike vector. The metric field $\boldsymbol{g}$ induces a 3-space metric $\boldsymbol{\gamma}$ on Σ_t, such that

$$\boldsymbol{\gamma} = \boldsymbol{g} + \boldsymbol{n} \otimes \boldsymbol{n}. \tag{3.13}$$

Furthermore, we may decompose the basis vector $\boldsymbol{\partial_t}$ into its normal and tangent components

$$\boldsymbol{\partial_t} = N\boldsymbol{n} + \boldsymbol{\beta}, \tag{3.14}$$

where $\boldsymbol{\beta} := \beta^i \boldsymbol{\partial}_i$ is called the shift vector. Notice that $\boldsymbol{\beta}$ is orthogonal to $\boldsymbol{n}$, i.e. the shift vector lives in the hypersurface Σ_t). One can therefore express the shift vector explicitly as $\boldsymbol{\beta} = -\boldsymbol{\gamma}\cdot\boldsymbol{\partial_t}$. Figure 3.2 gives a graphical explanation of $\boldsymbol{\beta}$. The line element described by

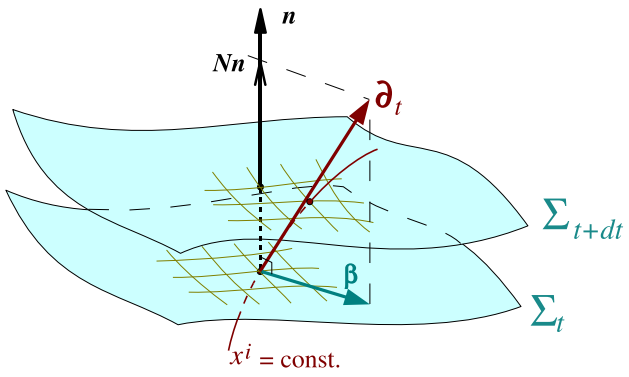

Figure 3.2: The relation between the shift vector $\boldsymbol{\beta}$, the normal unit vector $\boldsymbol{n}$, and the basis vector $\boldsymbol{\partial_t}$. Figure from [26].

the metric tensor $\boldsymbol{g}$ is therefore

$$ds^2 = -N^2 dt^2 + \gamma_{ij}\left(dx^i + \beta^i dt\right)\left(dx^j + \beta^j dt\right), \tag{3.15}$$

We may decompose the energy-momentum tensor as

$$\mathbf{T} = \mathbf{S} + \boldsymbol{n} \otimes \mathbf{J} + \mathbf{J} \otimes \boldsymbol{n} + E\,\boldsymbol{n} \otimes \boldsymbol{n}, \tag{3.16}$$

where $\mathbf{S}$ is the stress 3-tensor, $\mathbf{J}$ is the momentum density 3-vector, and E is the total energy density, as measured by the Eulerian observer (i.e. the observer whose 4-velocity is the unit normal $\boldsymbol{n}$). Their components are given by

$$\begin{aligned} E &= T_{\mu\nu}\, n^\mu\, n^\nu\,, \\ J_\alpha &= -\gamma^\mu_\alpha\, T_{\mu\nu}\, n^\nu\,, \\ S_{\alpha\beta} &= \gamma^\mu_\alpha\, \gamma^\nu_\beta\, T_{\mu\nu}\,. \end{aligned} \tag{3.17}$$

While the 3-space metric gives us all the purely intrinsic aspects of the hypersurface Σ_t geometry, we still need the information of its extrinsic geometry, i.e. how it is embedded in $(\mathcal{M}, \boldsymbol{g})$. Let us introduce the extrinsic curvature, a 3-tensor which measures the bending of Σ_t in $(\mathcal{M}, \boldsymbol{g})$. It is given by

$$\boldsymbol{K} = \frac{1}{2}\mathcal{L}_{\boldsymbol{n}}\boldsymbol{\gamma}, \tag{3.18}$$

where $\mathcal{L}_{\boldsymbol{n}}$ is the Lie derivative along the normal 4-vector. Its trace is therefore

$$K = \gamma^{ij}K_{ij} = \nabla_\mu n^\mu \,. \tag{3.19}$$

The tensors $\boldsymbol{\gamma}$ and $\boldsymbol{K}$ allow us to completely characterize the hypersurface Σ_t. We can now project Einstein equations (3.2) onto Σ_t, to obtain

$$(\partial_t - \mathcal{L}_{\boldsymbol{\beta}})\, K_{ij} = -D_i D_j N + N\left\{R_{ij} + K\, K_{ij} - 2K_{ik}K^k_j + 4\pi\left[(S-E)\gamma_{ij} - 2S_{ij}\right]\right\}\,, \tag{3.20}$$

where the operator $\boldsymbol{D}$ is the covariant derivative with respect to $\boldsymbol{\gamma}$, i.e. $D_\nu := \gamma^\mu_\nu \nabla_\mu$, and S is the trace of the stress 3-tensor $\mathbf{S}$. Furthermore, the Gauss-Codazzi equations (you can find their definition in [27]) allow us to derive two other constraint equations which must be solved together with (3.20): a scalar equation

$$R + K^2 - K_{ij}K^{ij} = 16\pi E, \tag{3.21}$$

which is the Hamiltonian constraint, and a 3-vector equation

$$D_j K^j_i + D_i K = 8\pi J_i, \tag{3.22}$$

which is the momentum constraint. Together, equations (3.20), (3.21) and (3.22) are fully equivalent to the equation (3.2).

3.3 Stationary, axisymmetric and asymptotically flat circular spacetimes

A stationary process is one which does not change over time. Whenever the dynamical processes occurring at the microscopic scale inside a star have a much smaller timescale than the time needed for changes to occur at the macroscopic scale, they can be regarded as quasi-stationary objects, i.e. a stationary solution of the star's structure remains valid for an appropriate timescale. A spacetime $(\mathcal{M}, \boldsymbol{g})$ is said to be stationary iff there exists a vector field $\boldsymbol{\xi}$ (called a Killing vector field), which is asymptotically timelike and is a solution of the Killing equation

$$\mathcal{L}_{\boldsymbol{\xi}}\boldsymbol{g} = 0. \tag{3.23}$$

If in addition, $\boldsymbol{\xi}$ is orthogonal to Σ_t, then $(\mathcal{M}, \boldsymbol{g})$ is also static (we will not treat such spacetimes in this thesis, as we intend to include rotation in our studies). A rotating source of gravity will necessarily produce a non-spherically symmetric spacetime. If such source is also stationary, then it necessarily has to be axisymmetric, because non-axisymmetric

spacetimes will radiate gravitational waves (and therefore, cannot be considered stationary). A spacetime is said to be axisymmetric iff there exists a Killing vector field $\boldsymbol{\chi}$, which vanishes on a timelike 2-surface of $\mathcal{M}$ (called the rotation axis), is spacelike everywhere else and whose orbits are closed curves, such that

$$\mathcal{L}_{\boldsymbol{\chi}} \boldsymbol{g} = 0. \tag{3.24}$$

The gravitational field of an isolated astrophysical object should vanish at infinity. In other words, the spacetime should tend to a Minkowsky spacetime far away from the source, i.e. it should be asymptotically flat[3]. A stationary axisymmetric spacetime $(\mathcal{M}, \mathbf{g})$ is asymptotically flat if at spatial infinity, we find the following limits:

$$\begin{aligned} \boldsymbol{\xi}\cdot\boldsymbol{\xi} &\to -1\,, \\ \boldsymbol{\xi}\cdot\boldsymbol{\chi} &\to 0\,, \\ \boldsymbol{\chi}\cdot\boldsymbol{\chi} &\to +\infty\,. \end{aligned} \tag{3.25}$$

Under all these assumptions, it it possible to show [42] that the vector fields $\boldsymbol{\xi}$ and $\boldsymbol{\chi}$ commute, and we therefore have the relation

$$\xi^\mu \nabla_\mu \chi^\nu - \chi^\mu \nabla_\mu \xi^\nu = 0. \tag{3.26}$$

This allows us to choose the Killing vector fields to be vector fields from the canonical basis, such that, taking spherical coordinates (t, r, θ, ϕ) as the basis coordinates (other choices would have been possible, such as cylindrical coordinates), we have

$$\begin{aligned} \boldsymbol{\xi} &= \boldsymbol{\partial_t}\,, \\ \boldsymbol{\chi} &= \boldsymbol{\partial_\phi}\,. \end{aligned} \tag{3.27}$$

As a consequence, equations (3.23) and (3.24) are respectively equivalent to

$$\begin{aligned} \partial_t g^{\mu\nu} &= 0\,, \qquad \text{(stationarity)} \\ \partial_\phi g^{\mu\nu} &= 0\,, \qquad \text{(axisymmetry)} \end{aligned} \tag{3.28}$$

i.e. the metric of a stationary axisymmetric asymptotically flat spacetime does not depend on the coordinates (t, ϕ). Finally, it is common to assume the absence of meridional convective currents on the source of the gravitational field. That is equivalent to impose the circularity condition, which is met by imposing that total energy-momentum tensor satisfies

$$\begin{aligned} \mathbf{T}\cdot\boldsymbol{\xi} &= \alpha\,\boldsymbol{\xi} + \beta\,\boldsymbol{\chi}\,, \\ \mathbf{T}\cdot\boldsymbol{\chi} &= \lambda\,\boldsymbol{\xi} + \kappa\,\boldsymbol{\chi}\,, \end{aligned} \tag{3.29}$$

which imposes that the 4-fluid velocity is

$$\mathbf{u} = u^t \left(\boldsymbol{\xi} + \Omega\,\boldsymbol{\chi}\right)\,, \tag{3.30}$$

[3]This need not be true in general. For instance, in the context of cosmology, one may want to consider different asymptotical behaviours, such as asymptotically de Sitter spacetimes. It applies in the analysis of isolated stellar type objects

where $\Omega = \frac{u^\phi}{u^t}$ is the angular velocity. As measured by the Eulerian observer, the fluid velocity (a three dimensional spacelike vector) will be

$$\boldsymbol{U} = \frac{1}{\Gamma}\,\boldsymbol{\chi}.\boldsymbol{u}\,. \tag{3.31}$$

It has been shown, in [41], that the assumption of the absence of meridional currents implies that the following terms of the metric $\boldsymbol{g}$ vanish:

$$g_{tr} = g_{t\theta} = g_{\phi r} = g_{\phi\theta} = 0\,. \tag{3.32}$$

3.4 The equations of relativistic rotating stars

We now have the tools to find a more general solution for rotating stars in general relativity. We will assume the star to be a stationary and axysymmetric perfect fluid with the energy momentum tensor given by eq. (3.7); we will also assume asymptotic flatness, and the circularity condition, which physically represents the absence of convective meridional currents. The latter is perhaps too restrictive, since we know that entropy gradients will imply convective currents. It does, however, greatly simplify the computation, and we argue that this is a valid approximation for the relevant astrophysical situations in which the meridional convective currents timescale is much larger than that of the star's rotation. In order to numerically solve the system of partial differential equations (PDE) composed by (3.20), (3.21) and (3.22), one needs to specify gauge conditions, i.e. a system of coordinates, and a slicing condition to describe the foliation. For the latter, we will use the maximal slicing condition, which is met by imposing that the trace of the extrinsic curvature (3.19) (the mean curvature of Σ_t) vanishes:

$$K = 0\,. \tag{3.33}$$

This type of foliation has a great advantage - by the definition (3.19), it implies an incompressibility condition on the velocity field of the Eulerian observer, which guarantees that there won't be coordinate singularities. We will now introduce the Dirac gauge, which will define the coordinate system of our star models.

3.4.1 The Dirac gauge for stationary axisymmetric and asymptotically flat circular spacetimes

As discussed in section 3.2, one can fully solve Einstein equations by numerically solving the system composed by equations (3.20), (3.21) and (3.22). While the PDE nature of equation (3.20) depends on the chosen gauge, equations (3.21) and (3.22) are almost invariantly elliptic equations (less often parabolic). They are, therefore, computationally expensive to solve for most numerical techniques. While this is not necessarily a problem for stationary models (where you can easily implement spectral methods, as will be used and discussed in chapter 4), it is indeed a problem for dynamical simulations, which are of great interest for relativistic astrophysical problems. A common strategy to overcome this difficulty is to

compute the constraint equations (3.21) and (3.22) only for the initial data, and freely solve the evolution equation (3.20). While mathematically it is correct to assume that if the initial data is constrained, the entire time evolution remains constrained as well, numerically this is not the case, and the violation of the constraint equations will grow at each time step. For simulations over long timescales, or which require short time steps, it is worth using a fully constrained formulation. A powerful technique to generate approximate solutions of the constraint equations (which are indeed exact if dealing with spherically symmetric spacetimes), is the so-called conformal flatness condition (CFC) (see for example [26], and references therein). Basically, it consists in writing the 3-space metric as

$$\gamma_{ij} = \psi^4 f_{ij}\,, \tag{3.34}$$

where $\boldsymbol{f}$ is the flat 3-space metric, and ψ is a conformal map, i.e. the 3-space is conformally flat. Within this approximation, the constraint equations become simple equations for the conformal map ψ. There are disadvantages though: i) mathematically, this is only an approximation of general relativity when dealing with rotating solutions, which might not be convenient in highly relativistic situations, ii) there are no gravitational waves in the flat 3-space $(\Sigma_t, \boldsymbol{f})$ (albeit it is nevertheless possible to perform an à posteriori study with a quadrupole formula [22]). We can however extend this formulation in such a way that we fully include the quadratic terms of Einstein equations in our computation, with the so called generalized Dirac gauge [20, 21]. In principle, any dynamical code based on the CFC approximation, could be extended to the Dirac gauge. As already mentioned, the stationary models we are presenting in this thesis, can serve as relativistic initial data for simulating a collapsing hot star, as well as to study a quasi-stationary evolution of the aftermath of a core-collapse or a neutron star merger. Keeping in mind the intention of combining this code with CoCoNuT [22] (Core Collapse with New Technologies - this is a general relativistic hydrodynamical code which uses the CFC approximation, allowing to perform gravitational collapse simulations, as well as the evolution of isolated compact stars) for future studies, we will use the generalized Dirac gauge to build our stationary models (in particular, to perform a dynamical evolution in the Dirac gauge, it is imperative that one uses initial data prepared with the same coordinates). In this section, we will describe the relevant ingredients of the Dirac gauge, and present the 3+1 decomposed Einstein equations under the already discussed symmetries.

Consider a conformal 3-space metric, defined as

$$\tilde{\gamma}^{ij} := \Psi^{-4}\gamma^{ij}, \quad \Psi := \left(\frac{\gamma}{f}\right)^{\frac{1}{12}} \tag{3.35}$$

where Ψ is the conformal factor, γ is the determinant of the 3-space metric $\boldsymbol{\gamma}$, and f is the determinant of the flat 3-space metric $\boldsymbol{f}$. We decompose the conformal metric into the flat metric and a potential h^{ij} which accounts for all quadratic terms of the 3-space solution, such that

$$h^{ij} := \tilde{\gamma}^{ij} - f^{ij}. \tag{3.36}$$

The Dirac gauge is a set of coordinates which meet the condition

$$\mathcal{D}_j h^{ij} = 0, \tag{3.37}$$

where $\mathcal{D}_j$ is the covariant derivative associated with the flat 3-space metric $\boldsymbol{f}$. This implies that $\mathcal{D}_j\tilde{\gamma}^{ij}=0$, and along with the maximal slicing condition (3.33), these proprieties greatly simplify the 3+1 decomposition of the Einstein equations, allowing for computationally efficient fully constrained formalism. Under this coordinate system, and with the imposed symmetries, the Einstein equations become

$$\begin{aligned}\Delta_* N &= \sigma_N\\ \Delta_* \beta^i &= \sigma_{\boldsymbol{\beta}}\\ \Delta_* Q &= \sigma_Q\\ \Delta_* h^{ij} &= \sigma_{\mathbf{h}},\end{aligned} \tag{3.38}$$

where $Q := \Psi^2 N$ determines the conformal factor. The differential operator is defined as $\Delta_* := f^{ij}\mathcal{D}_i\mathcal{D}_j + h^{kl}\mathcal{D}_k\mathcal{D}_l$, and the source terms are

$$\begin{aligned}
\sigma_N &:= \Psi^4 N\left[4\pi(E+S)+\tilde{A}_{kl}A^{kl}\right] - 2\tilde{D}_k\Phi\tilde{D}^k N\,,\\
\sigma_{\boldsymbol{\beta}} &:= 16\pi N\Psi^4 J^i + 2A^{ij}\mathcal{D}_j N - 12NA^{ij}\mathcal{D}_j\Phi - N\tilde{\gamma}^{im}\left(\mathcal{D}_k\tilde{\gamma}_{ml}+\mathcal{D}_l\tilde{\gamma}_{km}-\mathcal{D}_m\tilde{\gamma}_{kl}\right)A^{kl}\\
&\quad -\frac{1}{3}\left(\mathcal{D}^i(\mathcal{D}_j\beta^j)+h^{ik}\mathcal{D}_k\mathcal{D}_l\beta^l\right)\,,\\
\sigma_Q &:= \Psi^6\left[N\left(4\pi S+\frac{3}{4}\tilde{A}_{kl}A^{kl}\right)\right] + 2\Psi^2\left[N\left(\frac{1}{32}\tilde{\gamma}^{kl}\mathcal{D}_k h^{mn}\mathcal{D}_l\tilde{\gamma}_{mn}-\frac{1}{16}\tilde{\gamma}^{kl}\mathcal{D}_k h^{mn}\mathcal{D}_n\tilde{\gamma}_{ml}\right.\right.\\
&\quad \left.\left.+\tilde{D}_k\Phi\tilde{D}^k\Phi\right)+\tilde{D}_k\Phi\tilde{D}^k N\right]\,,\\
\sigma_{\mathbf{h}} &:= \frac{1}{Q}I^{ij}+\mathcal{D}_l h^{ik}\mathcal{D}_k h^{jl}+\tilde{\gamma}_{kl}\tilde{\gamma}^{mn}\mathcal{D}_m h^{ik}\mathcal{D}_n h^{jl}-\tilde{\gamma}_{nl}\mathcal{D}_k h^{mn}\left(\tilde{\gamma}^{ik}\mathcal{D}_m h^{jl}+\tilde{\gamma}^{jk}\mathcal{D}_m h^{il}\right)\\
&\quad -\frac{1}{2}\tilde{\gamma}^{ik}\tilde{\gamma}_{jl}\mathcal{D}_k h^{mn}\mathcal{D}_l\tilde{\gamma}_{mn}-2\left[8\tilde{D}^i\Phi\tilde{D}^j\Phi+\frac{4}{N}\left(\tilde{D}^i\Phi\tilde{D}^j N+\tilde{D}^j\Phi\tilde{D}^i N\right)\right]\\
&\quad +\frac{2}{3}\tilde{\gamma}^{ij}\left(\frac{1}{4}\tilde{\gamma}^{kl}\mathcal{D}_k h^{mn}\mathcal{D}_l\tilde{\gamma}_{mn}-\frac{1}{2}\tilde{\gamma}^{kl}\mathcal{D}_k h^{mn}\mathcal{D}_n\tilde{\gamma}_{ml}+8\tilde{D}_k\Phi\tilde{D}^k\Phi+\frac{8}{N}\tilde{D}_k\Phi\tilde{D}^k N\right)\\
&\quad +\frac{\Psi^4}{N^2}M^{ij}-4\Psi^4\left[\tilde{\gamma}_{kl}A^{ik}A^{jl}-4\pi\left(\Psi^4 S^{ij}-\frac{1}{3}S\tilde{\gamma}^{ij}\right)\right],
\end{aligned} \tag{3.39}$$

where $\tilde{D}_i$ is the covariant derivative associated with the conformal 3-metric, $\Phi = \ln\Psi$, the tensor A^{ij} stands for the traceless part of the conformal extrinsic curvature, defined as

$$\begin{aligned}
A^{ij} &:= \Psi^4\left(K^{ij}-\frac{1}{3}\gamma^{ij}K\right),\\
\tilde{A}_{ij} &:= \tilde{\gamma}_{ik}\tilde{\gamma}_{jl}A^{kl} = \psi^{-4}\left(K_{ij}-\frac{1}{3}\gamma_{ij}K\right),
\end{aligned} \tag{3.40}$$

the tensor I^{ij} is given by

$$\begin{aligned}
I^{ij} &= \mathcal{D}_k Q\left(\mathcal{D}^i h^{jk}+\mathcal{D}^j h^{ik}-\mathcal{D}^k h^{ij}\right)+2\tilde{\gamma}^{ik}\tilde{\gamma}^{jl}\mathcal{D}_k\mathcal{D}_l Q\\
&\quad +\left(h^{ik}\mathcal{D}_k h^{lj}+h^{kj}\mathcal{D}_k h^{il}-h^{kl}\mathcal{D}_k h^{ij}\right)\mathcal{D}_l Q\,,
\end{aligned} \tag{3.41}$$

and the tensor M^{ij} is given by

$$\begin{aligned} M^{ij} &= \mathcal{L}_{\boldsymbol{\beta}}\mathcal{L}_{\boldsymbol{\beta}}h^{ij} + \frac{4}{3}\mathcal{D}_k\beta^k\mathcal{L}_{\boldsymbol{\beta}}h^{ij} + 2\mathcal{L}_{\boldsymbol{\beta}}NA^{ij} + \frac{2}{3}\left[\mathcal{L}_{\boldsymbol{\beta}}(\mathcal{D}_k\beta^k) + \frac{2}{3}(\mathcal{D}_k\beta^2)^2\right]h^{ij} \\ &\quad - \left(\frac{2}{3}\mathcal{D}_k\beta^k - \mathcal{L}_{\boldsymbol{\beta}}\right)(L\beta)^{ij}, \end{aligned} \tag{3.42}$$

where $(L\beta)^{ij}$ stands for the conformal Killing operator associated with the flat metric acting on the shift vector $\boldsymbol{\beta}$, defined as

$$(L\beta)^{ij} := \mathcal{D}^i\beta^j + \mathcal{D}^j\beta^i - \frac{2}{3}\mathcal{D}_k\beta^k f^{ij}. \tag{3.43}$$

In short, the system of equations (3.38) are composed by one equation for the lapse function N, one equation for the conformal factor Ψ, three equations for the shift vector $\boldsymbol{\beta}$ which due to axisymmetry reduce to one, and six equations for the tensor field $\boldsymbol{h}$ which due to axisymmetry reduce to four (the diagonal terms plus the $h^{r\theta}$ term); along with equations (3.37), we have to solve ten equations to compute the metric potentials (seven equations for the gravitational field plus three gauge conditions).

3.4.2 The equilibrium equations

Let us define the operator $\perp$, which performs a projection orthogonal to the 4-fluid velocity

$$\perp^\mu_\nu = \delta^\mu_\nu + u^\mu u_\nu \tag{3.44}$$

Projecting the energy-momentum conservation equations (3.5) with the operator $\perp$, and expanding for the perfect fluid energy-momentum tensor (3.7) (according to the already imposed symmetries), one obtains the relativistic Euler equations

$$\frac{\partial_i p}{\varepsilon + p} + \partial_i\left(\nu - \ln\Gamma\right) + F\partial_i\Omega = 0, \qquad i = r, \theta \tag{3.45}$$

where $\nu = \ln N$ is a gravitational potential, $\Gamma = Nu^t$ is the Lorentz factor relating the Eulerian and the fluid comoving observers, $F = u_\phi u^t$, and $\Omega = \frac{u^\phi}{u^t}$ is the angular velocity.

Cold stars

Let us start by considering a star with a negligible temperature (that is, the temperature can be as high as $\sim 10^9 K$, however, the Fermi energy is such that $\varepsilon_{Fermi} \gg k_b T$, and therefore, we can safely neglect the temperature effects on the star's structure). We may therefore use a barotropic EoS, of the type

$$\begin{aligned} p &:= p(n_b)\,, \\ \varepsilon &:= \varepsilon(n_b)\,, \end{aligned} \tag{3.46}$$

where n_b stands for baryon number density. To integrate equations (3.45), let us define a thermodynamical potential, usually refereed to as the relativistic log-enthalpy

$$H = \ln \frac{\varepsilon + p}{m_b n_b}\,, \tag{3.47}$$

where m_b is the baryon mass (the term arises from the baryon rest-mass energy). Equations (3.45) now become

$$\partial_i \left(H + \nu - \ln \Gamma\right) = -F \partial_i \Omega\,, \qquad i = r, \theta. \tag{3.48}$$

The Schwarz theorem gives us an integrability condition on the quantity F and the angular velocity Ω

$$\partial_r F \partial_\theta \Omega = \partial_\theta F \partial_r \Omega\,. \tag{3.49}$$

This condition is clearly met by a rigidly rotating star, i.e. $d\Omega = 0$. More generally, this condition can be met by any star for which F depends uniquely of the angular velocity, i.e. $F := F(\Omega)$. Thus, $F(\Omega)$ can be physically interpreted as a rotation law. We can therefore find a first integral for the equilibrium equations (3.45)

$$H + \nu - \ln \Gamma + \int_{\Omega_0}^{\Omega} F(\Omega') d\Omega' = const, \tag{3.50}$$

where the constant in the right hand side corresponds to the central value of each of the scalar fields find in the left hand side. Furthermore, by the definition of the rotation law, one can define an implicit function,

$$F(\Omega) - \frac{\gamma_{\phi\phi}(\beta^\phi + \Omega)}{N^2 - \gamma_{\phi\phi}(\beta^\phi + \Omega)^2} = 0\,, \tag{3.51}$$

such that prescribing a rotation law, one can compute the corresponding angular velocity field.

Hot stars

Let us further generalize the previous analysis to a case with not necessarily barotropic, temperature dependent EoS, of the type

$$\begin{aligned} p &:= p(n_b, s_b)\,, \\ \varepsilon &:= \varepsilon(n_b, s_b)\,, \end{aligned} \tag{3.52}$$

where s_b stands for entropy per baryon. We will still make use of the previously defined relativistic log-enthalpy (3.47), which can be rewritten as

$$H = \ln \frac{h}{m_b N_b}\,, \tag{3.53}$$

where N_b is the total number of baryons, and $h = V(\varepsilon + p)$ is the specific enthalpy (with V standing for volume). The first law of thermodynamics

$$\begin{aligned} dh &= T dS + V dp + \mu_b dN_b \\ \Leftrightarrow dH &= \frac{T dS}{h} + \frac{dp}{\varepsilon + p} + \left(\frac{\mu_b}{h} - \frac{1}{N_b}\right) dN_b; \end{aligned} \tag{3.54}$$

with T standing for temperature, S standing for entropy[4] , and μ_b standing for baryon chemical potential, allows one to identify the temperature dependence of the equilibrium equations (3.45)

$$\partial_i \left(H + \nu - \ln \Gamma\right) = \frac{T\partial_i S}{h} + \left(\frac{\mu_b}{h} - \frac{1}{N_b}\right)\partial_i N_b - F\partial_i \Omega \,, \tag{3.55}$$

One can further simplify (3.54) with the Gibbs relation $h = TS + \mu_b N_b$, leading to

$$\begin{aligned} dH - \frac{dp}{\varepsilon + p} &= \frac{T}{h}\left(dS - \frac{S}{N_b}dN_b\right) \\ &= \frac{Te^{-H}}{m_b}\left(\frac{dS}{N_b} - \frac{S}{N_b^2}dN_b\right) = \frac{Te^{-H}}{m_b}ds_b, \end{aligned} \tag{3.56}$$

and therefore, we may still recast (3.45) as

$$\partial_i \left(H + \nu - \ln \Gamma\right) = \frac{Te^{-H}}{m_b}\partial_i s_b - F\partial_i \Omega \,. \tag{3.57}$$

Equations (3.57) are integrable if $T = 0$, if s_b is either constant or if it can be parametrized as a function of H, or if the term Te^{-H} can be parametrized as a function of s_b (which would force a rather artificial EoS, with a poor physical motivation), but not in general. To find a more general solution for the star equilibrium, one can use an iterative scheme to find scalar fields H and s_b which satisfy both equations (3.57). Let us introduce one such possible scheme, based on a fixed-point method:

We start by solving the radial equation for the enthalpy,

$$H = \left(H + \nu - \ln \Gamma\right)|_{r=0} - \nu + \ln \Gamma + \int_0^{r*} \frac{Te^{-H}}{m_b}\partial_r s_b dr' + \int_0^{r*} F\partial_r \Omega dr', \tag{3.58}$$

assuming an initial guess for this field and a radial profile for the entropy per baryon. As a following step, we take the Schwarz integrability condition on the relativistic log-enthalpy, $\partial_r\partial_\theta H = \partial_\theta\partial_r H$ to find an equation which allow us to determine the angular dependent higher multipoles of the s_b field

$$\partial_\theta s_b = \frac{\partial_\theta \left(Te^{-H}\right)}{\partial_r \left(Te^{-H}\right)}\partial_r s_b + \frac{m_b}{\partial_r \left(Te^{-H}\right)}\left(\partial_r F\partial_\theta \Omega - \partial_\theta F\partial_r \Omega\right) \tag{3.59}$$

As we have seen before, if one specifies a rotation law such that it depends only on the angular velocity, the (F, Ω) terms in the source of equation (3.59) vanish. Also, notice that in such case, one can find the same equation (3.59) by simply replacing (3.58) in the angular equilibrium equation (3.57), and taking a radial derivative in both sides of the equation.

[4] **Pitfall prevention:** do not confuse the trace of the stress tensor $S = \mathrm{Tr}\,\mathbf{S}$, introduced in section 3.2, with the star entropy field introduced here.

Equation (3.59) can easily be recast as a Poisson-like equation, which numerically is more convenient. We will therefore compute an angular Poisson equation for s_b

$$\Delta_{\theta\phi} s_b = \left(\partial^\theta + \frac{1}{\tan\theta}\right)\left[\frac{\partial_\theta\left(Te^{-H}\right)}{\partial_r\left(Te^{-H}\right)}\partial_r s_b\right], \tag{3.60}$$

where $\Delta_{\theta\phi}$ stands for the angular Poisson operator, defined as

$$\Delta_{\theta\phi} := \partial^\theta\partial_\theta + \frac{1}{\tan\theta}\partial_\theta + \frac{1}{\sin^2\theta}\partial^\phi\partial_\phi. \tag{3.61}$$

Stars out of β-equilibrium

The previous treatment of the stars hydrostatic equilibrium equations assumed implicitly that deviations from weak equilibrium could be neglected. Assuming, for illustrative purposes, a simplistic model in which the star is only composed by protons, neutrons and electrons, the condition for β-equilibrium is met if the chemical potentials are in an equilibrium state such that

$$\mu_p + \mu_e = \mu_n\,. \tag{3.62}$$

This would be the case for a completely deleptonized neutron star, or a neutron star with such opacities that neutrinos would be completely trapped. Let us finally deduce an equilibrium scheme for a star which has not yet achieved the β-equilibrium state, i.e. the equilibrium of a perfect fluid described by an EoS of the type

$$\begin{aligned} p &:= p(n_b, s_b, Y_L)\,, \\ \varepsilon &:= \varepsilon(n_b, s_b, Y_L)\,. \end{aligned} \tag{3.63}$$

where $Y_L := n_L/n_b$ is the lepton fraction. The first law of thermodynamics now reads

$$dH - \frac{dp}{\varepsilon + p} = \frac{e^{-H}}{m_b}\left(Tds_b + \mu_L dY_L\right)\,. \tag{3.64}$$

As a consequence, the Euler equations may be rewritten as

$$\partial_i\left(H + \nu - \ln\Gamma\right) = \frac{e^{-H}}{m_b}\left(T\partial_i s_b + \mu_L\partial_i Y_L\right) - F(\Omega)\partial_i\Omega\,, \tag{3.65}$$

and therefore, the scheme to numerically search for solutions of these equations now reads

$$\begin{aligned} H &= \left(H + \nu - \ln\Gamma\right)|_{r=0} - \nu + \ln\Gamma + \int_0^{r*}\frac{e^{-H}}{m_b}\left(T\partial_r s_b + \mu_L\partial_r Y_L\right) - F(\Omega)\partial_r\Omega dr'\,, \\ \Delta_{\theta\phi} s_b &= \left(\partial^\theta + \frac{1}{\tan\theta}\right)\left[\frac{\partial_\theta\left(Te^{-H}\right)}{\partial_r\left(Te^{-H}\right)}\partial_r s_b + \frac{\partial_\theta\left(\mu_L e^{-H}\right)\partial_r Y_L - \partial_r\left(\mu_L e^{-H}\right)\partial_\theta Y_L}{\partial_r\left(Te^{-H}\right)}\right]. \end{aligned} \tag{3.66}$$

To close the system (3.66), one needs a third equation to compute the lepton fraction correspondent to each stationary configuration. Such equation would be the Boltzmann transport

equation. We will discuss, in part III, future projects in the direction of a complete quasi-stationary model of a proto-neutron star. For the purpose of this thesis, we will only explore EoS with either a null lepton chemical potential $\mu_L = 0$, or a constant lepton fraction $Y_L = 0.4$ (the physical motivation for these choices will be explained in chapter 5). In both cases, the system (3.66) reduces to the system composed by equations (3.58) and (3.59), previously deduced for stars with finite temperature.

3.5 Global quantities

3.5.1 Baryonic mass

Let us start by introducing the baryon four-current

$$\boldsymbol{j}_b = n_b \boldsymbol{u} \,. \tag{3.67}$$

The baryon number conservation implies that

$$\nabla . \boldsymbol{j}_b = 0 \,. \tag{3.68}$$

This, in turn, allows us to recognize, by means of the divergence theorem, that the flux of the baryon four-current across the hypersurface Σ_t is a constant, in fact the total baryon number inside the star

$$N_b = \oint_{\Sigma_t} \boldsymbol{j}_b . \boldsymbol{n} \, d\Sigma_t = \int_{\Sigma_t} \boldsymbol{j}_b . \boldsymbol{n} \sqrt{\gamma} d^3 x \,. \tag{3.69}$$

From a physical point of view, it might be easier to understand equation (3.69) by recognizing the Lorentz factor $\Gamma = \boldsymbol{u}.\boldsymbol{n}$ in the inner product $\boldsymbol{j}_b.\boldsymbol{n}$, which therefore is equal to $n_b\Gamma$, the baryon number density according to the Eulerian observer. Therefore, (3.69) is equivalent to

$$N_b = \int_{\Sigma_t} n_b \Gamma \sqrt{\gamma} d^3 x \,, \tag{3.70}$$

the 3-space volume integral of the baryon number density. We can finally introduce the baryon mass of a star, by simply counting all baryons inside the star and multiplying by the mean baryon mass m_b

$$M_b = m_b N_b \,. \tag{3.71}$$

This mass definition does not include contributions from the gravitational energy; we know, however, that due to the mass-energy equivalence, the star's mass should involve all sources of energy. Because the energy of the gravitational field is not localizable, we cannot simply define some density field which integrating over a 3-space volume would give us the desired mass. Let us now introduce a definition for a gravitational mass of the star.

3.5.2 Komar mass

The Komar mass [28] is a definition of gravitational mass at infinity, valid only for stationary systems. Given the Killing vector $\boldsymbol{\xi}$ associated with stationarity, the Komar mass is defined as the flux of the tensor $\nabla\boldsymbol{\xi}$ over a closed 2-sphere $\mathscr{S}$ surrounding the star

$$M_g := -\frac{1}{8\pi}\oint_{\mathscr{S}} \nabla^\mu \xi^\mu dS_{\mu\nu}\,, \tag{3.72}$$

where $dS_{\mu\nu}$ is the area element of a 2-form normal to $\mathscr{S}$. Choosing $\mathscr{S}$ such that it is fully contained in the hypersurface Σ_t, and defined by r =const, we have

$$dS_{\mu\nu} = (s_\mu n_\nu - s_\nu n_\mu)\sqrt{q}d\theta d\phi\,, \tag{3.73}$$

where $\mathbf{s} = s^r\boldsymbol{\partial_r}$ is the unit normal of $\mathscr{S}$ in the 3-space $(\Sigma_t, \boldsymbol{\gamma})$, and q is the determinant of the 2-metric $\boldsymbol{q}$ induced by $\boldsymbol{\gamma}$ on $\mathscr{S}$. At first sight, one is led to think that M_g should depend on the choice of the 2-sphere $\mathscr{S}$. Komar showed [29] that due to the fact that $\boldsymbol{\xi}$ is a Killing vector, this is not the case as long as $\mathscr{S}$ lies outside the star. To see this, one may use the Gauss theorem, the Killing equations and Einstein equations to rewrite (3.72) as

$$M_g = 2\int_{\Sigma_t}\left(T_{\mu\nu} - \frac{1}{2}Tg_{\mu\nu}\right)n^\mu\xi^\nu\sqrt{\gamma}\,d^3x\,, \tag{3.74}$$

where $T := g_{\mu\nu}T^{\mu\nu}$ is the trace of the energy-momentum tensor. It is clear that outside the star, where the energy-momentum tensor $\mathbf{T}$ vanishes, there are no contributions for M_g, and therefore it is independent of the choice of surface $\mathscr{S}$. We may yet rewrite (3.74) in the 3+1 decomposition 3.2 (recall that in section (3.3), we have identified the Killing vector associated with stationarity $\boldsymbol{\xi}$, with the basis vector $\boldsymbol{\partial_t}$, defined in (3.14)), finally obtaining

$$M_g = 2\int_{\Sigma_t}\left(\frac{1}{2}N(E+S) - \gamma_{ik}J^i\beta^k\right)\sqrt{\gamma}\,d^3x\,. \tag{3.75}$$

A star is bound iff $M_g < M_b$, otherwise, the star is unstable (physically, if $M_g \geq M_b$, the star would explode, releasing its binding energy, which is the difference $M_g - M_b$, i.e. the energy needed to disperse all baryons from the star to infinity).

3.5.3 ADM mass

A different definition of a gravitational mass, which does not require any symmetry except for asymptotic flatness, has been introduced in the context of the ADM formalism, by Arnowitt, Deser & Misner, in their seminal paper published in 1962 [23]. The action functional of a gravitational field is

$$S_G = \frac{1}{16\pi}\int_{\mathscr{V}} R\sqrt{-g}\,d^4x + \frac{1}{8\pi}\oint_{\partial\mathscr{V}}(\mathscr{K} - \mathscr{K}_0)\sqrt{h}\,d^3x\,, \tag{3.76}$$

where $\mathscr{V}$ is an arbitrary region of the spacetime $(\mathcal{M}, \boldsymbol{g})$, bounded by a closed timelike hypersurface $\partial\mathscr{V}$, $\mathscr{K}$ is the extrinsic curvature of the boundary $\partial\mathscr{V}$ embedded in the spacetime

$(\mathcal{M}, \boldsymbol{g})$, $\mathscr{K}_0$ is a quantity independent of the metric $\boldsymbol{g}$, which is chosen to be the extrinsic curvature of the boundary $\partial\mathscr{V}$ embedded in the flat spacetime $(\mathcal{M}, \boldsymbol{\eta})$, so to avoid the divergence of the integral in the limit in which the boundary $\partial\mathscr{V}$ tends to infinity (for more details, see [27]), and finally, h is the determinant of 3-space metric $\boldsymbol{h}$, induced by $\boldsymbol{g}$ on $\partial\mathscr{V}$. The first term of the action (3.76) is known as the Einstein-Hilbert action. The second term is a boundary term, necessary for the well-posedness of the variational principle. We may now rewrite this action functional in the 3+1 decomposition. Consider a foliation of the region $\mathscr{V}$ by spacelike hypersurfaces Σ_t, bounded by the closed 2-surfaces $\mathscr{S}_t$

$$\mathscr{S}_t := \partial\mathscr{V} \cap \Sigma_t \,, \tag{3.77}$$

such that given two hypersurfaces Σ_{t1} and Σ_{t2}, the boundary of the spacetime region $\mathscr{V}$ is

$$\partial\mathscr{V} = \Sigma_{t2} \cup \Sigma_{t1} \cup \mathscr{B} \,, \tag{3.78}$$

where $\mathscr{B}$ is a timelike hypersurface, the intersection of all 2-surfaces $\mathscr{S}_t$. In the 3+1 formulation, the action (3.76) reads

$$(16\pi)\, S_G = \int_{t_1}^{t_2} dt \left\{ \int_{\Sigma_t} \left({}^3R + K^{ij}K_{ij} - K^2 \right) N\sqrt{\gamma}\, d^3x \; + 2 \oint_{\mathscr{S}_t} (k - k_0) N \sqrt{q}\, d^2x \right\} , \tag{3.79}$$

where ${}^3R$ is the Ricci scalar constructed from the induced 3-metric $\boldsymbol{\gamma}$, k is the extrinsic curvature of $\mathscr{S}_t$ embedded in the 3-space $(\Sigma_t, \boldsymbol{\gamma})$, k_0 is the extrinsic curvature of $\mathscr{S}_t$ embedded in the flat 3-space $(\Sigma_t, \boldsymbol{f})$, and q is the determinant of the 2-metric $\boldsymbol{q}$ induced by $\boldsymbol{\gamma}$ in the closed 2-surface $\mathscr{S}_t$. This action functional finally allows us to write the gravitational Hamiltonian

$$\begin{aligned} (16\pi)\, H_G \;\; = \;\; & \int_{\Sigma_t} \left[N(K^{ij}K_{ij} - K^2 - {}^3R) - 2\beta_i D_j (K^{ij} - K\gamma^{ij}) \right] \sqrt{\gamma}\, d^3x \\ & -2 \oint_{\mathscr{S}_t} \left[N(k - k_0) - \beta_i (K^{ij} - K\gamma^{ij}) s_j \right] \sqrt{q}\, d^2x \,, \end{aligned} \tag{3.80}$$

where $\boldsymbol{s}$ is the unit normal to $\mathscr{S}_t$. Solutions of Einstein equations must obey the Hamiltonian and momentum constraints (3.21) and (3.22). Therefore, the value of the Hamiltonian reduces to

$$H_G^{solution} = -\frac{1}{8\pi} \oint_{\mathscr{S}_t} \left[N(k - k_0) - \beta_i (K^{ij} - K\gamma^{ij}) s_j \right] \sqrt{q}\, d^2x \,. \tag{3.81}$$

The total energy contained in Σ_t, is therefore the limit of $H_G^{solution}$ when $\mathscr{S}_t$ is a 2-sphere at spatial infinity, evaluated for coordinates (t, x^i) that could be associated with some asymptotically inertial observer, such that the lapse function and shift vector are $N = 1$ and $\boldsymbol{\beta} = 0$. Such quantity is the definition of the ADM mass

$$\begin{aligned} M_{ADM} \;\; := \;\; & -\frac{1}{8\pi} \lim_{\mathscr{S}_t \to \infty} \oint_{\mathscr{S}_t} (k - k_0) \sqrt{q}\, d^2x \\ = \;\; & \frac{1}{16\pi} \lim_{\mathscr{S}_t \to \infty} \oint_{\mathscr{S}_t} \left[\mathcal{D}^j \gamma_{ij} - \mathcal{D}_i (f^{kl}\gamma_{kl}) \right] s^i \sqrt{q}\, d\theta d\phi \,. \end{aligned} \tag{3.82}$$

Albeit this seems to be a very different definition when compared to the Komar mass (3.72), it was shown in [30] and [31] that if the spacetime is stationary, and if Σ_t is orthogonal to the killing vector associated with stationary, $\boldsymbol{\xi}$, at spatial infinity, than the ADM mass and the Komar mass coincide

$$M_{ADM} = M_g \,. \tag{3.83}$$

3.5.4 Angular momentum

In the same fashion as we have defined the Komar mass in section 3.5.2, we can notice that for an axisymmetric spacetime, the existence of a Killing vector field $\boldsymbol{\chi}$ associated with symmetries of the rotation axis, guarantees a conserved quantity, associated with the angular momentum, and therefore define the angular momentum at infinity as

$$J := \frac{1}{16\pi} \oint_{\mathscr{S}} \nabla^\mu \chi^\mu dS_{\mu\nu} \,. \tag{3.84}$$

Again, similarly to how we arrived at (3.74), we can rewrite (3.84) as

$$J = -\int_{\Sigma_t} \left(T_{\mu\nu} - \frac{1}{2} T g_{\mu\nu} \right) n^\mu \chi^\nu \sqrt{\gamma}\, d^3x \,, \tag{3.85}$$

and noticing that from definition (3.17) we have $T_{\mu\nu} n^\mu \chi^\nu = -J_\nu \chi^\nu$, and that due to the fact that $\boldsymbol{\chi}$ is tangent to Σ_t, we have $n_\nu \chi^\nu = 0$, we can yet simplify (3.85) as

$$J = \int_{\Sigma_t} J_i \, \chi^i \sqrt{\gamma}\, d^3x \,, \tag{3.86}$$

with $\chi^\mu = (0, 0, 0, r \sin\theta)$. For rigidly rotating stars, we can also define the moment of inertia straightforwardly as

$$I = \frac{J}{\Omega} \,. \tag{3.87}$$

3.5.5 Circumferential radius

For any hypersurface Σ_t, the equatorial radius r_{eq} of the star is obtained by measuring the coordinate r in the equatorial plane $\theta = \frac{\pi}{2}$. This, of course, is a gauge dependent definition. To obtain a gauge independent measure of the stellar equator, let us introduce the circumferential radius, which is the circumference of the star in the equatorial plane, divided by 2π, that is

$$R_{eq} := \frac{1}{2\pi} \oint_{\substack{r=r_{eq} \\ \theta=\pi/2}} ds = \sqrt{\gamma_{\phi\phi}(r_{eq}, \pi/2)}\, r_{eq} \,, \tag{3.88}$$

Throughout this thesis, unless otherwise stated, we will only consider the circumferential radius of the star.

3.5.6 Virial identities

The generalization of the Newtonian virial theorem for general relativistic, stationary and asymptotically flat systems [32, 33], allows us to introduce two useful identities. These quantities are particularly good indicators to account both for the numerical error of a solution, as well as for the physical consistency of the model [38, 39].

GRV3

Let us start by introducing the identity $GRV3$ (GRV standing for General Relativistic Virial theorem, and the 3 recalling that the integrals are computed over the three dimensional subspace $(\Sigma_t, \boldsymbol{\gamma})$. It is derived from the fact that for a stationary asymptotically flat spacetime, the Komar mass (3.75) must equal the ADM mass (3.82) (see [33] for a full derivation). In general, it reads

$$\int_{\Sigma_t} \left[4\pi S - D^i\nu D_i\nu + \frac{1}{4}\gamma^{ij}\left(\Delta^l_{im}\Delta^m_{jl} - \Delta^l_{lm}\Delta^m_{ij}\right) + \frac{3}{4}\left(K_{ij}K^{ij} - K^2\right) - \frac{K}{N}\beta^i D_i\nu \right] \sqrt{\gamma}\, d^3x = 0\,, \tag{3.89}$$

where the tensor Δ^k_{ij} is defined as

$$\Delta^k_{ij} := \frac{1}{2}\gamma^{kl}\left(\mathcal{D}_i\gamma_{lj} + \mathcal{D}_j\gamma_{il} - \mathcal{D}_l\gamma_{ij}\right)\,. \tag{3.90}$$

In the Dirac gauge with maximal slicing condition, eq. (3.89) reduces to

$$\int_{\Sigma_t} \left[4\pi S - D^i\nu D_i\nu + \frac{1}{4}\gamma^{ij}\left(\Delta^l_{im}\Delta^m_{jl} - \Delta^l_{lm}\Delta^m_{ij}\right) + \frac{3}{4}\tilde{A}_{ij}A^{ij} \right] \sqrt{\gamma}\, d^3x = 0\,. \tag{3.91}$$

GRV2

Another useful virial identity is the GRV2, which in its most general form is valid for any asymptotically flat spacetime (no other symmetries are needed). Contrary to the GRV3, GRV2 is integrated over the meridional surface (hence the number 2 in its name), and it does not reduce to the virial theorem in the Newtonian limit. Let us consider the metric subspace $(\Sigma_{t\phi}, \boldsymbol{q})$, where $\Sigma_{t\phi}$ is a 2-surface of constant time and constant azimuthal angle, such that a family of nonintersecting $\Sigma_{t\phi}$'s give us a foliation of $(\Sigma_t, \boldsymbol{\gamma})$. We may define similar geometrical objects as those we have defined for Σ_t, namely the unit normal 4-vector $\boldsymbol{m}$, which lives in Σ_t and is oriented towards ϕ, the induced 2-metric $\boldsymbol{q}$

$$\boldsymbol{q} = \boldsymbol{\gamma} - \boldsymbol{m}\otimes\boldsymbol{m} = \boldsymbol{g} + \boldsymbol{n}\otimes\boldsymbol{n} - \boldsymbol{m}\otimes\boldsymbol{m}\,, \tag{3.92}$$

and the extrinsic curvature tensor $\boldsymbol{L}$, which analogously to $\boldsymbol{K}$, measures the bending of $\Sigma_{t\phi}$ in $(\Sigma_t, \boldsymbol{\gamma})$, and is given by

$$\boldsymbol{L} = -\frac{1}{2}\,{}^3\mathcal{L}_{\boldsymbol{m}}\boldsymbol{q}\,, \tag{3.93}$$

where ${}^3\mathcal{L}_{\mathbf{v}}$ stands for the Lie derivative along the vector field $\mathbf{v}$, in the 3-space $(\Sigma_t, \boldsymbol{\gamma})$. Projecting Einstein equations 3.2 along the normal vector $\boldsymbol{m}$, it is possible to derive the following identity (you may find the detailed derivation in [32])

$$\begin{aligned}\int_{\Sigma_{t\phi}} \Big[& 8\pi s - \mathscr{D}_a\nu\mathscr{D}^a\nu + m^i m^j\left(n^\sigma\nabla_\sigma K_{ij} - KK_{ij}\right) + L\frac{m^i}{N}D_iN \\ & - n^\sigma\nabla_\sigma K + \left(K_{ij}K^{ij} + K^2 + L_{ab}L^{ab} - L^2\right)\Big]\sqrt{q}\, d^2x \;=\; 0\,,\end{aligned} \tag{3.94}$$

where $\mathscr{D}_a$ is the covariant derivative associated with the induced metric $\boldsymbol{q}$, $s := T_{\mu\nu}m^\mu m^\nu$ is the matter stress in the direction of $\boldsymbol{m}$ as seen by the Eulerian observer, L is the trace of the

extrinsic curvature of $\Sigma_{t\phi}$, and q is the determinant of the induced metric $\boldsymbol{q}$. In the Dirac gauge with maximal slicing condition, and imposing all the symmetries of our star model, eq. (3.94) reduces to

$$\int_{\Sigma_{t\phi}} \left\{ 8\pi \left[(E+p)U^2 + p \right] + 3\tilde{A}_{i\phi} A^{i\phi} + \left(\gamma^{rr} + \frac{2}{r}\gamma^{r\theta} + \frac{1}{r^2}\gamma^{\theta\theta} \right) \partial_r \nu \partial_\theta \nu \right\} \sqrt{q}\, d^2x \;=\; 0\,. \quad (3.95)$$

Chapter 4

Numerical Solutions of Relativistic Hot Stars

In this chapter, we will provide an insight over the implementation strategy to solve the stellar structure of rotating compact stars with finite temperature. We will present the implemented codes (for rigid and differential rotation), and present test results employing a simple analytical EoS.

4.1 The BGSM scheme extended for hot EoS

Introduced in 1993, the BGSM algorithm [3] (sometimes also called the self-consistent-field method, for being based on a previously existing solution for Newtonian stars [40]), is a computationally efficient method to find solutions of barotropic perfect fluid stars, based on a fixed-point iteration of the log-enthalpy field, computed from the equilibrium equation (3.50). We will show how this algorithm can be adapted to non-barotropic perfect fluid stars with finite temperature, by replacing the analytical first integral (3.50), with the iterative scheme composed by equations (3.58) and (3.60). The algorithm then goes as follows:

To start with, you need to specify an initial configuration, and the star model, that is:

• Prescribe an initial (spherical) guess for the log-enthalpy profile, which in our codes will be

$$H = H_c \left(1 - \frac{r^2}{R_s^2}\right), \tag{4.1}$$

were H_c is the central value of H (it won't change throughout the iterations, therefore will be a parameter of the star model), and R_s will be the star surface for the initial guess. Note that in [51], it was shown that for a rigidly rotating barotropic star, the scheme will always converge exponentially for any initial guess of H.

• Prescribe a monopolar entropy per baryon profile (i.e. a spherical profile corresponding to the $l = 0$ term of a multipole expansion of s_b; this will remain fixed as the monopolar

term of the the s_b profile, while the higher multipoles are to be computed by the iterative scheme).

- Provide a choice of: i) the angular velocity Ω for rigidly rotating
  ii) the central angular velocity Ω_c for differentially rotating stars, plus a rotation law of the form $F = F(\Omega)$.

The initial values for the metric potentials are set to 1, and the initial fluid velocity (according to the Eulerian observer) is set to $U = 0$. U will increase gradually (by increasing linearly the angular velocity Ω) throughout the iterations until it achieve the desired rotation frequency is achieved.

- Prescribe a finite temperature EoS, of the form $[\varepsilon(H, s_b), p(H, s_b)]$.

Once provided the initial data, each iteration follows as:

1. compute $\varepsilon(H, s_b)$ and $p(H, s_b)$ from the EoS,

2. if solving a differentially rotating star, compute the angular velocity field Ω from the implicit equation (3.51),

$$F(\Omega) - \frac{\gamma_{\phi\phi}(\beta^\phi + \Omega)}{N^2 - \gamma_{\phi\phi}(\beta^\phi + \Omega)^2} = 0\,, \tag{4.2}$$

3. with the energy density ε, the pressure p, the star fluid velocity U and the Lorentz factor Γ, compute the source terms of the energy-momentum tensor (rhs of Einstein equations) (3.17), which written in an explicit form read

$$\begin{aligned} E &= \Gamma^2(\varepsilon + p) - p\,, \\ J^\phi &= (E + p)U^\phi\,, \\ S^{ij} &= (E + p)U^i U^j + p\gamma^{ij}\,, \\ S^i_i &= (E + p){U^\phi}^2 + 3p\,, \end{aligned} \tag{4.3}$$

   (recall that we imposed the circularity condition, therefore only the azimuthal component of vector $\boldsymbol{U}$ is non-zero),

4. solve the Einstein eqs (3.38) for the metric,

5. update the star fluid velocity from

$$U^\phi = \frac{1}{N}\left(\Omega r \sin\theta + \beta^\phi\right)\,, \tag{4.4}$$

   and the Lorentz factor Γ from

$$\Gamma = (1 - U^2)^{-1/2}\,, \tag{4.5}$$

6. compute the radial equilibrium equation (3.58) to obtain the log-enthalpy field H,

$$H = (H + \nu - \ln\Gamma)|_{r=0} - \nu + \ln\Gamma + \int_0^{r*} \frac{Te^{-H}}{m_b}\partial_r s_b dr' + \int_0^{r*} F\partial_r\Omega dr', \tag{4.6}$$

7. compute from equation (3.60) the higher multipoles of the entropy per baryon field s_b that fulfill the equilibrium for the current iteration,

$$\Delta_{\theta\phi} s_b = \left(\partial^\theta + \frac{1}{\tan\theta}\right)\left[\frac{\partial_\theta\left(Te^{-H}\right)}{\partial_r\left(Te^{-H}\right)}\partial_r s_b\right], \tag{4.7}$$

8. go back to step 1., until convergence of H and s_b is achieved (i.e. when the field's relative difference between two consequent iteration steps is smaller than the desired precision).

4.2 Code implementation

We implemented the above described algorithm in two codes available in the numerical relativity library LORENE [15], namely HotRNS, for Hot (rigidly) Rotating Neutron Stars, and HotRNS_diff, which handles the case of differential rotation. LORENE is a C++ library based on multi-domain spectral methods [24], widely used in the literature to compute stationary relativistic objects, e.g. to build initial data for dynamical relativistic simulations. In short, a spectral method is a numerical technique which consists in recasting a function as a sum of basis functions, and represent it by its basis coefficients, such that differential equations of this function becomes an algebraic relation between these coefficients. Such a method allows one to compute rather efficiently accurate numerical solutions of PDE problems. Of course, one has to assure that the function is continuous throughout the entire domain correspondent to the numerical grid where one intends to perform calculations, otherwise, the scheme will not converge due to the Gibbs phenomenon. Therefore the need to use several numerical domain, corresponding to different regions of the function where such condition is fulfilled, whenever dealing with functions which may involve discontinuities. Both codes use spherical coordinates. For each domain $\mathcal{D}_\mathcal{N}$, there is a map between the spherical coordinates and the numerical coordinates

$$\begin{aligned} [-1,1]\times[0,\pi]\times[0,2\pi] &\longrightarrow \mathcal{D}_\mathcal{N}\,, \\ (\xi,\theta',\phi') &\longmapsto (r,\theta,\phi)\,, \end{aligned} \tag{4.8}$$

with the exception of the core domain $\mathcal{D}_0$, for which $\xi \in [0,1]$. This choice of coordinates allows us to use Chebyshev polynomials as basis functions to decompose the radial component of a function. In general, scalar functions are decomposed as

$$f(r,\theta,\phi) \longmapsto f(\xi,\theta',\phi') \simeq \sum_{i=0}^{n_r}\sum_{j=0}^{n_\theta}\sum_{k=-n_\phi}^{n_\phi} c_{ijk} T_i(\xi)\cos(j\theta)\, e^{ik\phi}\,, \tag{4.9}$$

where $T_n(\xi)$ are the Chebyshev polynomials of first kind (in the core domain, even Chebyshev polynomials $T_{2n}(\xi)$ are used), and (n_r, n_θ, n_ϕ) are the number of collocation points, i.e. the numerical grid points where the basis coefficients are evaluated.

The user can specify any analytical or a tabulated EoS (for the latter case, we have use a bidimensional version of the standard interpolating Swesty algorithm [45], assuring thermodynamical consistency).

To improve convergence, the following strategies have been implemented:

- during the first ten iterations, we will compute the equilibrium of a cold, non rotating star;
- after the first ten iterations, during the following ten iterations, the angular velocity Ω (its central value Ω_c in the case of differential rotation), will be linearly increased from zero to the desired value of Ω (entropy is still not taken into account at this point), i.e. it's value will be multiplied by a coefficient during those ten iterations, varying as

$$\Omega^i = \frac{i-10}{10}\Omega\,, \quad i \in [10, 20]\,; \tag{4.10}$$

- after the first twenty iterations, during the following twenty iterations,the entropy per baryon field s_b is multiplied by a factor growing linearly from zero to one, in a similar way to that was done with the angular velocity (4.10) (at this point, eq. (3.60) is not yet being computed, i.e. we are only taking into account the monopolar term of s_b);
- after the first forty iterations, we start computing the multipolar terms of the entropy per baryon field s_b with eq. (3.60), and during the following twenty iterations, the multipolar terms of s_b will be multiplied by a linearly increasing factor, in the same way as described in the previous steps;
- at the end of each iteration, we will relax the quantities ν and $Q\,(= \Psi^2 N$, the solution of the third Poisson equation in system (3.38)), i.e. at the end of each iteration, we modify the quantity $f = \nu, Q$ with some relaxation parameter w as

$$f^{i+1} = w\, f^{i+1} + (1-w)\, f^i\,. \tag{4.11}$$

In our codes, the numerical domains $\mathcal{D}_\mathcal{N}$ are spherical domains. This raises a limitation on the capability of the code to find solutions without imposing any approximation to the equations. We observed that equation (3.59) (which physically is only defined in the interior of the star), becomes numerically unstable when computed outside the star for non-trivial entropy per baryon monopolar profiles. Now, rapidly rotating stars, as well as strongly differentially rotating stars, have large deviations from spherical symmetry, and for that reason, when using spherical domains, one has to compute the fields outside the star, for some region of the domain which contains the stellar equator. For this reason, our equilibrium solver is only capable of solving non-approximated solutions up to some rotation frequency limit, which depends on the EoS, the central log-enthalpy H_c, and of course on the monopolar profile specified to the entropy per baryon field s_b. In order to be able to use the code in more general situations, we implemented an approximation to equation (3.59): when the star flatness (i.e. the ratio between the polar radius and the equatorial coordinate radius) becomes lower than some threshold, we restrain the computation of (3.59) to a spherical domain which covers at least the entire polar radius of the star (it can cover a larger radius for analytical EoS), but not the entire equatorial radius. As we will show below in figure 4.4, for an analytic EoS this threshold is considerably high. We will discuss, in part III of this thesis, projects for future work which might allow us to develop a more robust numerical code.

We observed as well the emergence of aliasing instabilities, which are a non-physical divergence of higher frequency modes, when computing rapidly rotating stars (which require more

iterations for convergence). To handle these instabilities, when computing the source term for ((3.59)), we implemented the de-aliasing technique usually referred to as the truncating 2/3-rule (see [34] for example), i.e. we set to zero two thirds of the higher frequency spectral coefficients for each field in the source term before proceeding to any multiplication.

4.3 The relavitistic ideal gas

In order to properly test the code, we will use an analytical EoS, so to avoid any numerical errors from the EoS construction and interpolation. For that purpose, we will use the simplest possible example of a relativistic gas with finite temperature: the ideal gas.

For a single-species (let's say baryons) ideal gas, one may write the energy density as (see, for example, [35])

$$\varepsilon = \frac{1}{\gamma_a - 1} n_b^{\gamma_a} \Phi^{(\gamma_a - 1)} e^{s_b(\gamma_a - 1)} + m_b n_b \,. \tag{4.12}$$

where γ_a is the adiabatic index, and Φ is a constant which depends on the gas specific characteristics. The temperature and chemical potential are given by the relations

$$\begin{aligned} \mu_b &= \left(\frac{\partial \varepsilon_{int}}{\partial n_b}\right)\bigg|_{V,S} = (\Phi\, n_b)^{(\gamma_a - 1)} \left(\frac{\gamma_a}{\gamma_a - 1} - s_b\right) e^{s_b(\gamma_a - 1)} \,, \\ T &= \left(\frac{\partial \varepsilon / n_b}{\partial s_b}\right)\bigg|_{V,n_b} = (\Phi\, n_b)^{(\gamma_a - 1)}\, e^{s_b(\gamma_a - 1)} \,, \end{aligned} \tag{4.13}$$

where $\varepsilon_{int} := \varepsilon - m_b n_b$ is the internal energy density (the microscopic kinetic and potential energy of the gas as a whole). From the Gibbs relation $\varepsilon + p = (T s_b + \mu_b) n_b$, we can obtain pressure as

$$p = n_b^{\gamma_a} \Phi^{(\gamma_a - 1)} e^{s_b(\gamma_a - 1)} \,. \tag{4.14}$$

Finally, identifying the pressure coefficient $k = \Phi^{(\gamma_a - 1)}$, we can rewrite our EoS in terms of the log-enthalpy H and the entropy per baryon s_b as

$$\begin{aligned} p(H, s_b) &= k\, n_b(H, s_b)^{\gamma_a} e^{(\gamma_a - 1) s_b} \,, \\ \varepsilon(H, s_b) &= \frac{k}{\gamma_a - 1} n_b(H, s_b)^{\gamma_a} e^{(\gamma_a - 1) s_b} + m_b n_b(H, s_b) \,, \\ T(H) &= m_b \frac{\gamma_a - 1}{\gamma_a} \left(e^H - 1\right) \,, \\ n_b(H, s_b) &= \left(m_b \frac{\gamma_a - 1}{\gamma_a\, k} \left(e^H - 1\right)\right)^{\frac{1}{\gamma_a - 1}} e^{-s_b} \,. \end{aligned} \tag{4.15}$$

For an EoS to be physically consistent, we must assure that sound doesn't propagate at superluminal speeds on the corresponding fluid, and to assure microscopic stability, the sound speed c_s must always be real. This translates as

$$1 > c_s^2 = \frac{\partial p}{\partial \varepsilon}\bigg|_S \geqslant 0 \,. \tag{4.16}$$

A sufficient (but not necessary) condition to verify both limits expressed in (4.16) for the ideal gas is (assuming $\gamma_a > 1$)

$$\frac{\gamma_a}{\gamma_a - 1} \geqslant s_b \,. \tag{4.17}$$

4.4 Test results

Having verified that in the limit of zero entropy per baryon, both codes verify the results of the equivalent codes implemented for cold neutron stars, namely rotstardirac and rotstardirac_diff, we are going to explore the code limitations prescribing three distinct profiles for the monopolar part of s_b, as represented in figure 4.1: a constant profile s_0, for which we have an analytical solution of the equilibrium equations, and two non-constant monopolar profiles,

$$\begin{aligned} s_1 &= \frac{1}{2} + \frac{s_0\, r^2}{10} \,, \\ s_2 &= s_0\, e^{-\frac{r^2}{2^3}} \,. \end{aligned} \tag{4.18}$$

The purpose of these profiles is uniquely for testing the liability of the code, there was

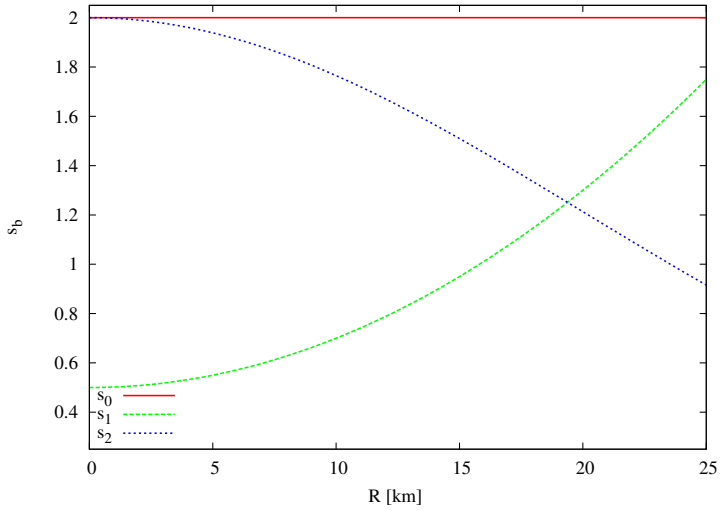

Figure 4.1: Profiles for the monopolar term of s_b

no physical motivation for these choices. On the following results, we will take the constant profile to be $s_0 = 2$ (in units of Boltzmann constant). Furthermore, we will take the adiabatic index to be $\gamma_a = 2$, and the pressure coefficient to be $k = 200 MeV\, fm^3$ (for such choice of parameters, at zero entropy per baryon, EoS ((4.15)) roughly fit the typical mass/radius profiles of a neutron star. Unless stated otherwise, we will consider models with a central log-enthalpy of $H_c = 0.3$, and we will end the computation when the variation of the log-enthalpy field is smaller than 10^{-7}.

	$f_{rot}\,[Hz]$	$M_g\,[M_\odot]$	$R_{eq}\,[Km]$	r_p/r_{eq}	$GRV2$	$GRV3$
s_0	382.84	4.73	47.37	0.58	-7.43 e-7	1.32 e-6
$s_{1\,apprx}$	721.85	2.26	22.65	0.64	-9.45 e-4	9.35 e-4
s_1	650	2.18	20.26	0.75	-3.34 e-6	2.38 e-5
$s_{2\,apprx}$	490	4.40	37.65	0.57	1.01 e-2	5.73 e-3
s_2	395	3.79	28.72	0.76	2.35 e-5	-4.69 e-5

Table 4.1: Star configurations for the different s_b profiles. The subscript $apprx$ stand for approximate solutions, meaning that we implement the approximation described above. f_{rot} stand for the rotating frequency, M_g stand for the Komar mass, R_{eq} is the equatorial circular radius, r_p/r_{eq} is the flatness (the ratio between the polar and equatorial coordinate radius), and ($GRV2$, $GRV3$) are the virial identities.

4.4.1 Rigid rotation

Let us start by discussing the tests made to the HotRNS code. For the constant entropy per baryon profile, we could verify the very same results we obtain with the previously implemented code rotstar_dirac (notice that in such case, (3.58) reduces to the analytical first integral of cold stars (3.50), while equation (3.59) is trivially fulfilled). In figure 4.2, we show isocontour lines[1] for the log-enthalpy field of a star rotating at the Kepler frequency, with the constant profile s_0, for which the equilibrium scheme reduces to the standard analytical first integral obtained in [3]. As described above, for the non-constant entropy per baryon profiles, our code is not able to find non-approximated solutions when approaching the rotation velocity of the Kepler frequency. We show below some examples of parameter choices for which the implemented approximation becomes stronger than desired (in the sense that the coordinate equatorial radius of the star is large compared to the coordinate radius of the spherical domain in which the higher multipoles of s_b are computed, being the latter, for the case presented in figure 4.3, $\sim 73\%$ of the earlier), along with the maximum rotation for which the code can provide a non-approximated solution under such parameters choice. In figure 4.3, we show the isocontour lines for the pseudo-log enthalpy and entropy per baryon of a rapidly rotating star, with the non-constant radial profile s_1. The maximum rotation frequency for which we can obtain a solution without requiring any approximation is $f_{rot} = 650\,Hz$ (i.e. 90% of the frequency for the rapidly rotating star in 4.3). We show its log-enthalpy and entropy per baryon profiles in figure 4.4. Finally, we show in figure 4.5 the isocontour plots for a rapidly rotating star with the non-constant monopolar profile s_2. The maximum rotation frequency for which we can obtain a non-approximated solution is $f_{rot} = 395\,Hz$ (i.e. 81% of the frequency for the rapidly rotating star in 4.5). We show its log-enthalpy and entropy per baryon profiles in figure 4.6. Despite the code limitations, we have shown here that nevertheless, it allows us to compute non-approximated solutions of rigidly rotating stars with analytical EoS for remarkably fast rotations. In figure 4.7 we exemplify the influence of temperature in the mass-radius profiles for the different choices of

[1]For all the isocontour plots presented in this thesis, the dash-point lines represent the numerical domains, the dashed lines represent negative values of the plotted field, thin continuous lines represent positive values of the plotted field, and thick lines represent the star surface.

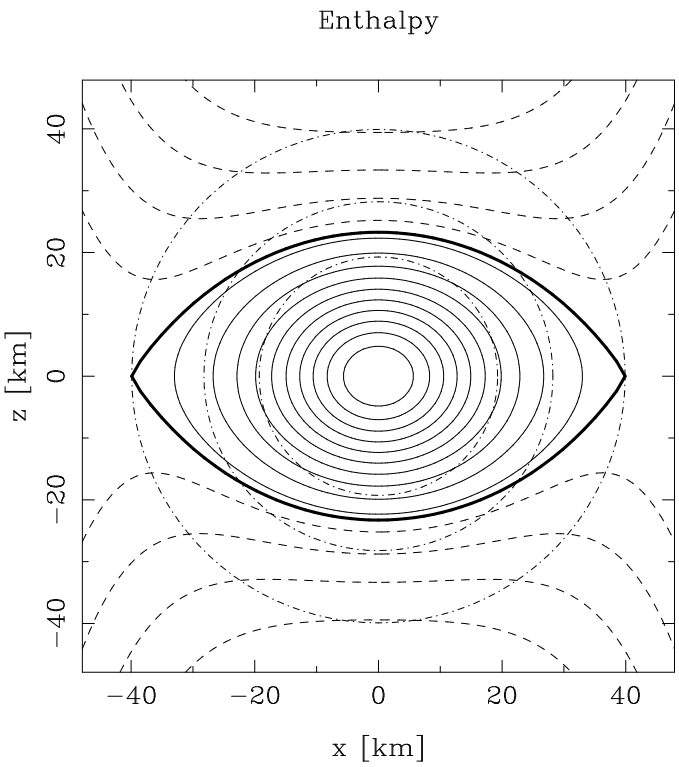

Figure 4.2: Isocontour enthalpy lines for the s_0 radial entropy profile ($f_{rot} = 382.84\,Hz$)

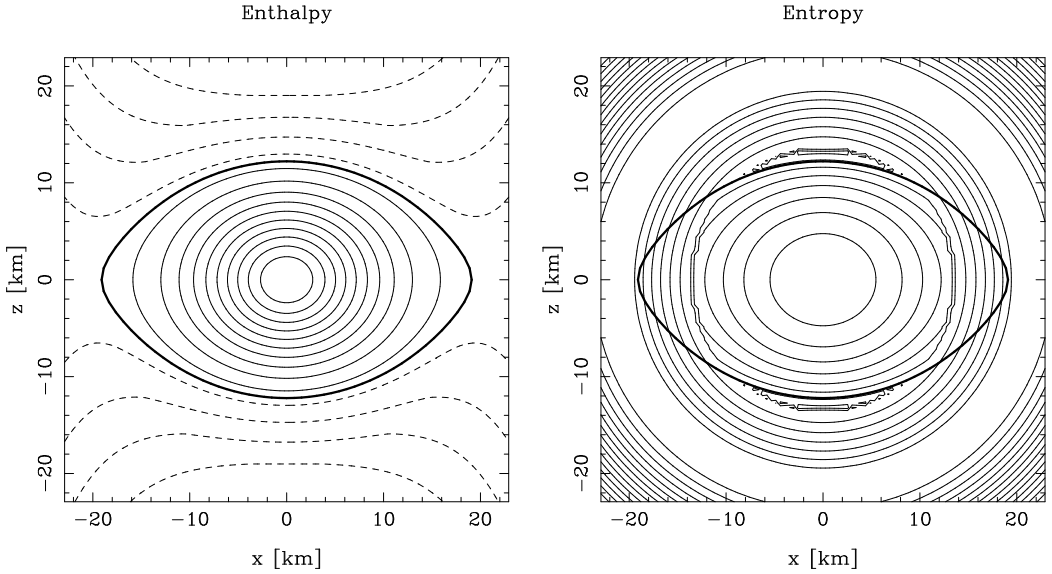

Figure 4.3: Isocontour lines of log-enthalpy and entropy per baryon for a rapidly rotating star with the s_1 entropy per baryon monopolar profile ($f_{rot} = 721.85\,Hz$)

entropy per baryon monopolar profiles. Of course that, as we will later show with a realistic EoS, the dramatic impact of temperature shown in 4.7 is a mere artifact of the ideal gas EoS. As expected, the larger the entropy field, the more energy the star will have, and therefore,

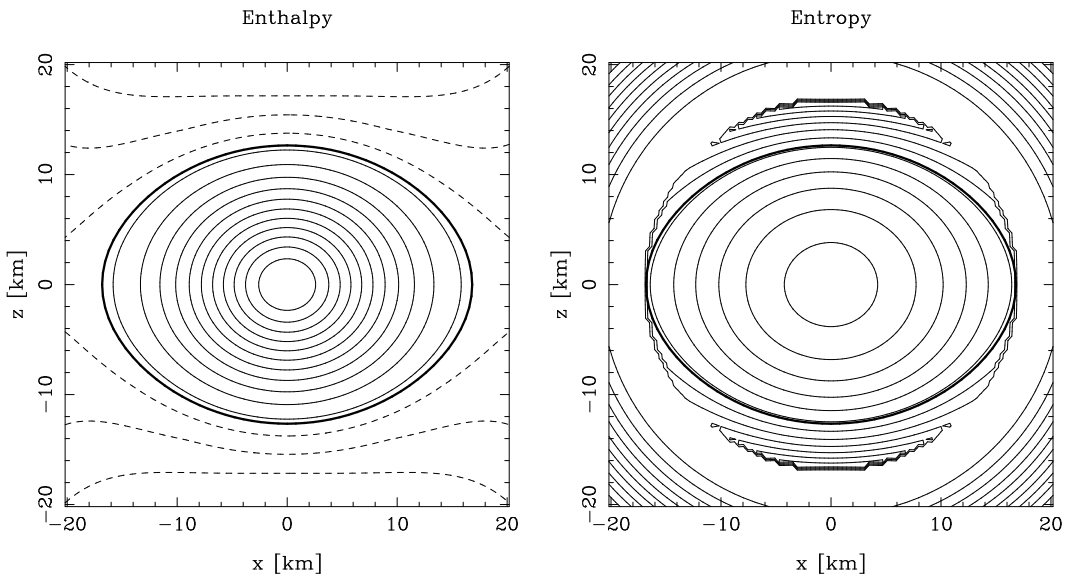

Figure 4.4: Isocontour lines of log-enthalpy and entropy per baryon for the fastest rotation up to which the code can provide a solution without approximations, using the s_1 entropy radial profile ($f_{rot} = 650\,Hz$)

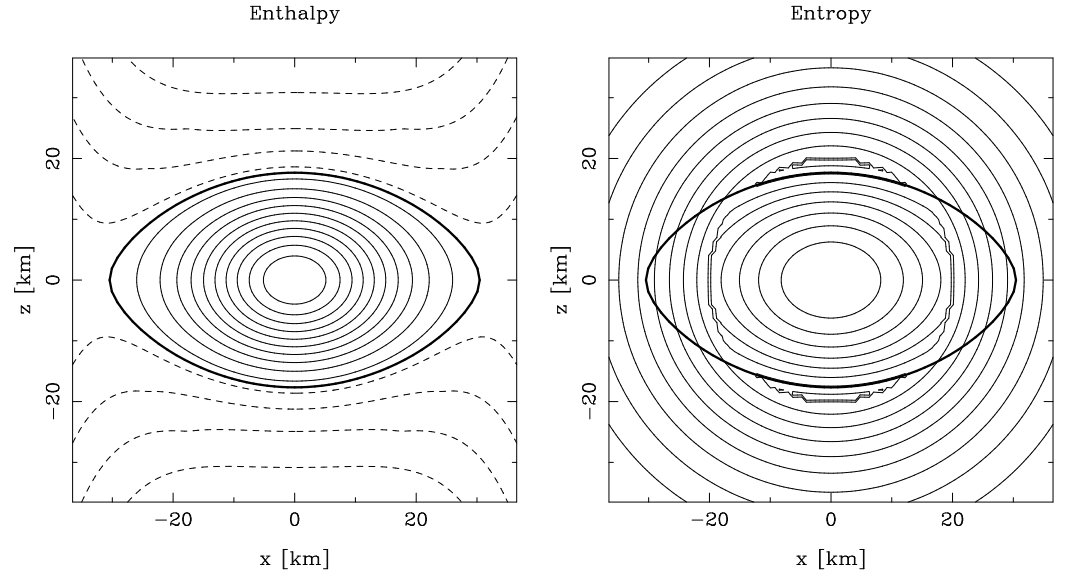

Figure 4.5: Isocontour lines of log-enthalpy and entropy per baryon for a rapidly rotating star with the s_2 entropy per baryon monopolar profile ($f_{rot} = 490\,Hz$)

the larger its mass. Also, the larger its radius, the larger the angular momentum will be, and therefore, the smaller the maximal rotation velocity.

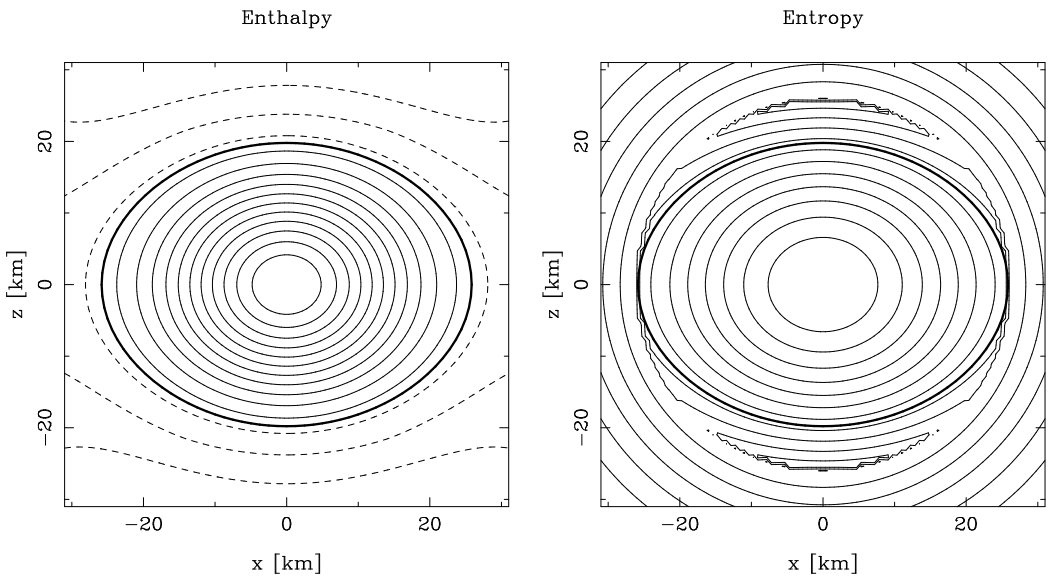

Figure 4.6: Isocontour lines of enthalpy and entropy for the fastest rotation up to which the code can provide a solution without approximations, using the s_2 entropy radial profile ($f_{rot} = 395\,Hz$)

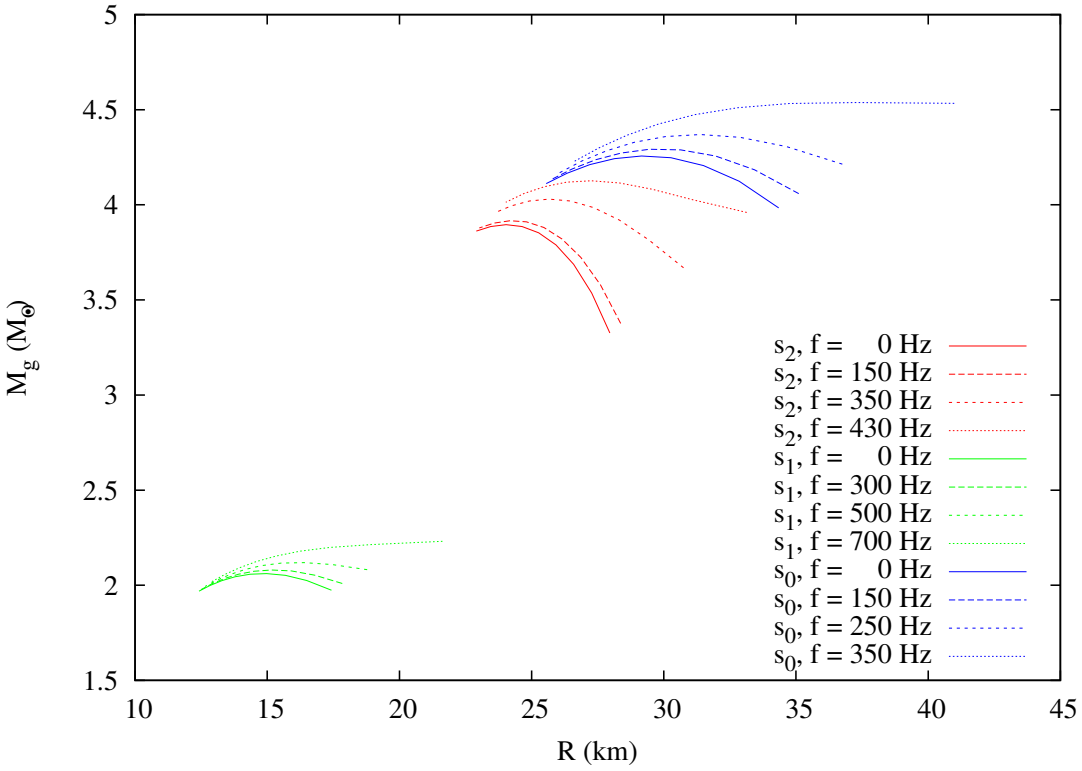

Figure 4.7: Mass-radius profiles for the ideal gas EoS

a	$M_g\,[M_\odot]$	$R_{eq}\,[Km]$	R_p/R_{eq}	$GRV2$	$GRV3$
2	4.32	34.92	0.82	-2.61 e-7	-2.08 e-6
0.95	5.71	40.68	0.51	-1.50 e-5	2.55 e-5
0.75	7.18	47.50	0.35	-1.67 e-5	2.14 e-5

Table 4.2: Star configurations for the constant s_0 entropy per baryon profile, for different values of the parameter a.

a	$M_g\,[M_\odot]$	$R_{eq}\,[Km]$	R_p/R_{eq}	$GRV2$	$GRV3$
1	2.13	18.32	0.84	3.29 e-4	2.93 e-4
0.6	2.31	20.23	0.51	-5.22 e-6	4.14 e-6

Table 4.3: Star configurations for the constant s_1 monopolar profile, for different values of the parameter a.

4.4.2 Differential rotation

We will now discuss the tests made to the HotRNS_diff code. We will consider a linear rotation law

$$F(\Omega) = \left(\frac{R_{eq}}{a}\right)^2 (\Omega_c - \Omega)\,, \tag{4.19}$$

where a is a free parameter describing the degree of differential rotation, and Ω_c is the central angular velocity, which for the purpose of the following tests we set to the value $\Omega_c = 2\pi \times 1000\,rad/s$ (recall that when testing rigid rotation , we found the maximum rotations of all three entropy per baryon profiles to be much lower than $f_{rot} = 1000\,Hz$). Again, for the constant entropy profile, we could verify the very same results we obtain with the previously implemented code rotstar_dirac_diff. In table 4.2, we describe the global quantities for solutions with the constant entropy per baryon profile s_0, with different degrees of differential rotation, and we show the correspondent isocontour enthalpy plots in figures 4.8, 4.9 and 4.10. Again, at constant entropy per baryon, all solutions presented here are solutions without approximations. For non-constant entropy per baryon monopolar profiles, the code is however only stable for a smaller range of values of the parameter a. These numerical instabilities can in any case be overcome by imposing the approximation earlier described on the entropy per baryon field, however, if one wants to keep low deviations on the virial identities, one has to constrain the level of differential rotation for which solutions can be considered credible. We show in table 4.3 the global quantities for solutions with the entropy per baryon profile s_1. The correspondent isocontour log-enthalpy and entropy per baryon plots are shown in figures 4.11 and 4.12. Finally, we show in table 4.4 the global quantities for solutions with s_2 monopolar profile, and the correspondent isocontour log-enthalpy and entropy per baryon plots in figures 4.13 and 4.14. For the later case, with $a = 1$, the solution is an approximated one. We have shown that for differentially rotating stars, the code has strong limitations on the ability to find solutions of stars which are strongly deformed in the polar points, for models with non-constant entropy per baryon fields. It does nevertheless allow us to find interesting non-trivial, non-approximated solutions, such as those we have

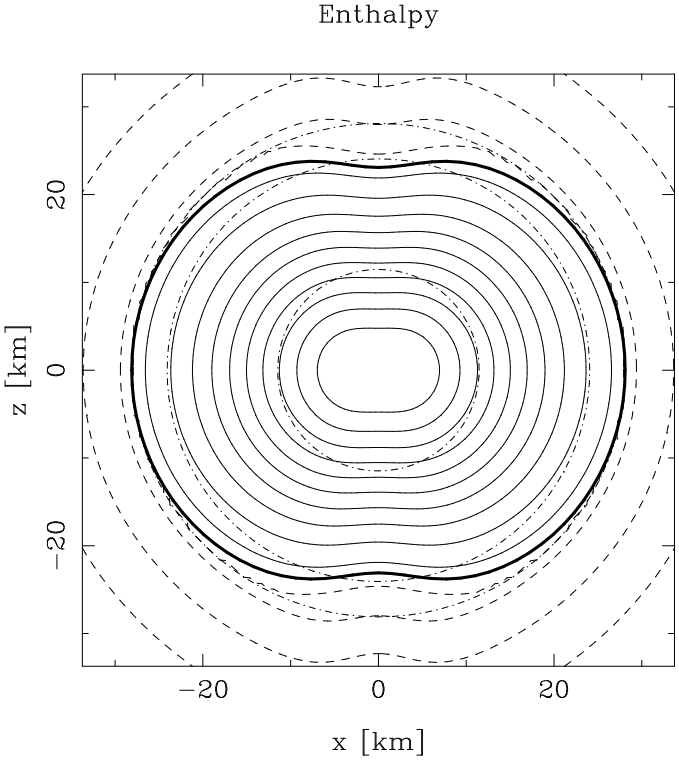

Figure 4.8: Isocontour log-enthalpy lines for the s_0 entropy per baryon profile, a=2

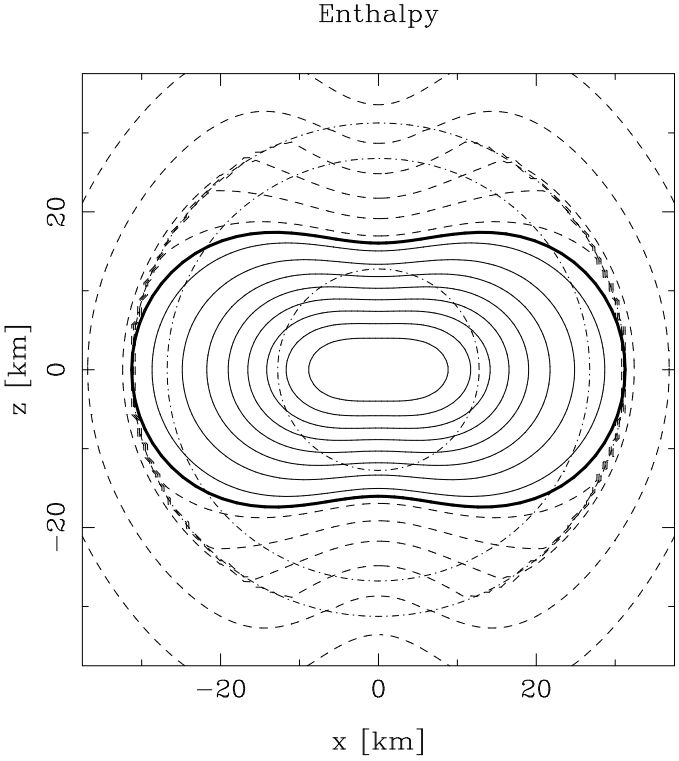

Figure 4.9: Isocontour log-enthalpy lines for the s_0 entropy per baryon profile, a=0.95

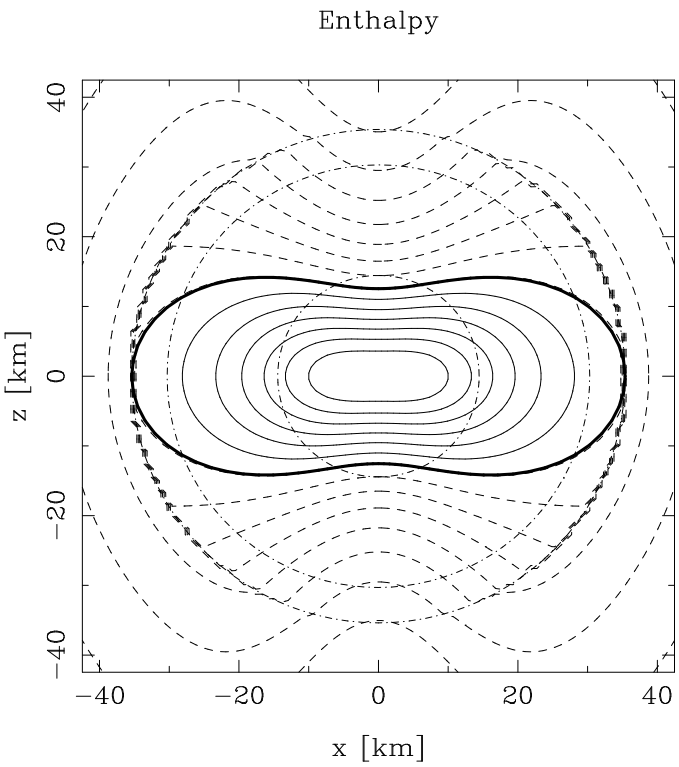

Figure 4.10: Isocontour log-enthalpy lines for the s_0 entropy per baryon profile,a=0.75

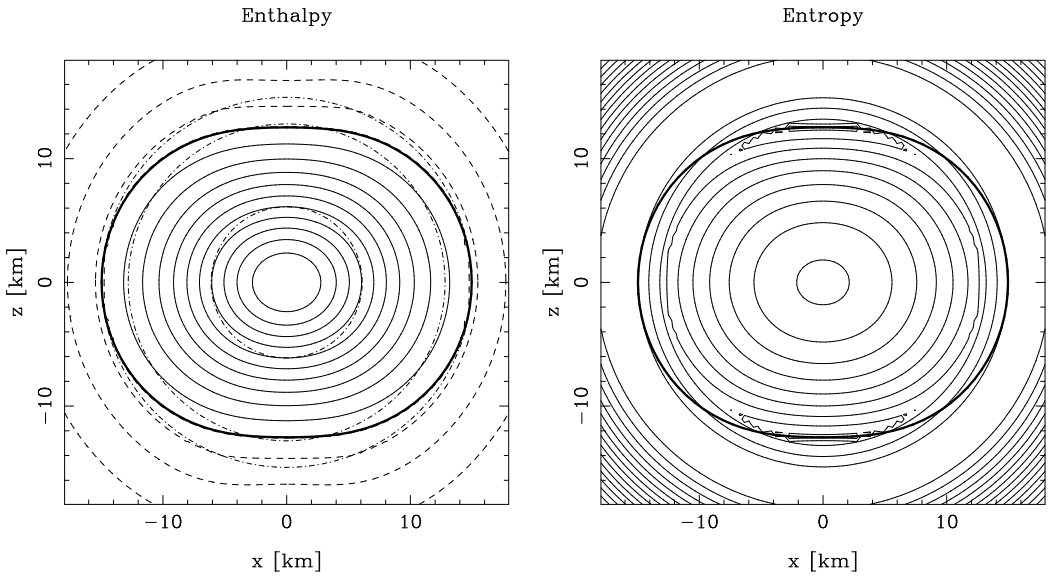

Figure 4.11: Isocontour lines of log-enthalpy and entropy per baryon for a differentially rotating star with the s_1 monopolar profile, a=1

shown in figures 4.11 and 4.12.

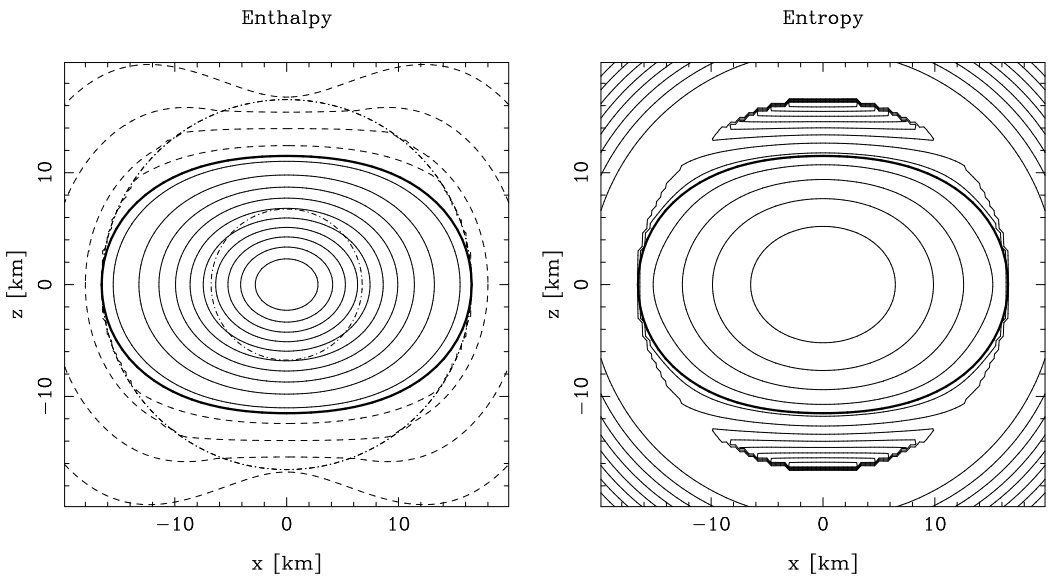

Figure 4.12: Isocontour lines of log-enthalpy and entropy per baryon for a differentially rotating star with the s_1 monopolar profile,a=0.6

a	$M_g\,[M_\odot]$	$R_{eq}\,[Km]$	R_p/R_{eq}	$GRV2$	$GRV3$
2.85	3.44	28.23	0.91	3.08 e-3	-2.29 e-5
1	4.43	32.00	0.63	2.04 e-2	-1.15 e-2

Table 4.4: Star configurations for the constant s_2 monopolar profile, for different values of the parameter a.

4.5 Summary

Let us now summarize the main findings from our tests to both codes with an analytical EoS (4.15). Again, we recall that we have verified that both codes do perfectly agree with the results of the previously implemented codes for cold relativistic rotating stars in Dirac gauge, in the corresponding limit of $s_b = 0$. The codes have further been tested for the case of a constant s_b profile, as well two non-constant s_b profiles (4.18) with different behaviors: the first growing quadratically towards the star's surface, implying a smaller entropy per baryon inside the star, and the second decaying as a Gaussian function towards the stars surface, having therefore a larger entropy per baryon inside the star. In it's present form, the codes has a limited capability to find solutions of rapidly rotating, or strongly differentially rotating stars with non-constant s_b profiles. In those limits, we implemented an approximation to the angular hydrostatic equilibrium equation. We observed that when implementing this approximation, the maximum deviation of this equation from zero is of the order of the virial identity GRV2.

For the code HotRNS, we found that:

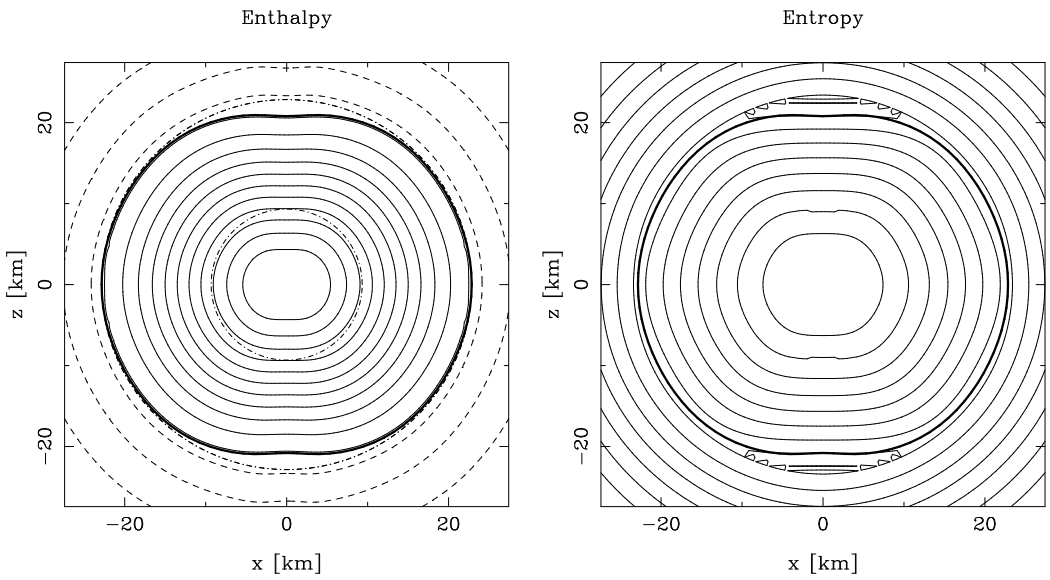

Figure 4.13: Isocontour lines of log-enthalpy and entropy per baryon for a differentially rotating star with the s_2 monopolar profile, a=2.85

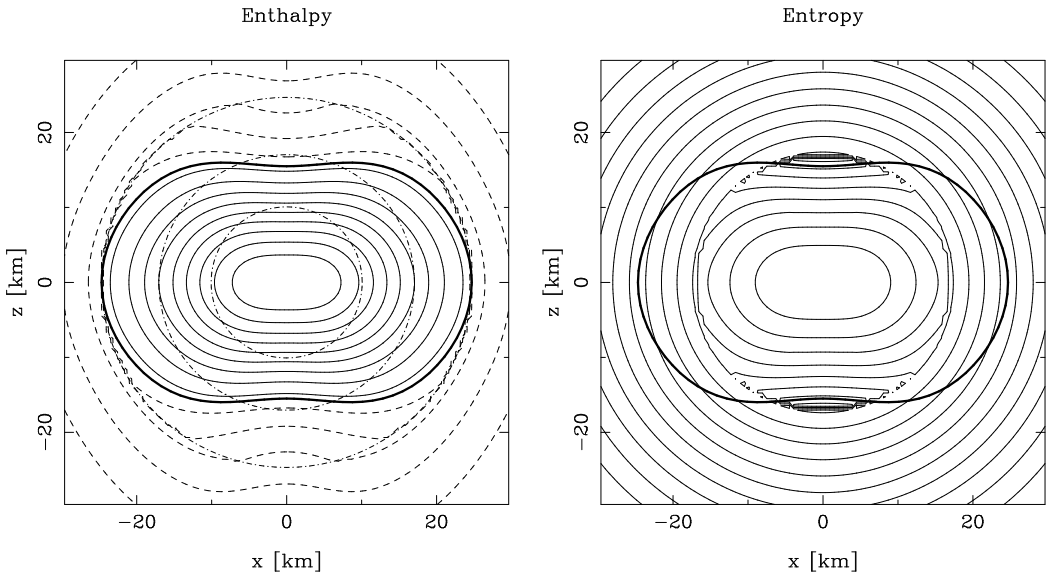

Figure 4.14: Isocontour lines of log-enthalpy and entropy per baryon for a differentially rotating star with the s_2 monopolar profile, a=1

• When using the constant profile s_0, for which our scheme reduces to the well known BGSM scheme, the code handles easily the calculation, leading to a good numerical accuracy (the virial identities GRV2 and GRV3 have similar values to those we obtain when computing a polytropic star with the rotstardirac code).

• When using the non-constant s_b profiles, in its present state, the code requires an

approximation on the multipolar terms of the entropy per baryon field for rapidly rotating star models.

- Using the non-constant profile s_1, employing the described approximation on s_b, we obtained acceptable numerical accuracies (the virial identities GRV2 and GRV3 are of order $\sim 10^{-4}$) for the fastest rotating model for which we obtained convergence. The code was able to converge without any approximation for a star model rotating at 90% of the rotation frequency of the fastest rotating solution for which our code converged (employing the approximation in the s_b field), with a good numerical accuracy.

- Using the non-constant profile s_2, employing the described approximation on s_b, we obtained rather low numerical accuracies (with GRV2 of order $\sim 10^{-2}$ and GRV3 of order $\sim 10^{-3}$) for the fastest rotating model for which we obtained convergence. In contrast with what was observed with the non-constant profile s_1, for s_2, the deformation on the s_b profile due to rotation was larger. This larger deviation from the spherically symmetric profile assumed for the outer domain, is the origin of such lower accuracy. The code was able to converge without any approximation for a star model rotating at 81% of the rotation frequency of the fastest rotating solution for which our code converged (employing the approximation in the s_b field), with a good numerical accuracy.

- The mass-radius relations shown in figure 4.7, are consistent with the physical expectation one would have: the larger the amount of entropy inside the star, the larger its energy, and therefore, the larger its mass, and the larger its radius; also, the faster the star's rotation, the larger the radius, and the larger the maximum mass supported by such star.

For the code HotRNS_diff, we found that:

- Again, when using the constant profile s_0, the code handles easily the calculation, leading to a good numerical accuracy (the virial identities GRV2 and GRV3 have similar values to those we obtain when computing a polytropic star with the rotstardirac_diff code).

- When using a non-constant s_b profile, in its present state, the code has a rather limited reliability. We have tested the code using a linear rotation law (4.19), such that the star rotates faster in its core, and slower in its surface. Such star models will therefore lead to a stronger deformation towards the stellar core. It becomes rather difficult task to appropriately compute the angular dependence of the s_b field when attempting to model strongly differentially rotating stars.

- Using the non-constant profile s_1, we have presented, in figures 4.11 and 4.12, two differentially rotating solutions for which with didn't impose any approximation on the s_b multipolar terms. We obtained a good numerical accuracies, with virial identities respectively of order $\sim 10^{-4}$ and $\sim 10^{-6}$.

- Using the non-constant profile s_2, we have presented, in figures 4.13 and 4.14, two differentially rotating solutions, the latter employing the approximation on the s_b multipolar

terms. In both cases, the virial identities seem to indicate a poor numerical accuracy (being clearly the case for the approximated solution).

Chapter 5

The Nuclear Equation of State

So far, we have seen how to solve the equations of a relativistic differentially rotating star, with hot matter and a constant lepton fraction, and we have explored solutions of a (not so realistic) compact star whose matter could be described as an ideal gas. To model a realistic hot neutron star, we need to derive a suitable EoS capable of properly describing the behavior of nuclear matter at finite density, finite temperature and finite chemical potential. Of course, if this EoS will be the source term of Einstein equations, one has to guarantee general covariance of the underlying theory. The Einstein equivalence principle tell us that a local free falling frame exists for which gravity and inertial forces locally compensate each other, i.e. a microscopic (therefore local) description of matter, is consistent with a locally flat spacetime, for which reason we don't need to take the curvature of spacetime into account in the EoS underlying theory. The relevant physical interaction we need to care for is the strong interaction, which is described by the theory of quantum chromodynamics (QCD). In short, one can think of it as an extended version of quantum electrodynamics (QED); whereas the latter has one (electric) charge and photons as the interaction mediators, QCD has three charges, referred to as color charge, and gluons, which are photon-like massless fields, as their interaction mediators. Color charge is carried by quarks, a family of spin-1/2 fundamental particles quarks, which along with gluons, are the constituents of all hadronic states of matter. There are six flavors of quarks: up *'u'* quarks, down *'d'* quarks, strange *'s'* quarks, charmed *'c'* quarks, bottom *'b'* quarks, and top *'t'* quarks. All these flavors represent quarks of different masses, which carry a unit of any of the three above mentioned color charges (and carry as well a fraction of unit of electric charge). Again, like in QED, QCD is symmetric with respect to all three charges, described by the SU(3) group. Albeit all similarities, QCD has nevertheless a more complicated structure than QED. For example, while photons are electrically neutral, and simply respond to electric charge presence and dynamics, gluons have the ability of changing a quark color into another: they carry color themselves. It follows that unlike QED, QCD is a self-interacting field theory: gluons respond to presence and motion of color-charges, and they carry color-charge themselves, therefore, gluons will also interact among themselves, unlike what happens among the electrically neutral photons. Another remarkable difference between QED and QCD is the so-called confinement. While the electromagnetic field between two charges quickly diminishes with distance, allowing

electrons to be ejected from atoms, the reason for which we can observe them in nature, the gluon field, having color-charge itself, will act constantly between quark-antiquark pairs, regardless of their distance. The energy one would need to break such a pair, does therefore greatly exceeds the energy needed to form a new quark-antiquark pair; in other words, an attempt to eject a quark from a hadron, would only lead to the formation of a new hadron, and therefore, we cannot observe isolated quarks directly. This elegant theory is fully described by the Lagrangian density

$$\mathscr{L} = \bar{\psi}_f \left(i\gamma^\mu D_\mu - m_f \right) \psi_f - \frac{1}{4} G^\alpha_{\mu\nu} G^{\mu\nu}_\alpha, \tag{5.1}$$

where f stands for flavor index and α for color index, ψ_f is a Dirac spinor representing a quark with the correspondent mass m_f, γ^μ are the Dirac matrices, the covariant derivative operator is

$$D_\mu = \partial_\mu + i t_\alpha A^\alpha_\mu, \tag{5.2}$$

with t_α the Gell-Mann matrices (generators of the SU(3) group), and A^α_μ the gluon fields, and finally, $G^\alpha_{\mu\nu}$ is the gluon field strength tensor

$$G^\alpha_{\mu\nu} = \partial_\mu A^\alpha_\nu - \partial_\nu A^\alpha_\mu - g_s f^{\alpha\beta\gamma} A^\beta_\mu A^\gamma_\nu, \tag{5.3}$$

where g_s is the coupling constant of the strong interaction, and $f^{\alpha\beta\gamma}$ are the structure constants of the SU(3) group. Now, the QCD coupling constant is of order unity. Because gluons are self-interacting fields, this leads to perturbation theory being only applicable for processes of very high energies, at temperatures and densities irrelevant for modeling neutron stars. There is a numerical approach to QCD, named lattice QCD, however, for the moment, it is not computationally practical for calculations at the large density regimes of a neutron star. Even a derivation of the "true" interaction between hadrons from QCD remains a very complex task despite intensive efforts. There are therefore many uncertainties about the behavior of dense and hot matter. This represents therefore a major difficulty in neutron star modeling: one cannot make an ab initio description of nuclear matter, by building an EoS from the first principles of QCD. An alternative approach would be to work with an effective field theory, i.e. a simpler model, which reduces the number of degrees of freedom, keeping the main ingredients (the appropriate ingredients for the case study) of the real underlying theory, which in itself is not a trivial task neither. In an initial and simplistic approach, one might say that for the task of describing matter in a neutron star, we are mostly concerned with a proper microscopic many-body description of nucleonic matter at supra-nuclear densities, and their interactions. We would therefore need an effective model capable of properly describing nucleonic degrees of freedom, which could be obtained directly from QCD if such task was computationally practical in the relevant energy and density limits. Walecka [43, 44] developed such a model, based on a relativistic mean field theory (RMF). He proposed a $(\sigma - \omega)$ model, describing a system of Dirac baryons interacting via meson fields, the latter being treated on the mean field limit. Because RMF is an effective model, those are not necessarily existing mesons. His approach can readily be employed for building a model for hadronic (other than nucleonic) degrees of freedom. In fact, if one neglects the possibility of a transition to the quark-gluon plasma in the center of the star, the relevant degrees of freedom for matter in a neutron star, or in a core collapse supernova, are not quarks and gluons, but hadrons. Due to the inherent difficulty in

finding an appropriate method to compute the actual state of such system, most models, as RMF models, rely on phenomenological "in-medium" interactions, whose parameters have to be adjusted to existing experimental or observational data. Microscopic many-body calculations (Brueckner-Hartree-Fock, Monte Carlo techniques, renormalisation group, ...) starting from the fundamental hadronic two- and three-body forces can to some extent constrain the phenomenological models, too. But since it is impossible to solve the strongly interacting many-body problem exactly, these calculations contain, in addition to the uncertainties on the fundamental forces, more or less controlled approximations, and the constraints have to be regarded with some care.

In this thesis, we will employ such an effective model for hadronic matter, assuring the compatibility with the existing constraints. Among the constraints, particular attention will be paid to the recent discovery of two neutron stars with a mass of about 2 $M_\odot$ [**?**, 107], which triggered intensive discussions about the composition of matter at the center of neutron stars and the EoS at very high densities. Most models predict the onset of non-nucleonic degrees of freedom, such as hyperons (strange baryons) or mesons (pions, kaons), at about twice the value of nuclear matter saturation density, i.e. for cold neutron stars with a mass above roughly $1.4M_\odot$. These additional degrees of freedom soften the EoS and lower the maximum mass. In particular, the classical models with hyperons predict maximum masses of $\sim 1.4M_\odot$, well below the highest observed ones. This leads to the so-called "hyperon puzzle".

Different solutions have been proposed to overcome this problem. A possible solution is that a transition to quark matter appears at sufficiently low densities, such that hyperons have not yet softened the EoS too much. Phenomenological quark models can easily be supplemented with the necessary repulsion at high densities, and maximum neutron star masses above $2M_\odot$ can be obtained [93].Another possibility is to modify the hyperonic interactions at high densities. Experimental data are scarce and furnish only weak constraints on the interactions at densities below nuclear matter saturation density. At the relevant densities in the center of neutron stars, almost nothing is known about the hyperon-nucleon (YN) and hyperon-hyperon (YY) interactions. In phenomenological models, the interaction can thus be adjusted to provide the necessary repulsion. This will be the case of our model.

Presently available EoS models which include all hyperons and cover the entire range in baryon number density n_B, temperature T and hadronic charge fraction, $Y_Q = n_Q/n_B$, necessary for appropriately modeling an hot neutron star (as well as a core-collapse supernova, or binary neutron star mergers), are either not compatible with some constraints from nuclear physics and/or with a neutron star maximum mass of $2M_\odot$ [69, 72], or consider only Λ-hyperons [74]. We will now introduce an EoS which takes into account the entire baryon octet, and yet, is well compatible with the presently existing constraints.

In our proto-neutron star model, we will fix Y_Q by the condition of β-equilibrium and assuming that neutrinos freely leave the system, i.e. a vanishing lepton number chemical potential

$$\mu_L = 0 \ . \tag{5.4}$$

Albeit muons might have a non-negligble influence on the EoS at the very center of the proto-neutron star [72], they will not be considered. This condition might not be very realistic, since in the early phases neutrinos are trapped. Assuming a fixed lepton fraction would therefore be more appropriate [58]. In part III of this thesis, we will discuss future projects for

implementing a neutrino transport equation in our model, and considering the corresponding evolution of the hadronic charge Y_Q inside the star, allowing for a more complete study of proto-neutron stars evolution.

5.1 Statistical model for inhomogeneous matter

At subsaturation densities and low temperatures, nucleonic matter is unstable with respect to variations in the particle densities and becomes inhomogeneous, i.e. nuclei or more generally nuclear clusters are formed. The critical temperature is of the order ~ 15 MeV just below saturation, and decreases to about 1 MeV at lower densities. Below a density of roughly $n_b \sim 10^{-4}\text{fm}^{-3}$, the cluster size is very small compared with its mean free path, such that matter can be described as a noninteracting gas of nuclei, nucleons and leptons in thermodynamic equilibrium. This approach is generally called "nuclear statistical equilibrium" (NSE). In the last years several models have been developed to go beyond a pure NSE and take into account the interaction of clusters and the surrounding medium at higher densities [78, 80, 81, 83]. In stellar matter, particular attention has to be paid to the interplay between the short-range nuclear interaction and the long-range Coulomb interaction, which determines sizes and shapes of the nuclear clusters, and thus influences strongly the transition to homogeneous matter [78].

In the present EoS, clustered matter is described within the extended NSE model of Hempel & Schaffner-Bielich [80]. Nuclei are treated as classical Maxwell-Boltzmann particles. For the description of nucleons, we employ a RMF approach, similarly to the earlier mentioned Walecka model (for which we will give a detailed description in section 5.2), with the same parametrization as for the description of homogeneous matter. Several thousands of nuclei are considered, including light ones other than the α-particle. If available, nuclear binding energies are taken from experimental measurements [90]. In particular for neutron rich nuclei, where no measurement exists, they are complemented with values from theoretical nuclear structure calculations [91]. Several corrections are considered to describe the modifications of cluster properties in medium: screening of the Coulomb energies by the surrounding gas of electrons, excited states, and excluded-volume effects.

5.2 Relativistic mean field model for homogeneous matter

RMF is a field theoretical description of hadrons interactions, suitable for a self-consistent description of nucleons at supra-nuclear densities. As mentioned before, Homogeneous matter will be described within a phenomenological RMF. In short, the idea is that the interaction between baryons is mediated by meson fields, inspired by the meson exchange models of the nucleon-nucleon interaction. Notice that, RMF being an effective model, those are not necessarily existing mesons, but introduced on a phenomenological basis with their quantum numbers in different interaction channels. The coupling constants are adjusted to a chosen

set of nuclear observables. Earlier models introduced non-linear self-couplings of the meson fields in order to reproduce correctly nuclear matter saturation properties. More recently, density-dependent couplings between baryons and the meson fields have become widely used in the literature, existing many different parameterizations for such models (see [92], and references therein, for an insight on several different parameter sets). In our model, we will use density-dependent couplings.

The RMF Lagrangian density is given by

$$\begin{aligned}\mathscr{L} &= \sum_{j\in\mathcal{B}} \bar{\psi}_j \left(i\gamma_\mu\partial^\mu - m_j + g_{\sigma j}\sigma + g_{\sigma^* j}\sigma^* - g_{\omega j}\gamma_\mu\omega^\mu - g_{\phi j}\gamma_\mu\phi^\mu - g_{\rho j}\gamma_\mu\vec{\rho}^\mu\cdot\vec{I}_j \right)\psi_j \\ &+\frac{1}{2}(\partial_\mu\sigma\partial^\mu\sigma - m_\sigma^2\sigma^2) + \frac{1}{2}(\partial_\mu\sigma^*\partial^\mu\sigma^* - m_{\sigma^*}^2\sigma^{*2}) \\ &-\frac{1}{4}W^\dagger_{\mu\nu}W^{\mu\nu} - \frac{1}{4}P^\dagger_{\mu\nu}P^{\mu\nu} - \frac{1}{4}\vec{R}^\dagger_{\mu\nu}\cdot\vec{R}^{\mu\nu} \\ &+\frac{1}{2}m_\omega^2\omega_\mu\omega^\mu + \frac{1}{2}m_\phi^2\phi_\mu\phi^\mu + \frac{1}{2}m_\rho^2\vec{\rho}_\mu\cdot\vec{\rho}^\mu \,, \end{aligned} \tag{5.5}$$

where ψ_j stands for the Dirac field of baryon j (the sum include the baryons $B = n$, p, Λ, Σ, and Ξ, and their correspondent antiparticles), m_j is the bare mass of the baryon j, $\vec{I}_j$ is the isospin operator, and $W_{\mu\nu}, P_{\mu\nu}, \vec{R}_{\mu\nu}$ are the vector meson field tensors of the form

$$V^{\mu\nu} = \partial^\mu V^\nu - \partial^\nu V^\mu \,. \tag{5.6}$$

σ, σ^* are scalar-isoscalar meson fields, coupling to all baryons (σ) and to strange baryons (σ^*), respectively. Some models introduce an additional scalar-isovector coupling via a $\vec{\delta}$-meson, which we do not consider here. The first step to build an EoS from a field theory, is to obtain a partition function, by solving the path integral of the Lagrangian density over the baryon Dirac fields

$$\mathcal{Z} = \int \mathcal{D}\bar{\psi}_j\mathcal{D}\psi_j \exp\left[\int_0^\beta d\tau \int d^3x \mathscr{L}\right] \,, \tag{5.7}$$

with $\beta := 1/T$. This allows us to compute the grand-canonical thermodynamical potential Ω

$$\Omega = -T\ln\mathcal{Z} \,. \tag{5.8}$$

In the mean field approximation, the meson fields are replaced by their respective mean-field expectation values, which are given in uniform matter as

$$m_\sigma^2\bar{\sigma} + g_2\bar{\sigma}^2 + g_3\bar{\sigma}^3 = \sum_{i\in B} g_{\sigma i} n_i^s \tag{5.9}$$

$$m_{\sigma^*}^2\bar{\sigma}^* = \sum_{i\in B} g_{\sigma^* i} n_i^s \tag{5.10}$$

$$m_\omega^2\bar{\omega} + c_3\bar{\omega}^3 = \sum_{i\in B} g_{\omega i} n_i \tag{5.11}$$

$$m_\phi^2\bar{\phi} = \sum_{i\in B} g_{\phi i} n_i \tag{5.12}$$

$$m_\rho^2\bar{\rho} = \sum_{i\in B} g_{\rho i} t_{3i} n_i \,, \tag{5.13}$$

where $\bar{\rho} = \langle \rho_3^0 \rangle$, $\bar{\omega} = \langle \omega^0 \rangle$, $\bar{\phi} = \langle \phi^0 \rangle$, and t_{3i} represents the third component of isospin of baryon i with the convention that $t_{3p} = 1/2$. The scalar density of baryon i is given by

$$n_i^s = \langle \bar{\psi}_i \psi_i \rangle = \frac{1}{\pi^2} \int k^2 \frac{M_i^*}{\sqrt{k^2 + M^{*2}}} \{ f[\epsilon_i(k)] + \bar{f}[\epsilon_i(k)] \} dk \ , \tag{5.14}$$

and the number density by

$$n_i = \langle \bar{\psi}_i \gamma^0 \psi_i \rangle = \frac{1}{\pi^2} \int k^2 (f(\epsilon_i(k)) - \bar{f}(\epsilon_i(k))) dk \ . \tag{5.15}$$

f and $\bar{f}$ represent here the occupation numbers of the respective particle and antiparticle states with the single-particle energies, $\epsilon_i(k) = \sqrt{k^2 + M^{*2}}$, which reduce to a step function at zero temperature. The effective baryon mass M_i^* depends on the scalar mean fields as

$$M_i^* = M_i - g_{\sigma i} \bar{\sigma} - g_{\sigma^* i} \bar{\sigma}^* \ , \tag{5.16}$$

and the effective chemical potentials, $(\mu_i^*)^2 = (M_i^*)^2 + k_{Fi}^2$, are related to the chemical potentials via

$$\mu_i^* = \mu_i - g_{\omega i} \bar{\omega} - g_{\rho i} \, t_{3i} \bar{\rho} - g_{\phi i} \bar{\phi} - \Sigma_0^R \ . \tag{5.17}$$

The rearrangement term Σ_0^R is present in models with density-dependent couplings,

$$g_j(n_B) = g_j(n_0) h_i(x) \ , \quad x = n_B / n_0 \ , \tag{5.18}$$

to ensure thermodynamic consistency. It is given by

$$\begin{aligned} \Sigma_0^R \ = \ & \sum_{j \in B} \left(\frac{\partial g_{\omega j}}{\partial n_j} \bar{\omega} n_j + t_{3j} \frac{\partial g_{\rho j}}{\partial n_j} \bar{\rho} n_j + \frac{\partial g_{\phi j}}{\partial n_j} \bar{\phi} n_j \right. \\ & \left. - \frac{\partial g_{\sigma j}}{\partial n_j} \bar{\sigma} n_j^s - \frac{\partial g_{\sigma^* j}}{\partial n_j} \bar{\sigma}^* n_j^s \right) \ . \end{aligned} \tag{5.19}$$

The grand-canonical potential per unit volume of the hadronic phase therefore reads

$$\begin{aligned} \frac{\Omega}{V} = & \frac{1}{2} \left(m_\sigma^2 \sigma^2 - m_\omega^2 \omega_0^2 - m_\rho^2 \rho_{03}^2 - m_\phi^2 \phi_0^2 \right) - \Sigma_0^R \sum_i n_i \\ & - 2T \sum_i \int \frac{d^3k}{(2\pi)^3} \left[\ln \left(1 + e^{-\beta(\epsilon_i(k) - \mu_i^*)} \right) + \ln \left(1 + e^{-\beta(\epsilon_i(k) + \mu_i^*)} \right) \right] \ . \end{aligned} \tag{5.20}$$

And finally, the relevant quantities to build the energy-momentum tensor for the perfect fluid, i.e. pressure and energy density, can be derived from the grand-canonical potential, being $p = -\Omega/V$ and

$$\begin{aligned} \varepsilon \ = \ & \frac{1}{2} \left(m_\sigma^2 \sigma^2 + m_\omega^2 \omega_0^2 + m_\rho^2 \rho_{03}^2 + m_\phi^2 \phi_0^2 \right) \\ + \ & 2 \sum_i \int \frac{d^3k}{(2\pi)^3} \epsilon_i(k) \left(\frac{1}{e^{\beta(\epsilon_i(k) - \mu_i^*} + 1} + \frac{1}{e^{\beta(\epsilon_i(k) + \mu_i^*} + 1} \right) . \end{aligned} \tag{5.21}$$

In this thesis, we will consider the DD2 parameterization [81], where the following form for the density dependence of the isoscalar couplings is assumed [81],

$$h_i(x) = a_i \frac{1 + b_i(x + d_i)^2}{1 + c_i(x + d_i)^2} \tag{5.22}$$

and

$$h_i(x) = a_i \, \exp[-b_i(x - 1)] - c_i(x - d_i) \; . \tag{5.23}$$

for the isovector ones.

Similar to many recent works [93, 74, 94], for the hyperonic coupling constants, we will follow a symmetry inspired procedure. The individual isoscalar vector meson-baryon couplings are expressed in terms of $g_{\omega N}$ and a few additional parameters, $\alpha, \theta, z = g_1/g_8$ (see e.g. [37]), as follows

$$\begin{aligned}
\frac{g_{\omega\Lambda}}{g_{\omega N}} &= \frac{1 - \frac{2z}{\sqrt{3}}(1-\alpha)\tan\theta}{1 - \frac{z}{\sqrt{3}}(1-4\alpha)\tan\theta} \; , \; \frac{g_{\phi\Lambda}}{g_{\omega N}} = -\frac{\tan\theta + \frac{2z}{\sqrt{3}}(1-\alpha)}{1 - \frac{z}{\sqrt{3}}(1-4\alpha)\tan\theta} \; , \\
\frac{g_{\omega\Xi}}{g_{\omega N}} &= \frac{1 - \frac{z}{\sqrt{3}}(1+2\alpha)\tan\theta}{1 - \frac{z}{\sqrt{3}}(1-4\alpha)\tan\theta} \; , \; \frac{g_{\phi\Xi}}{g_{\omega N}} = -\frac{\tan\theta + \frac{z}{\sqrt{3}}(1+2\alpha)}{1 - \frac{z}{\sqrt{3}}(1-4\alpha)\tan\theta} \; , \\
\frac{g_{\omega\Sigma}}{g_{\omega N}} &= \frac{1 + \frac{2z}{\sqrt{3}}(1-\alpha)\tan\theta}{1 - \frac{z}{\sqrt{3}}(1-4\alpha)\tan\theta} \; , \; \frac{g_{\phi\Sigma}}{g_{\omega N}} = \frac{-\tan\theta + \frac{2z}{\sqrt{3}}(1-\alpha)}{1 - \frac{z}{\sqrt{3}}(1-4\alpha)\tan\theta} \; , \\
\frac{g_{\phi N}}{g_{\omega N}} &= -\frac{\tan\theta + \frac{z}{\sqrt{3}}(1-4\alpha)}{1 - \frac{z}{\sqrt{3}}(1-4\alpha)\tan\theta} \; .
\end{aligned} \tag{5.24}$$

Assuming an underlying $SU(6)$-symmetry, we will take $\tan\theta = 1/\sqrt{2}$, corresponding to ideal ω-ϕ-mixing, $\alpha = 1$, and $z = 1/\sqrt{6}$. Extending the above procedure to the isovector sector would lead to contradictions with the observed nuclear symmetry energy. $g_{\rho N}$ is therefore left as a free parameter and the remaining hyperonic isovector couplings are fixed by isospin symmetry.

The information from hypernuclear data on hyperonic single-particle mean field potentials is then used to constrain the scalar coupling constants. The potential for particle j in k-particle matter is given by

$$U_j^{(k)}(n_k) = M_j^* - M_j + \mu_j - \mu_j^* \; . \tag{5.25}$$

We will assume here standard values [93, 74] in symmetric nuclear matter at saturation density, n_0: $U_\Lambda^{(N)}(n_0) = -30$ MeV, $U_\Xi^{(N)}(n_0) = -18$ MeV, and $U_\Sigma^{(N)}(n_0) = +30$ MeV.

Apart from a few light double-Λ-hypernuclei, that constrain only the low density behavior, almost no information is available on the hyperon-hyperon (YY)-interaction and the corresponding couplings, in particular σ^* and ϕ, are only very poorly constrained. As mentioned above, we fix the ϕ-couplings via the relations in eqs. (5.24) and neglect σ^* for simplicity in the first version (I) of our EoS. Without the coupling to σ^*, the YY-interaction is very repulsive already at low densities. We obtain $U_\Lambda^{(\Lambda)}(n_0/5) = 7$MeV, $U_\Xi^{(\Xi)}(n_0/5) = 47$MeV, and $U_\Sigma^{(\Sigma)}(n_0/5) = 26$MeV, whereas the data on double-Λ-hypernuclei suggest a weakly attractive potential at least for Λ-hyperons, $U_\Lambda^{(\Lambda)}(n_0/5) \approx -1$MeV [95, 96]. Although, as

shown in [97, 99], the σ^* has only a weak influence on the EoS and proto-neutron star properties, we include a second version (II) of the EoS with a σ^*-coupling adjusted to have $U_\Lambda^{(\Lambda)}(n_0/5) = -0.4$MeV, $U_\Xi^{(\Xi)}(n_0/5) = -0.4$MeV, and $U_\Sigma^{(\Sigma)}(n_0/5) = -0.4$ MeV.

5.3 Compatibility with constraints

The interaction between nucleons can be constrained by data of finite nuclei and nuclear matter properties. The latter are chosen in general as the coefficients of a Taylor expansion of the energy per baryon of isospin symmetric nuclear matter around the saturation density. Values with a reasonable precision can be obtained for the saturation density (n_{sat}), binding energy (E_B), incompressibility (K), symmetry energy (J) and its slope (L). In addition, much effort has been recently devoted to theoretical ab initio calculations of pure neutron matter in order to constrain the equation of state. This quantity is particularly interesting for the EoS of compact stars, completing the information about symmetric matter. The only constraint on the interactions at super-saturation density, arises from the recent observation of two massive neutron stars, indicating the the maximum mass of a cold, spherically symmetric neutrons stars should be above $2M_\odot$. A summary and discussion of all available constraints can be found in [99].

The present parameterization, DD2, has been chosen since it agrees well with most of the established constraints. The values for $n_{sat} = 0.149\,\mathrm{fm}^{-3}$, $E_B = 16.0$ MeV and $K = 243$ MeV are within standard ranges [99]. The compatibility of J and L with ranges derived in [100] (light grey rectangle) and [99] (dark grey rectangle), respectively, are shown in figure 5.1. For comparison we show the values for two other interactions, that of the Lattimer and Swesty EoS (LS) [101] and that for TM1, too. These two interactions have been employed in other recently developed general purpose EoS including non-nucleonic degrees of freedom, e.g. [69, 102, 72].

In figure 5.2, we show pressure and energy per baryon for pure neutron matter below saturation density. The green band represents the results from the ab initio calculations from [104], including an estimate of the corresponding uncertainties. In contrast to LS and TM1, the interaction DD2 employed here is in reasonable agreement with the ab initio calculations.

In figure 5.3, we show mass-radius relations of cold spherically symmetric neutron stars within different general purpose EoS models. Purely nucleonic versions are shown as plain lines and models including hyperons as dashed or dotted lines. The latter are the extension of the LS EoS with Λ-hyperons ("LS220Λ") [108], the extension of the EoS by Shen et al. ("STOS") employing the TM1 interaction [112] with Λ-hyperons ("STOSΛ") [102] and all hyperons ("STOSY") [69], and the two models including Λ-hyperons within the same nuclear model as the present one from Ref. [74], ("BHBΛ") and ("BHBΛΦ"). It is evident from the figure that there are only two EoS including hyperons compatible with the $2M_\odot$-constraint: BHBΛΦ containing only Λ-hyperons and the present DD2Y(I). The two models are the same, except for the particle content. The additional hyperonic degrees of freedom in DD2Y(I) slightly reduce the maximum mass with respct to BHBΛΦ, but it remains above $2M_\odot$. The additional attractive YY-interaction in DD2Y(II) reduces the maximum mass to 1.87 $M_\odot$, thus below the observational limit. A summary of cold neutron star properties for

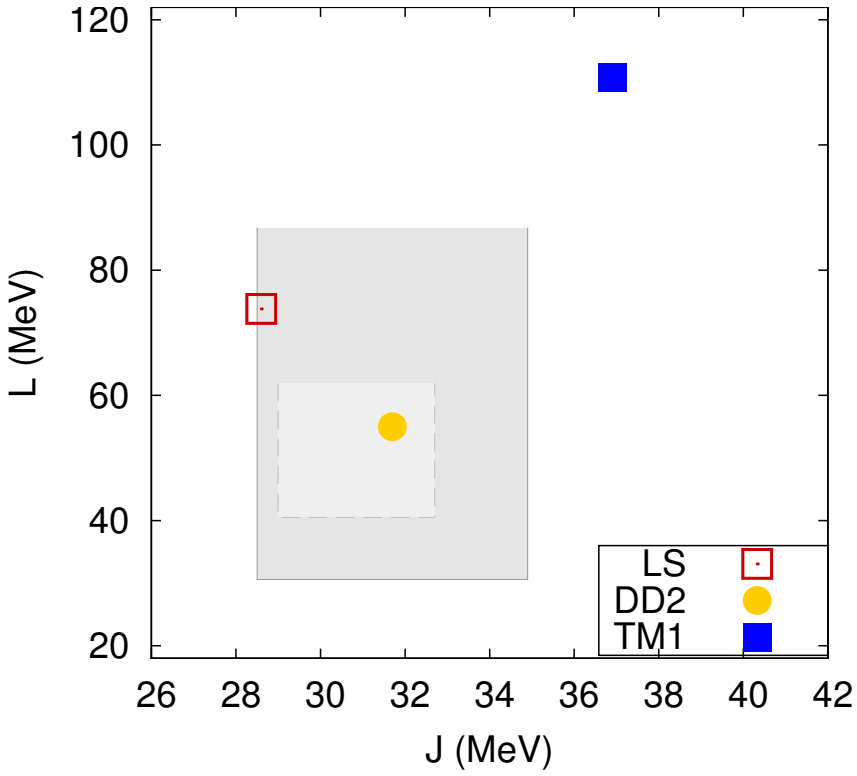

Figure 5.1: Values of J and L in different nuclear interaction models. The two grey rectangles correspond to the range for J and L derived in Ref. [100] (light grey) and Ref. [99] (dark grey) from nuclear physics experiments.

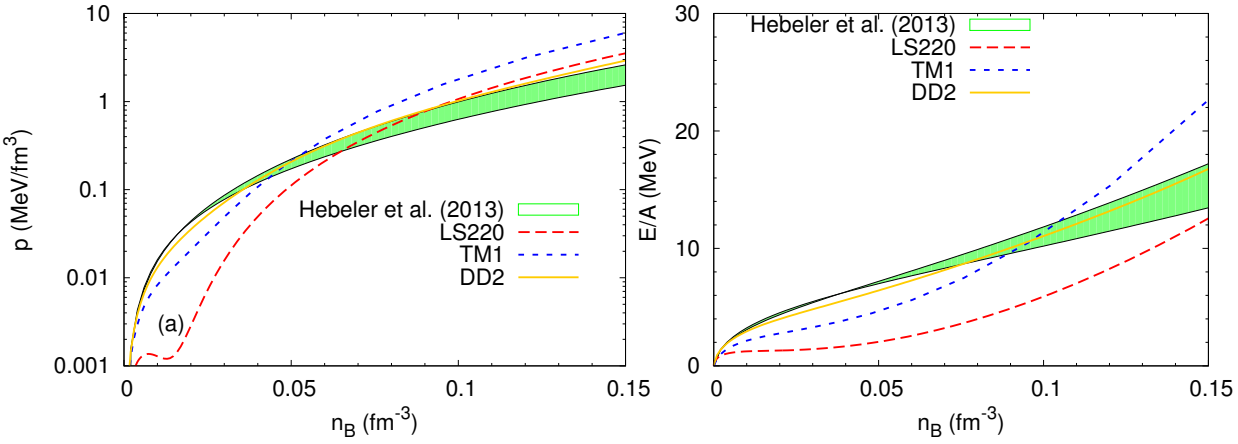

Figure 5.2: Pressure (left panel) and energy per baryon (right panel of pure neutron matter as function of baryon number density within different nuclear interaction models compared with the ab initio calculations of Ref. [104], indicated by the green band.

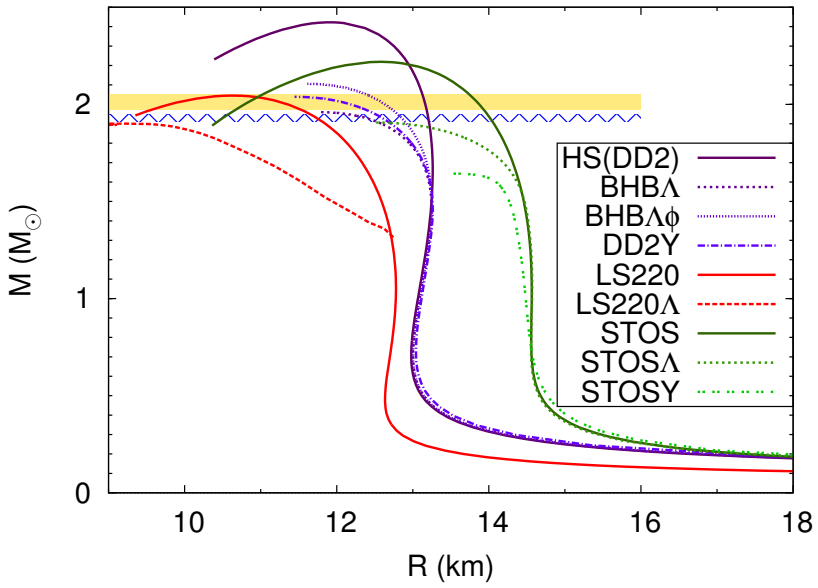

Figure 5.3: Gravitational mass versus circumferential radius for a cold spherically symmetric neutron stars within different EoS models. The two horizontal bars indicate the two recent precise NS mass determinations, PSRJ1614-2230 [105] (hatched blue) and PSR J0348+0432 [107] (yellow).

the different EoS is given in table 5.1.

As already mentioned in [99], the overall hyperon content within the EoS remains similar between the models containing only Λ-hyperons and the corresponding ones with the full baryonic octet. For cold NSs, this can be seen from table 5.1. In figure 5.4, the regions where the overall hyperon fraction exceeds 10^{-4} are compared for BHBΛ and DD2Y(I). Again, although as expected hyperons are slightly more abundant in the full model, the shape of the regions remains the same and only small quantitative differences are observed. The bump in the curves arises from the competition between light nuclear clusters and hyperons in this particular temperature and density domain and does not exist in EoS build on nuclear models without light clusters [99].

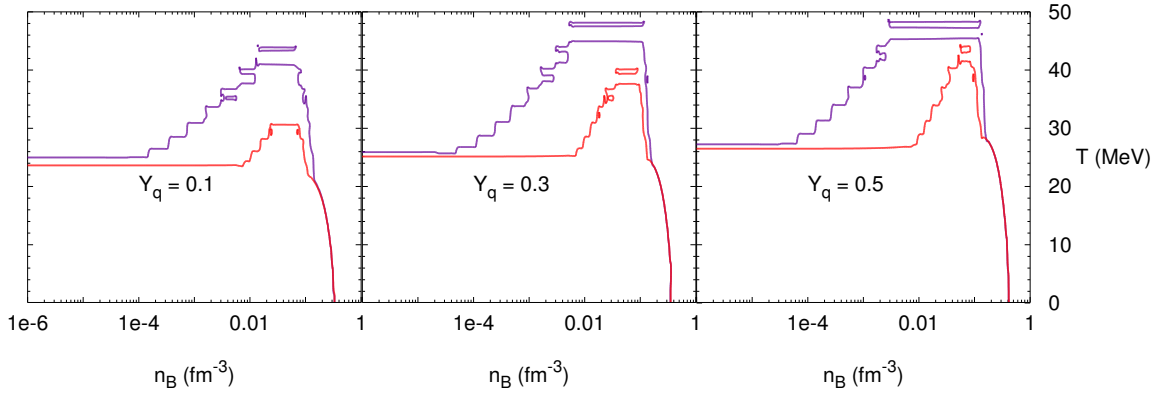

Figure 5.4: The lines delimit the regions in temperature and baryon number density for which the overall hyperon fraction exceeds 10^{-4}, which are situated above the lines. The dark purple line corresponds to the BHBΛ model and light red line to the DD2Y(I) model. Different charge fractions are shown as indicated within the panels.

Model	M_{max} $[M_\odot]$	$R_{1.4}$ [km]	f_S	$n_B^{(c)}$ [fm^{-3}]
HS(DD2)	2.42	13.2	-	0.84
BHBΛ	1.96	13.2	0.05	0.95
BHB$\Lambda\Phi$	2.11	13.2	0.05	0.95
DD2Y(I)	2.04	13.2	0.04	0.99

Table 5.1: Properties of spherically symmetric neutron stars in β-equilibrium at zero temperature: Maximum mass, radius at a fiducial mass of $M = 1.4M_\odot$, the total strangeness fraction, f_S, representing the integral of the strangeness fraction $Y_s/3$ over the whole star as in [93], and the central baryon number density. In addition to the EoS presented here, for comparison the values for the purely nucleonic version HS(DD2) and the two version including Λ-hyperons are listed.

Chapter 6

A Proto-Neutron Star Model

In the previous chapter, we have introduced a new EoS, with an appropriate microphysical description of relativistic matter at finite temperature, suitable for supernova simulations, binary compact mergers simulations, and proto-neutron stars modeling. To conclude this thesis, we will now explore the viability of the code introduced in chapter 4 when using a realistic EoS, by applying the EoS introduced in chapter 5. We compare three different β-equilibrated models: a purely nucleonic one HS(DD2), a model containing only Λ-hyperons BHB$\Lambda\Phi$, and finally the version with all hyperonic degrees of freedom DD2Y(I). We will use the s_b profiles s_0 (constant), and s_2 (4.18) (gaussian curve), introduced earlier in chapter 4. We do not present results for the s_1 entropy per baryon profile, as it leads to star models with a central temperatures of the order of $\sim 10^{-3}\, MeV$, which would not be realistic at all for our purposes of modeling stationary proto-neutron stars. Unless for the mass-radius profiles, all the solutions we will present in this section take the central log-enthalpy to be $H_c = 0.3$.

6.1 Rigid rotation

Let us start our analysis by exploring results for rigidly rotating stars. We show in figures 6.1,6.2 and 6.3, isocontour lines for the log-enthalpy field of stars rotating at Kepler frequency, with the constant profile s_0, respectively for HS(DD2), BHB$\Lambda\phi$ and DD2Y(I), and in figures 6.4, 6.5 and 6.6, the correspondent plots for the log-enthalpy and entropy per baryon fields, for the fastest rotation achieved (already in Kepler frequency for the HS(DD2) and BHB$\Lambda\phi$) with the non-constant profile s_2, employing the approximation earlier described in chapter 4. Finally we show in figures 6.7, 6.8 and 6.9 the profiles for the maximum rotation for which we were able to obtain a solution without imposing any approximations. The global quantities for all this plots are presented in table 6.1. As compared to the case of the analytical EoS for the ideal gas, used to test the code in chapter 4, with a tabulated EoS, the code is more limited in its ability to find solutions for stars with non-constant s_b profiles without requiring approximations on the equations of hydrostatic equilibrium. In particular, the maximum spinning frequency for which we found solutions without implementing any approximation

		$f_{rot}\,[Hz]$	$M_g\,[M_\odot]$	$T_c\,[MeV]$	$R_{eq}\,[Km]$	r_p/r_{eq}	$GRV2$	$GRV3$
s_0	HS(DD2)	908	2.27	53.87	20.56	0.59	$1.86e^{-3}$	$1.52e^{-3}$
	BHB$\Lambda\phi$	913.63	2.11	47.35	20.30	0.58	$2.31e^{-4}$	$-1.95e^{-4}$
	DD2Y(I)	916.3	1.99	40.71	19.59	0.60	$4.34e^{-3}$	$1.68e^{-3}$
$s_{2\,apprx}$	HS(DD2)	933	2.29	53.91	20.37	0.58	$1.08e^{-3}$	$-6.54e^{-4}$
	BHB$\Lambda\phi$	945.5	2.12	47.43	19.92	0.57	$1.36e^{-3}$	$-7.99e^{-4}$
	DD2Y(I)	936	2.00	40.70	18.98	0.60	$7.74e^{-4}$	$-4.86e^{-4}$
s_2	HS(DD2)	620	2.03	54.05	16.19	0.85	$1.52e^{-3}$	$8.58e^{-4}$
	BHB$\Lambda\phi$	650	1.91	47.28	15.71	0.85	$-7.19e^{-5}$	$-2.01e^{-4}$
	DD2Y(I)	310	1.73	40.61	14.53	0.96	$7.48e^{-4}$	$-8.41e^{-4}$

Table 6.1: Star configurations for the different s_b profiles. The subscript *apprx* stand for approximate solutions, meaning that we implement the approximation described in chapter 4. f_{rot} stand for the rotating frequency, M_g stand for the Komar mass, T_c is the central temperature, R_{eq} is the equatorial circular radius, r_p/r_{eq} is the flatness (the ratio between the polar and equatorial coordinate radius), and ($GRV2$, $GRV3$) are the virial identities.

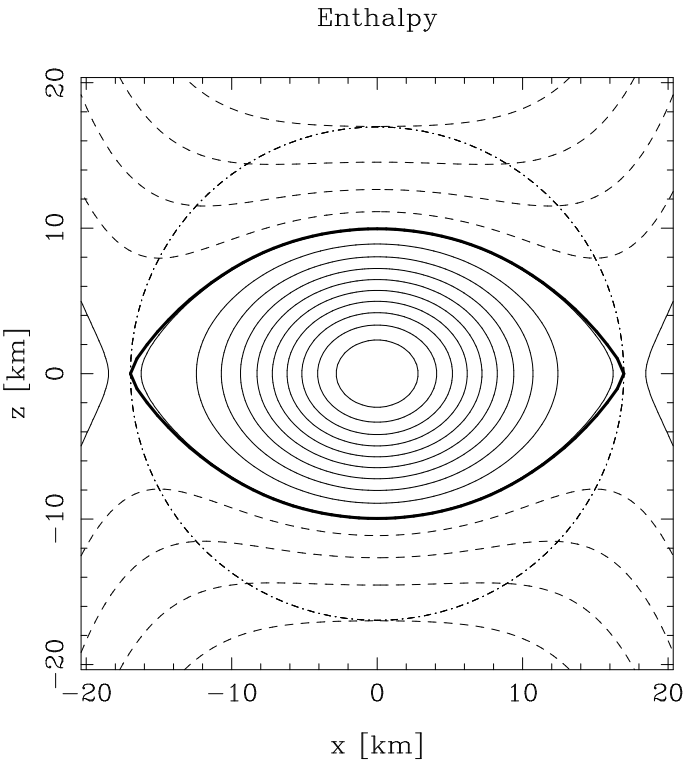

Figure 6.1: Isocontour enthalpy lines for the HS(DD2) EoS, using s_0 profile ($f_{rot} = 908\,Hz$)

was (as a percentage of the frequency of the maximum rotation achieved) of only 33% for the DD2Y(I) EoS, increasing by a factor of two for the the BHB$\Lambda\phi$ and HS(DD2) EoS, achieving 66%. It seems to be the case that increasing the amount of degrees of freedom on an EoS, makes it more difficult to be managed by our code in its present state. Of course, for the

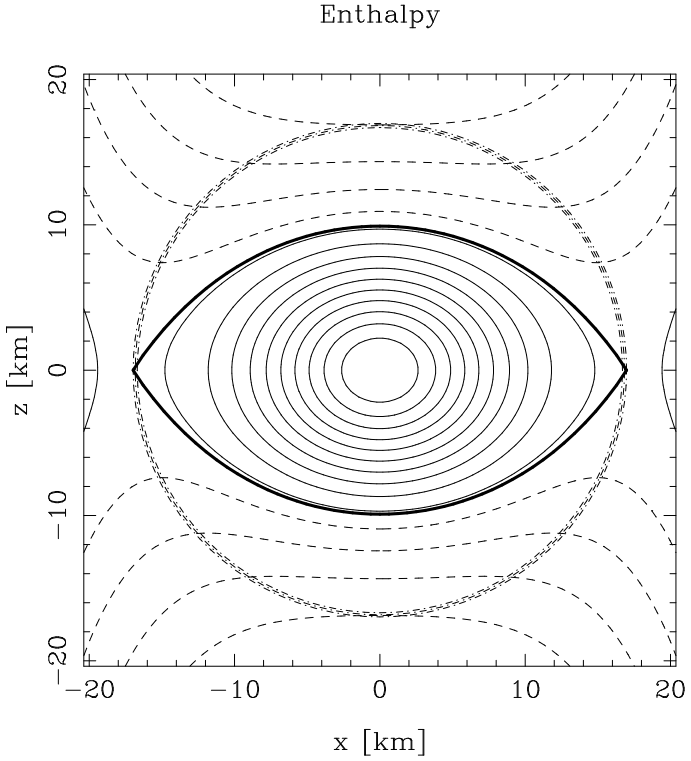

Figure 6.2: Isocontour enthalpy lines for the BHB$\Lambda\phi$ EoS, using s_0 profile ($f_{rot} = 913.63\,Hz$)

case of a tabulated EoS, the virial identities are in general larger than what we found for the analytical EoS. This is because the tabulated EoS was computed numerically, therefore, the numerical error from the computation and the interpolation of the EoS propagates through the code numerical error.

6.1.1 Mass Radius Relations

Let us now explore the mass-radius curves for the three equations of state. Here, we will show the impact of the different s_b profiles, as well as different rotation frequencies. We show in figures 6.10, 6.11 and 6.12, the mass-radius curves for stars rotating at different velocities, using both s_b profiles, respectively for the EoS HS(DD2), BHB$\Lambda\phi$, and DD2Y(I). Unlike the behavior observed in figure 4.7 for the ideal gas EoS, for a realistic EoS, the impact of using different s_b profiles is not nearly as dramatic. We can observe that regardless of the amount of degrees of freedom we include in the EoS, in the region close to the proto-neutron star's maximum mass, where the star's compactness is larger, the two chosen s_b profiles nearly coincide. It is in the region of where the star's compactness is smaller, with larger radii, that we observe the constant s_b profile, which models a star with a larger entropy profile, and therefore more internal energy, leading to larger masses. This is perhaps not too surprising: in the region of larger compactness, the star's radius is smaller, therefore, the difference between the two s_b profiles is not as big as for stars with larger radii (as can be seen in figure 4.1). As for the effect of rotation, like it was to be expected, the larger the spinning

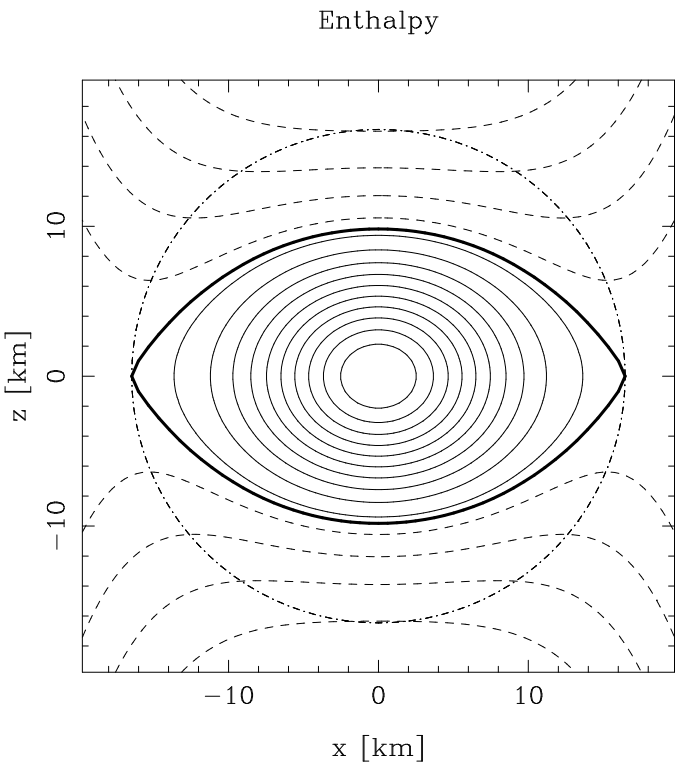

Figure 6.3: Isocontour enthalpy lines for the DD2Y(I) EoS, using s_0 profile ($f_{rot} = 916.3\,Hz$)

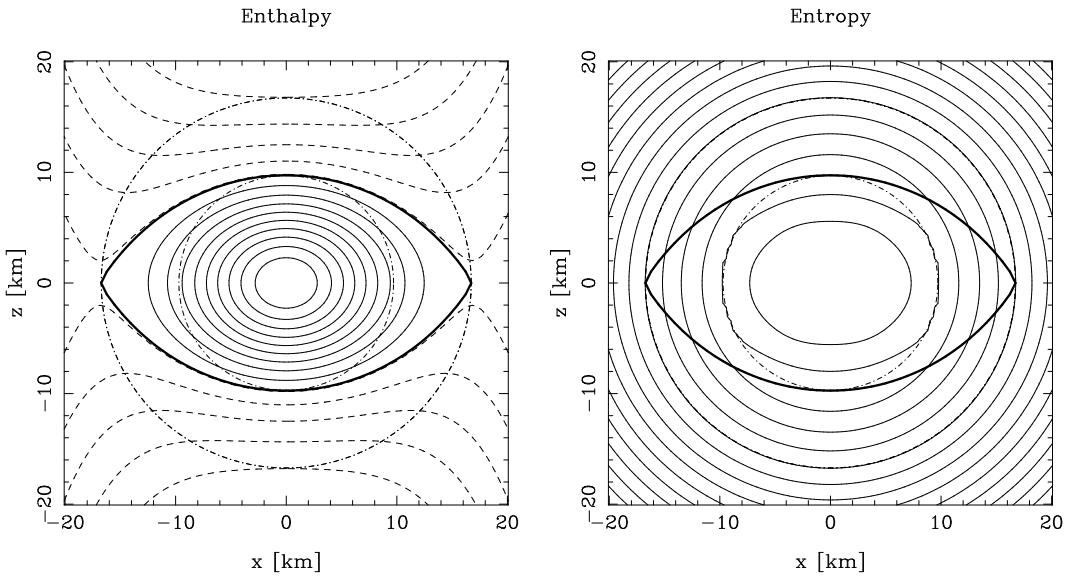

Figure 6.4: Isocontour lines of log-enthalpy and entropy per baryon for a rapidly rotating star with the s_2 profile, for the HS(DD2) EoS ($f_{rot} = 933\,Hz$)

frequency, the larger the star's kinetic energy, therefore the larger its maximum mass is. Let us now compare the mass-radius curves of the three EoS, fixing the spinning frequency. In figures 6.13, 6.14 and 6.15, we compare the mass-radius curves of the three EoS, using the two s_b profiles, for spinning frequencies of, respectively, 100 Hz, 600 Hz and 900 Hz.

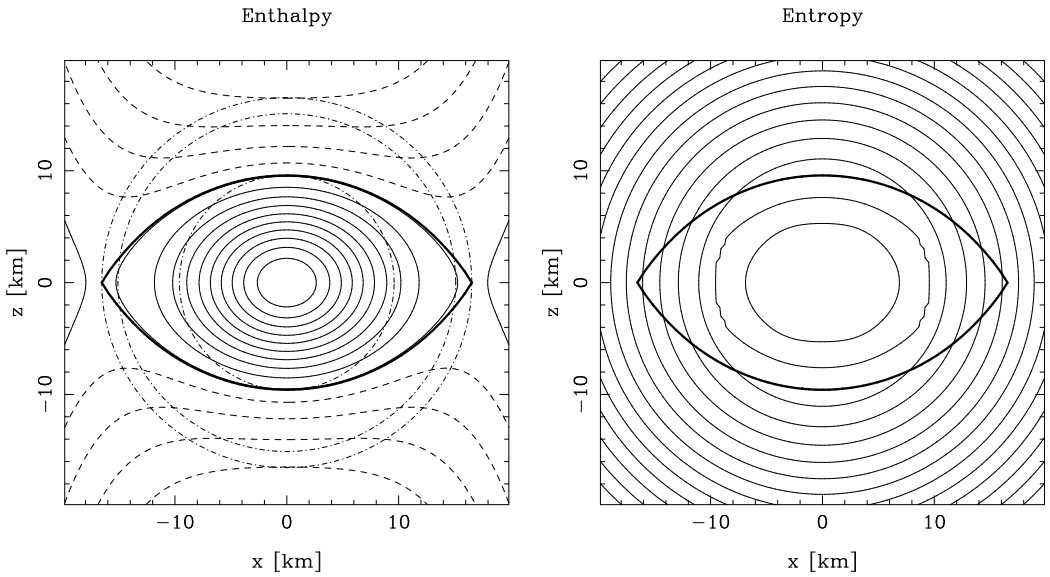

Figure 6.5: Isocontour lines of log-enthalpy and entropy per baryon for a rapidly rotating star with the s_2 profile, for the BHB$\Lambda\phi$ EoS ($f_{rot} = 945.5\,Hz$)

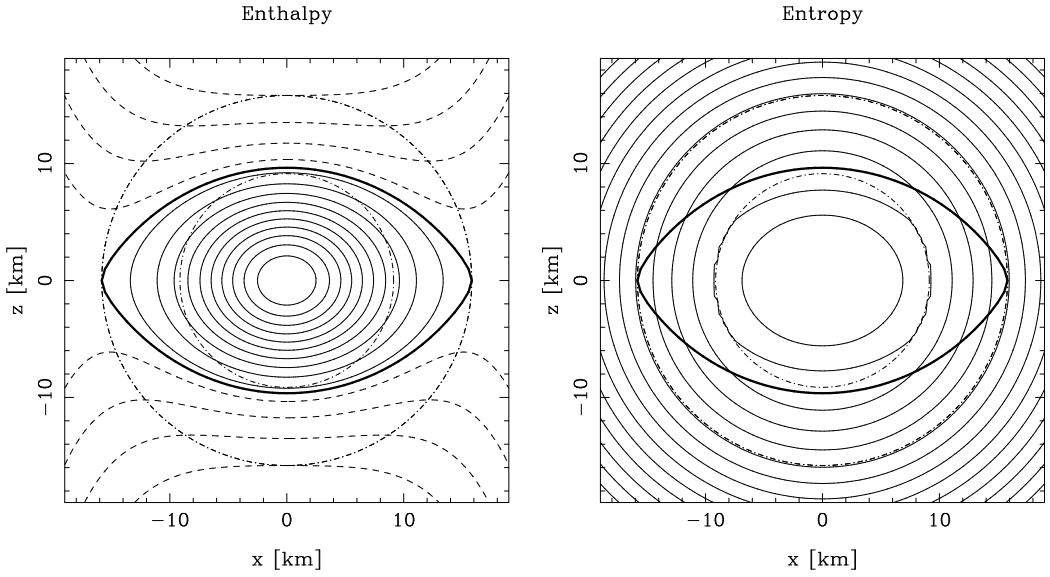

Figure 6.6: Isocontour lines of log-enthalpy and entropy per baryon for a rapidly rotating star with the s_2 profile, for the DD2Y(I) EoS ($f_{rot} = 936\,Hz$)

As we mentioned before, the presence hyperonic degrees of freedom soften the EoS. This can be very clearly observed in all three plots; the purely nucleonic EoS HS(DD2) leads to considerably larger maximum masses as compared to the hyperonic EoS, while the restriction of the hyperonic degrees of freedom to include only Λ hyperons, as in BHB$\Lambda\phi$, soften less the EoS then in the scenario in which all hyperonic degrees of freedom are included. For slowly rotating stars, in the smaller compactness region, the difference between the three EoS is less noticeable. In figure 6.13, fixing the spinning frequency at 100 Hz, one can observe that

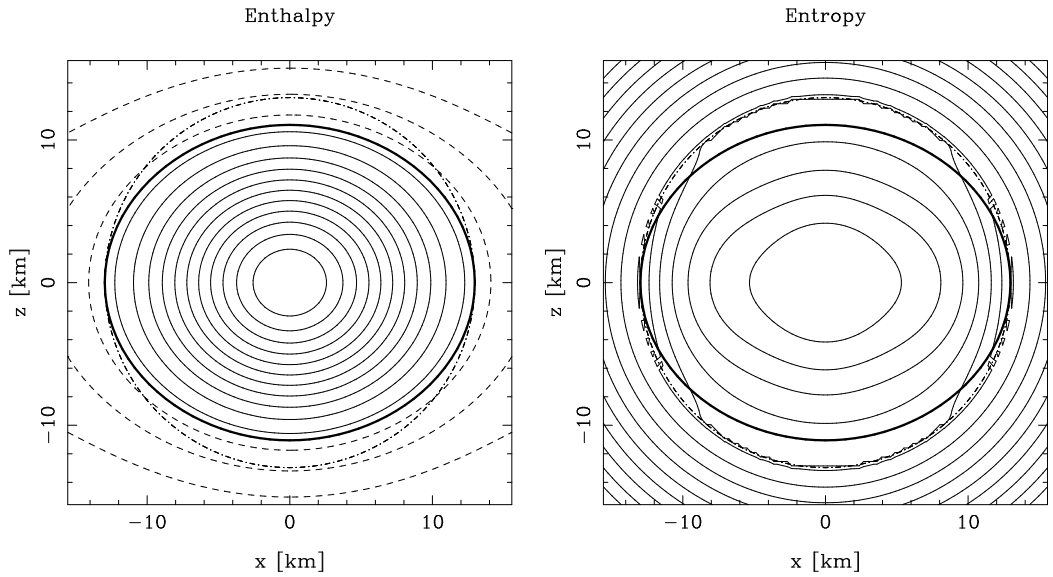

Figure 6.7: Isocontour lines of enthalpy and entropy for the fastest rotation up to which the code can provide a solution without approximations, using the s_2 profile, with the HS(DD2) EoS ($f_{rot} = 620\,Hz$)

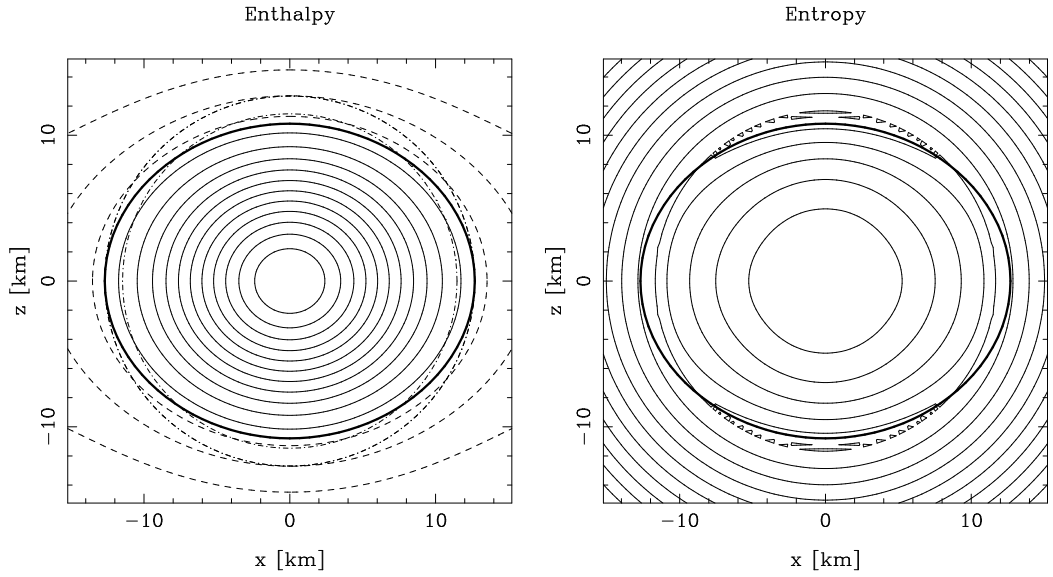

Figure 6.8: Isocontour lines of enthalpy and entropy for the fastest rotation up to which the code can provide a solution without approximations, using the s_2 profile, with the BHB$\Lambda\phi$ EoS ($f_{rot} = 650\,Hz$)

at lower masses, all EoS will nearly coincide, according to the chosen s_b profile. For star's with larger spinning frequency, because the mass generally increases across the mass-radius curve, the distinction among different EoS becomes more clear; as seen in figure 6.15, for the chosen s_b profiles, for star's rotating at 900 Hz, no point coincides across the mass-radius curves of different EoS. In table 6.2, we show the obtained maximum masses obtained for

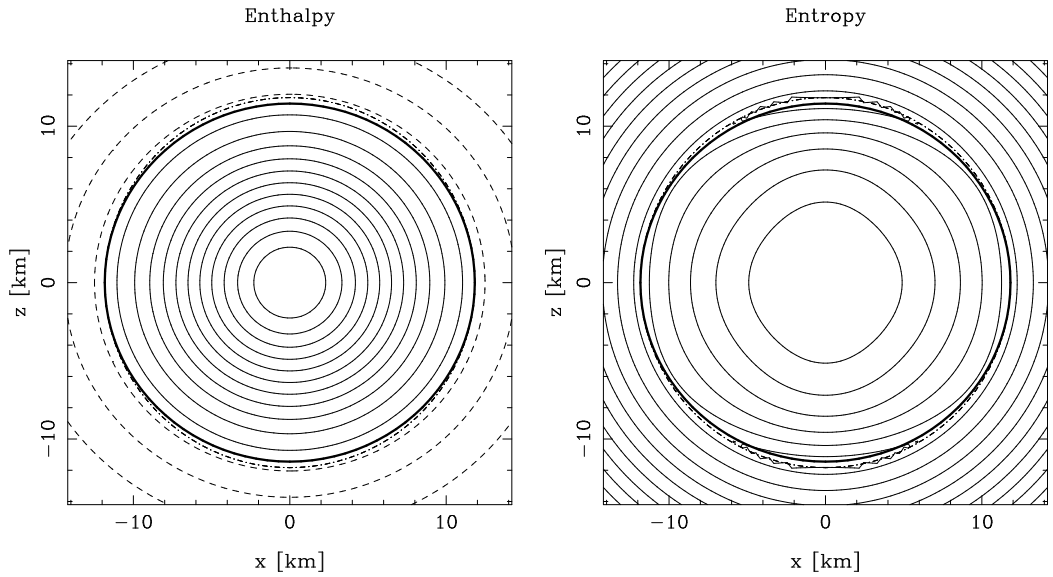

Figure 6.9: Isocontour lines of enthalpy and entropy for the fastest rotation up to which the code can provide a solution without approximations, using the s_2 profile, with the DD2Y(I) EoS ($f_{rot} = 310\,Hz$)

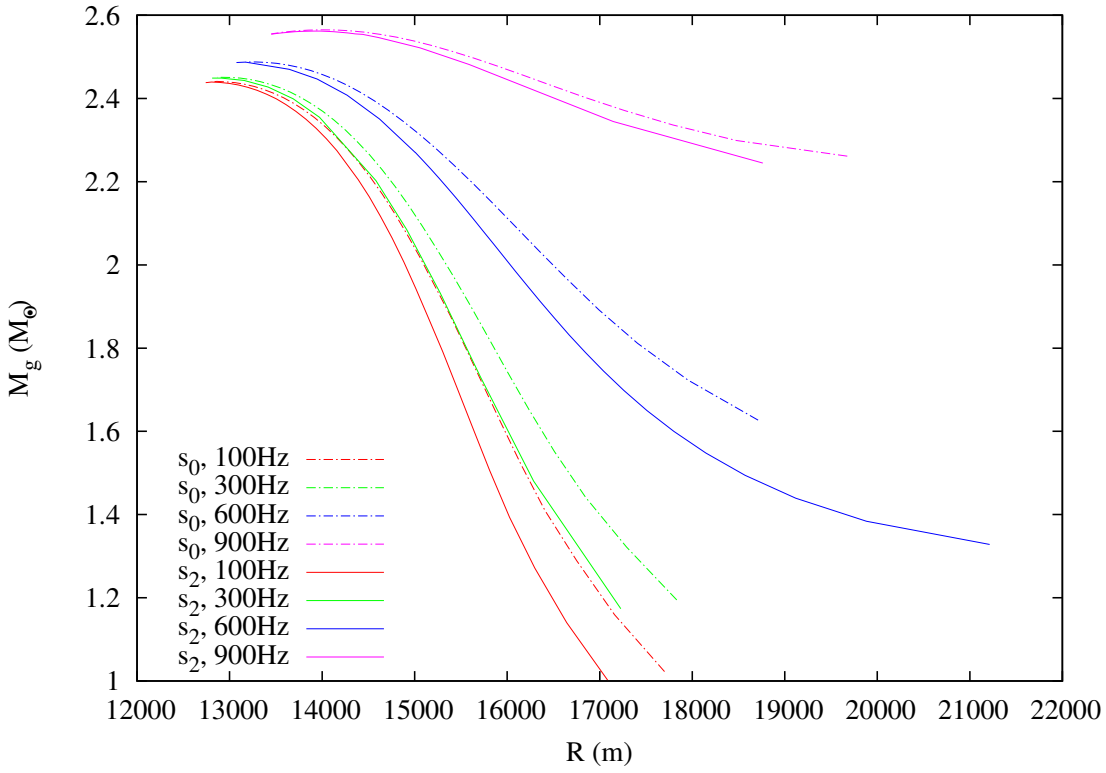

Figure 6.10: Mass-radius profiles for the HS(DD2) EoS

all the mass-radius curves presented in this section. As already mentioned, for the chosen s_b

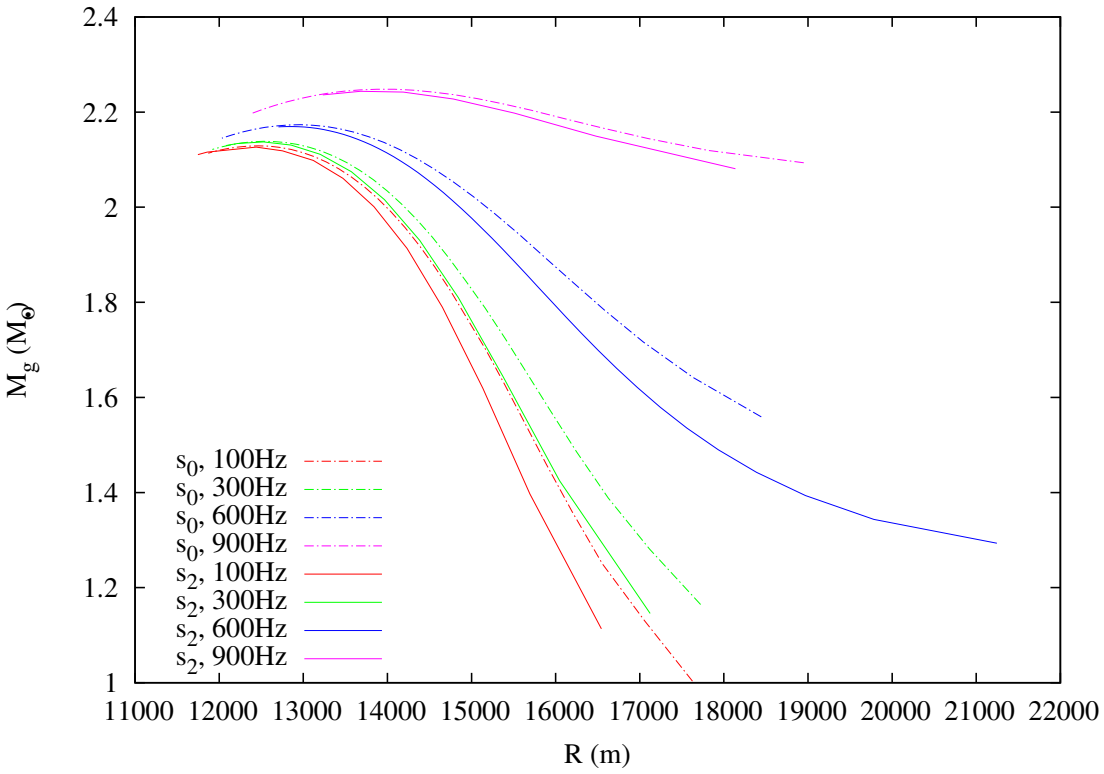

Figure 6.11: Mass-radius profiles for the BHB$\Lambda\phi$ EoS

profiles, the obtained maximum masses are nearly independent of the chosen s_b profile. One can also appreciate in table 6.2 the fact that, for the EoS and s_b profiles we are comparing, the increase in maximum mass with the kinetic energy of the star's rotation frequency is somewhat independent of presence of hyperonic degrees of freedom in the EoS. Once again, it is worth stating that the DD2Y(I) EoS (as well as the other two EoS used in this chapter), achieve maximum masses consistent with the mass of the heaviest pulsar yet observed, PSR J0348+0432, with $M = 2.01 \pm 0.04\, M_\odot$.

		100 Hz	300 Hz	600 Hz	900 Hz
HS(DD2)	s_0	2.44	2.45	2.49	2.57
	s_2	2.44	2.45	2.49	2.56
BHB$\Lambda\phi$	s_0	2.13	2.14	2.17	2.23
	s_2	2.13	2.13	2.17	2.24
DD2Y(I)	s_0	2.00	2.01	2.05	2.11
	s_2	2.00	2.01	2.04	2.11

Table 6.2: Maximum gravitational masses (in units of solar mass) for the three EoS, using two s_b profiles, at different velocities.

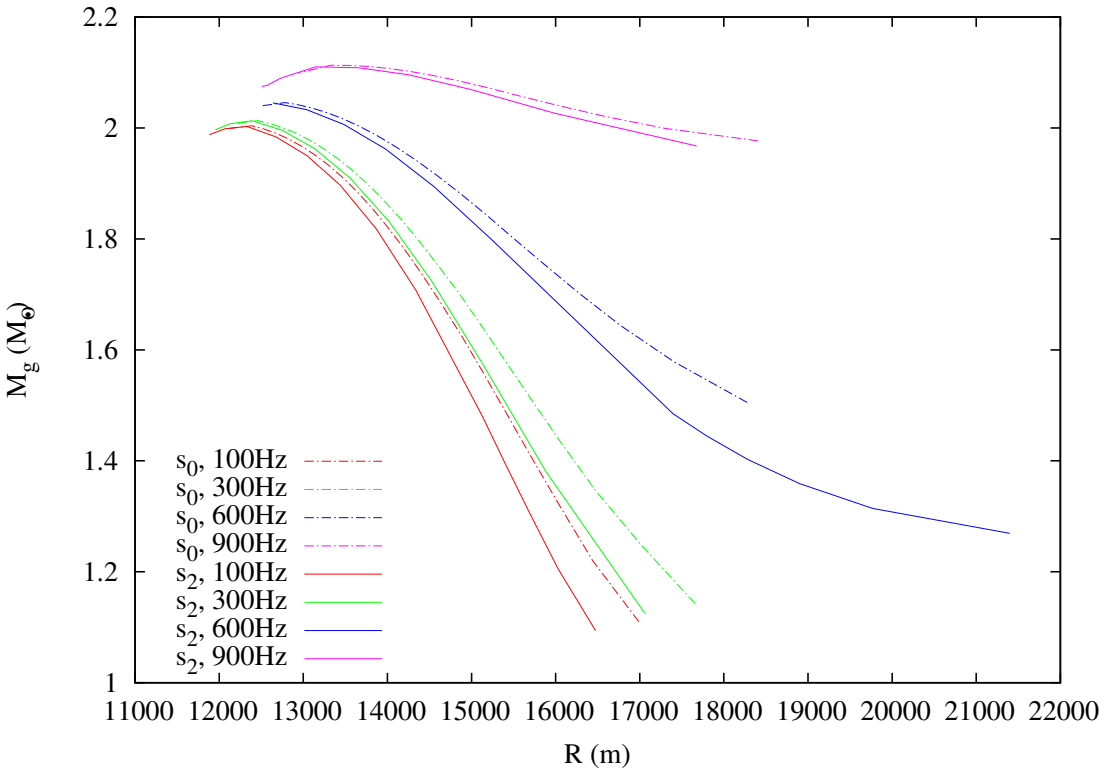

Figure 6.12: Mass-radius profiles for the DD2Y(I) EoS

6.2 Differential rotation

To conclude this chapter, we will explore some differentially rotating solutions, employing the same linear rotation law 4.19, described earlier in chapter 4. All solutions presented in this section have a central of the angular velocity $\Omega_c = 2\pi \times 1000\, rad/s$.

We show in figures 6.16,6.17 and 6.18, isocontour lines for the log-enthalpy field of differentially rotating stars with the constant profile s_0, respectively for HS(DD2) (with $a = 0.23$), BHB$\Lambda\phi$ (with $a = 0.24$) and DD2Y(I) (with $a = 0.25$). In figures 6.19 and 6.20, we show the corresponding plots for the log-enthalpy and entropy per baryon fields respectively for the EoS HS(DD2) and BHB$\Lambda\phi$, using the non-constant s_2 profile, all with the rotation parameter $a = 0.4$, and in figures 6.21 and 6.22, the same plots with the rotation parameter $a = 1$. Unfortunately, so far, when using the EoS DD2Y(I) with the non-constant s_2 profile, we have not been able to find a convergence for differentially rotating configurations with any considerable deviation from spherical symmetry (up to now, the largest flatness obtained was 0.97). All the solutions obtained for the non-constant s_b profile required an approximation of the hydrostatic equilibrium. We present the global quantities in table 6.3.

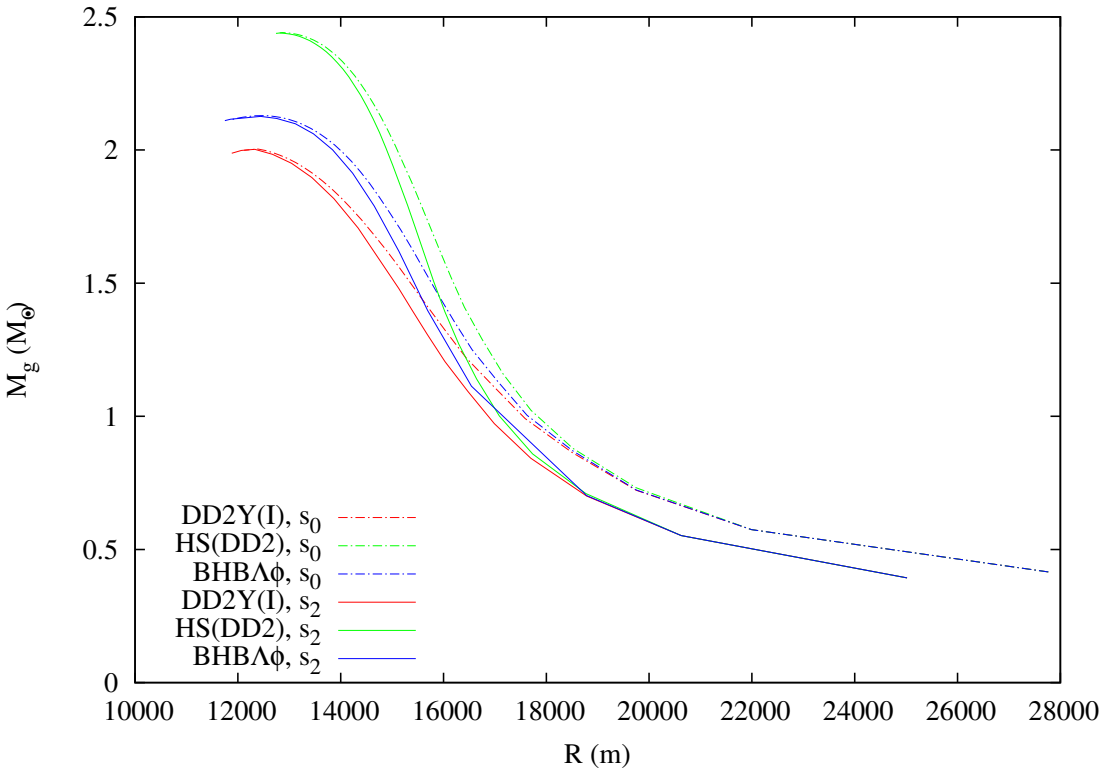

Figure 6.13: Mass-radius profiles for all EoS, rotating at 100 Hz

		a	$M_g\,[M_\odot]$	$T_c\,[MeV]$	$R_{eq}\,[Km]$	r_p/r_{eq}	$GRV2$	$GRV3$
s_0	HS(DD2)	0.23	2.34	53.87	20.52	0.57	$8.29e^{-6}$	$-2.72e^{-6}$
	BHB$\Lambda\phi$	0.24	2.16	47.35	19.69	0.59	$3.28e^{-5}$	$-4.08e^{-5}$
	DD2Y(I)	025	2.03	40.71	18.81	0.61	$4.34e^{-3}$	$1.68e^{-3}$
s_2	HS(DD2)	0.4	2.21	53.87	17.23	0.73	$7.92e^{-4}$	$-5.39e^{-4}$
		1	2.02	53.87	15.54	0.89	$1.82e^{-4}$	$-9.27e^{-5}$
	BHB$\Lambda\phi$	0.4	2.06	47.35	16.76	0.73	$6.89e^{-4}$	$-4.74e^{-4}$
		1	1.89	47.35	15.10	0.89	$8.15e^{-5}$	$-4.85e^{-5}$

Table 6.3: Global quantities of the obtained configurations of differentially rotating stars.

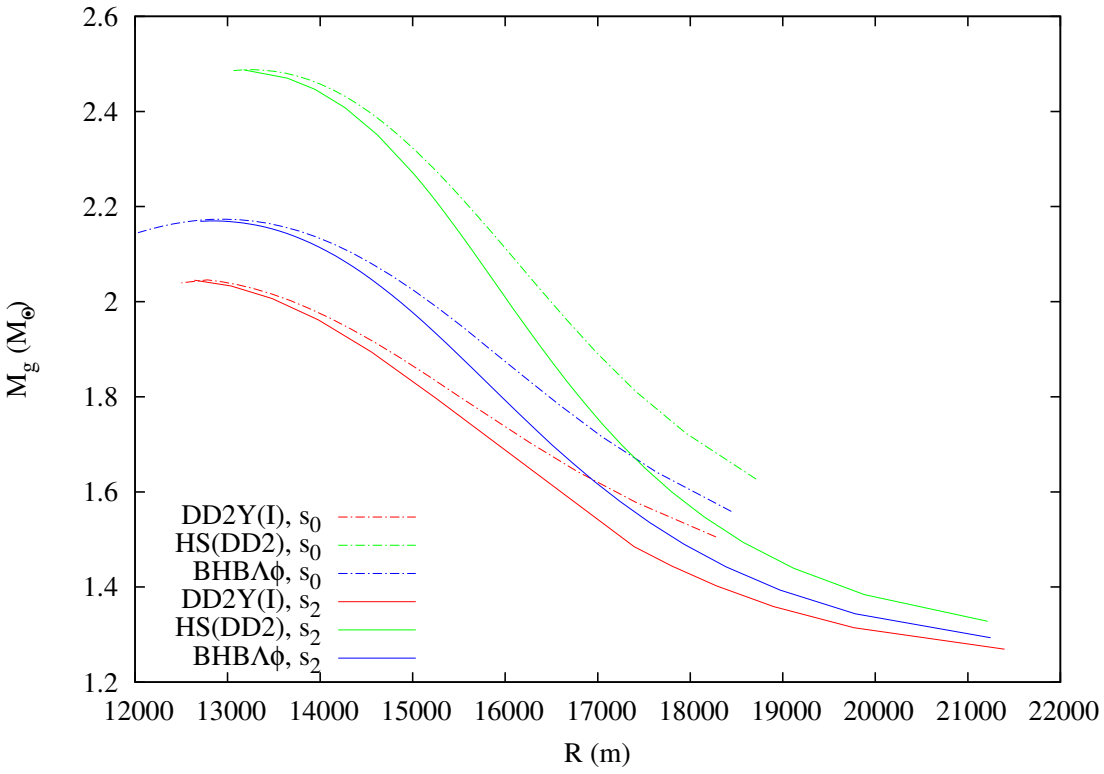

Figure 6.14: Mass-radius profiles for all EoS, rotating at 600 Hz

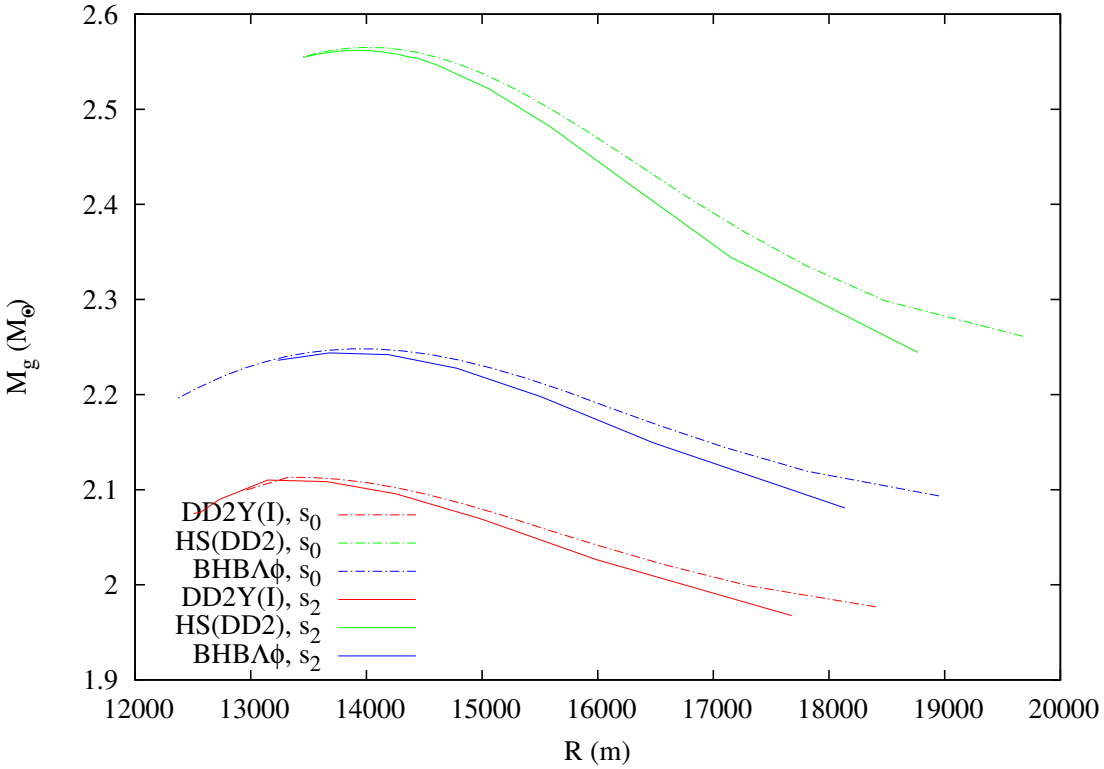

Figure 6.15: Mass-radius profiles for all EoS, rotating at 900 Hz

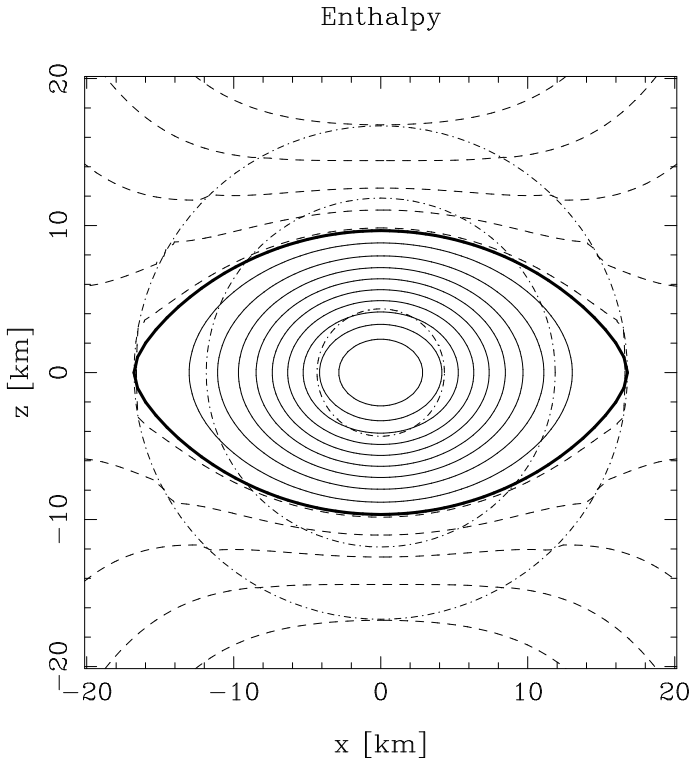

Figure 6.16: Isocontour enthalpy lines for the HS(DD2) EoS, using s_0 profile

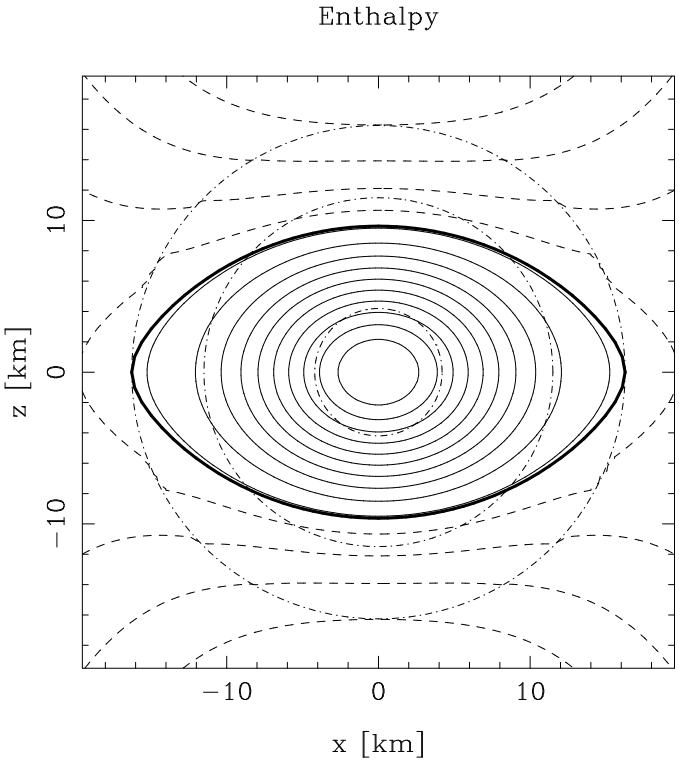

Figure 6.17: Isocontour enthalpy lines for the BHB$\Lambda\phi$ EoS, using s_0 profile

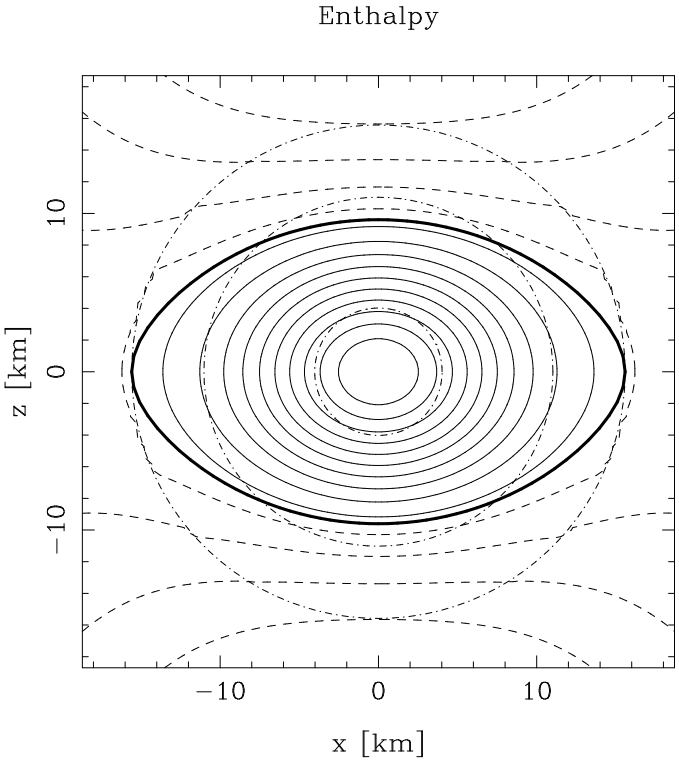

Figure 6.18: Isocontour enthalpy lines for the DD2Y(I) EoS, using s_0 profile

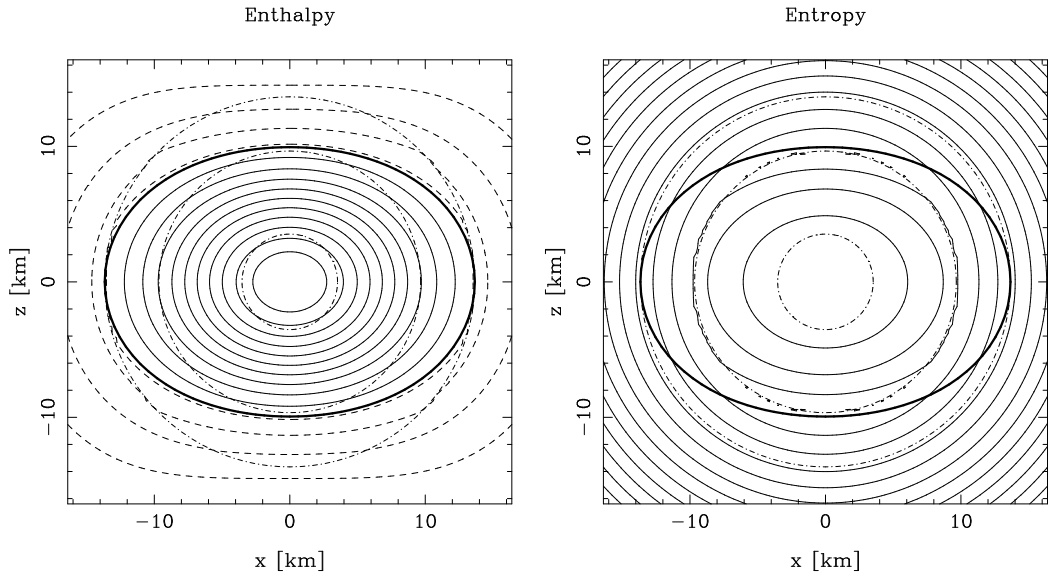

Figure 6.19: Isocontour lines of log-enthalpy and entropy per baryon for a differentially rotating star with the s_2 profile and $a = 0.4$, for the HS(DD2) EoS.

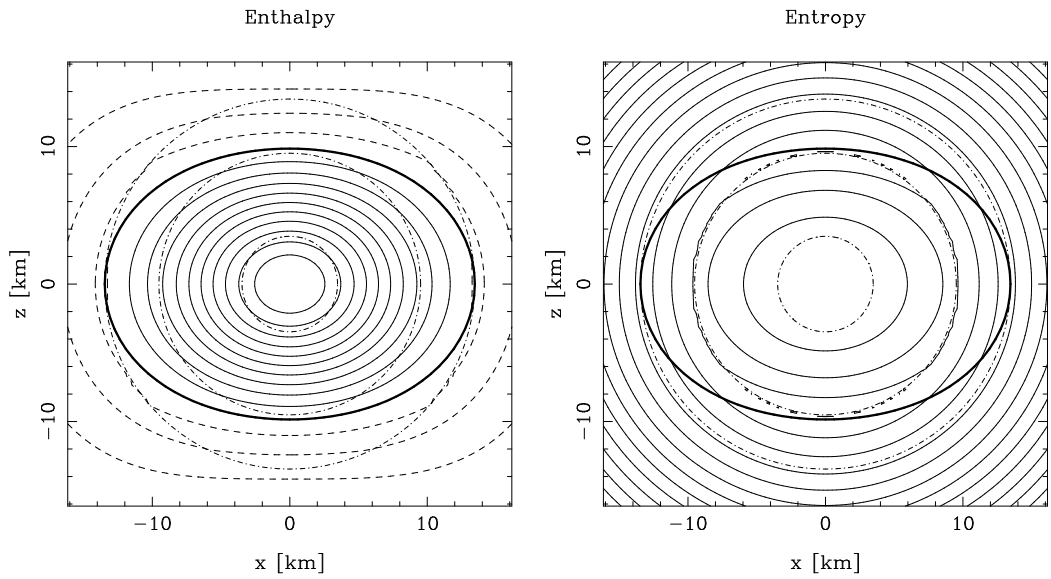

Figure 6.20: Isocontour lines of log-enthalpy and entropy per baryon for a differentially rotating star with the s_2 profile and $a = 0.4$, for the BHB$\Lambda\phi$ EoS.

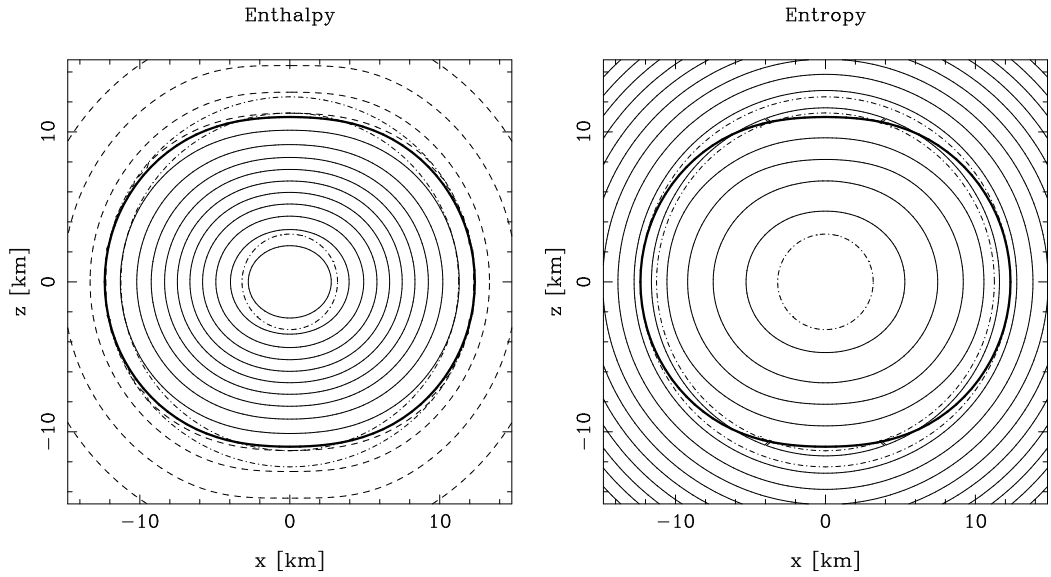

Figure 6.21: Isocontour lines of enthalpy and entropy for a differentially rotating star with the s_2 profile and $a = 0.1$, with the HS(DD2) EoS.

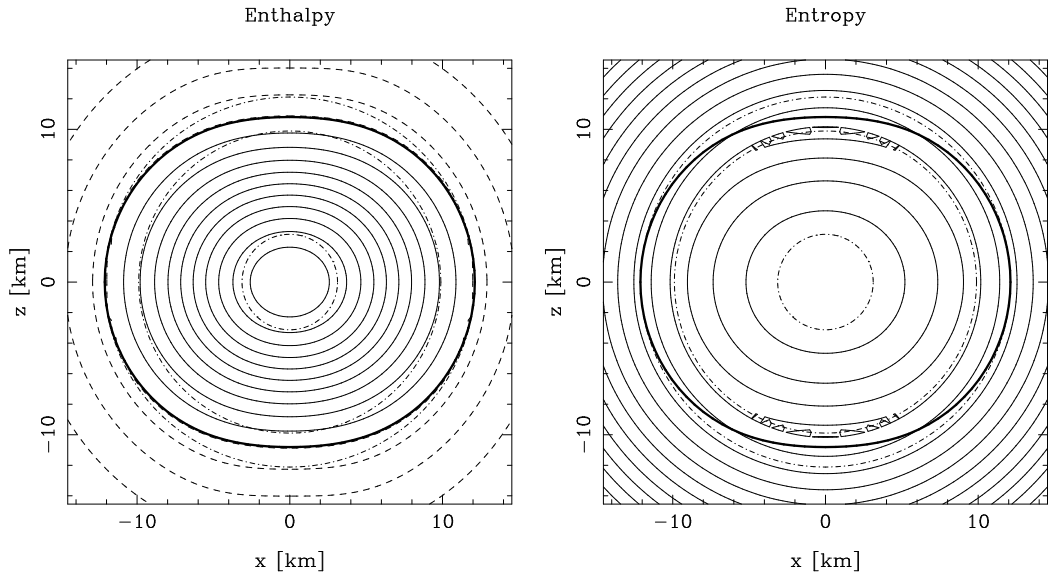

Figure 6.22: Isocontour lines of enthalpy and entropy for a differentially rotating star with the s_2 profile and $a = 0.1$, with the BHB$\Lambda\phi$ EoS.

Part III

Conclusions and Future Work

Simulating the evolution of a proto-neutron star is a challenging task. As of today, a multi-dimensional hydrodynamical model following the first minutes of evolution a proto-neutron star is yet unattainable. The fact that after seconds of strong hydrodynamical instabilities, the proto-neutron star enter in a Kelvin-Helmholtz phase, allow us to explore the possibility of studying its evolution as a series of stationary equilibrium configurations. While such studies are not new in the literature, with the motivation to develop such quasi-stationary models of proto-neutron stars using a different approach, we have presented in this thesis a new self-consistent scheme to compute equilibrium configurations of generally rotating relativistic stars, able to deal with non-barotropic EoS. The codes will be made publicly available in LORENE [15], an open source C++ spectral methods package for numerical relativity. We have explored the limitations of the code, both using a simple analytical EoS, and a set of three realistic EoS.

The behavior and composition of matter at the large densities and temperatures of a proto-neutron star, is still largely unknown, and is not easy to study, as it is not possible to reproduce such extreme conditions in earth based experiments. One needs therefore to use neutron stars observable quantities to transform them in laboratories to study hot and dense matter. One particular problem raised in the attempt do describe neutron star matter is the so called hyperon puzzle: while we expect the appearance of hyperonic degrees of freedom to be energetically favored in the conditions of the formation of a proto-neutron star, they soften the EoS, leading to a maximum neutron star mass lower than the heavier observed pulsars. In this thesis, we presented a new EoS, based on a phenomenological field theoretical model with a parametrization for which it is possible to include all existing hyperonic degrees of freedom respecting all the available constraints from experiments and observations. We used β-equilibrated versions of this new EoS to test the viability of our new codes using realistic equations of state, explored its results at different rotation frequencies and different, constant and non-constant, entropy per baryon profiles, and found the codes to provide the results that we would intuitively expect for rigidly rotating models, however, the code displayed stronger limitations when dealing with differentially rotating models.

In their present form, the codes have limitations in dealing with rapid rotation or strong differential rotation. The apparent reason for this to happen is related to the need to use spherical numerical grids in our numerical schemes: rapidly rotating stars, as well as strongly deformed differentially rotating stars, are axisymmetric objects which considerably deviate from spherical symmetry. To address these limitations, in future projects I wish to implement new versions of this code using adaptative numerical spectral grids, i.e. numerical domains which adapt to the star surface. I believe this could greatly improve the limits of convergence of these codes without requiring any approximations to the hydrostatic equilibrium equations. A self-consistent solution to the equilibrium of generally rotating hot neutron stars without any approximations to the equations solved, would definitely be an interesting tool both for the advances in the literature of evolutionary models of proto-neutron stars, as to the literature of finite temperature in relativistic stars by itself.

The recent detection of gravitational waves by LIGO have opened a new era in astronomy. They allowed for the first direct detection of a black hole; in fact, gravitational waves may carry information which we may not find in electromagnetic radiation. They may be a

valuable tool to develop the field of asteroseismology of neutron stars: born in catastrophic events, proto-neutron stars radiate gravitational waves due to their oscillations. By computing the spectrum of these oscillations, i.e. their frequencies and damping times, one can in principle know what information from the proto-neutron star composition can be learned and distinguished by observing their gravitational radiation. In future work, I plan to study the quasi-normal modes of proto-neutron stars, using solutions computed from the codes presented in this thesis, including therefore the effects of rapid and differential rotation.

In recent years, a lot of attention has been devoted to the discovered approximate no-hair relations found for relativistic stars: these are relations among multipole moments, such as the I-Q relations (among the moment of inertia and the quadrupole moment), which are approximately independent of the star's EoS. As mentioned in chapter 2, it was found for models of slowly rotating proto-neutron stars that the I-Q relations break-down in the presence of entropy gradients. Recently [111], different multipole moments relations have been found for slowly differentially rotating relativistic stars (where differential rotation was included as a small perturbation). In future work, I plan to use the codes developed during this thesis to explore the validity of the existing approximate no-hair relations in more general setups, and research the possible existence of other multipole momentum relations for stars at finite temperature, or alternatively research the physics behind the reason why these relations break-down when temperature is not negligible.

As mentioned in the beginning of this conclusions, the spirit of the project I undertook for my PhD studies, was to develop a tool to allow us to build a quasi-stationary model of a proto-neutron star. I surely plan to give continuation to this project. In future work, I plan to couple the developed codes to a two dimensional Boltzmann equation for neutrino transport, and use such code to study the physics of proto-neutron stars cooling.

Bibliography

[1] J. Goussard, P. Haensel, and J. Zdunik, "Rapid uniform rotation of protoneutron stars," *A&A*, vol. 321, pp. 822–834, 1997.

[2] J. Goussard, P. Haensel, and J. Zdunik, "Rapid differential rotation of protoneutron stars and constraints on radio pulsars periods," *A&A*, vol. 330, pp. 1005–1016, 1998.

[3] S. Bonazzola, E. Gourgoulhon, M. Salgado, and J. Marck, "Axisymmetric rotating relativistic bodies: a new numerical approach for "exact" solutions," *A&A*, vol. 278, pp. 421–443, 1993.

[4] D. R. Lorimer and M. Kramer, *Handbook of Pulsar Astronomy*. Oct. 2012.

[5] S. A. Colgate and R. H. White, "The Hydrodynamic Behavior of Supernovae Explosions," *ApJ*, vol. 143, p. 626, Mar. 1966.

[6] H.-T. Janka, K. Langanke, A. Marek, G. Martínez-Pinedo, and B. Müller, "Theory of core-collapse supernovae," *Phys. Rep.*, vol. 442, pp. 38–74, Apr. 2007.

[7] H.-T. Janka, "Conditions for shock revival by neutrino heating in core-collapse supernovae," *A&A*, vol. 368, pp. 527–560, Mar. 2001.

[8] X. Roca-Maza, J. Piekarewicz, T. Garcia-Galvez, and M. Centelles, "Influence of the nuclear symmetry energy on the structure and composition of the outer crust," *ArXiv e-prints*, Sept. 2011.

[9] J. M. Lattimer and M. Prakash, "Neutron star observations: Prognosis for equation of state constraints," *Phys. Rep.*, vol. 442, pp. 109–165, Apr. 2007.

[10] V. Ravi and P. D. Lasky, "The birth of black holes: neutron star collapse times, gamma-ray bursts and fast radio bursts," *MNRAS*, vol. 441, pp. 2433–2439, July 2014.

[11] T. Tsujimoto and T. Shigeyama, "Enrichment history of r-process elements shaped by a merger of neutron star pairs," *A&A*, vol. 565, p. L5, May 2014.

[12] J. M. Weisberg and J. H. Taylor, "The Relativistic Binary Pulsar B1913+16: Thirty Years of Observations and Analysis," in *Binary Radio Pulsars* (F. A. Rasio and I. H. Stairs, eds.), vol. 328 of *Astronomical Society of the Pacific Conference Series*, p. 25, July 2005.

[13] F. Ozel and P. Freire, "Masses, Radii, and Equation of State of Neutron Stars," *ArXiv e-prints*, Mar. 2016.

[14] J. Antoniadis, P. C. C. Freire, N. Wex, T. M. Tauris, R. S. Lynch, M. H. van Kerkwijk, M. Kramer, C. Bassa, V. S. Dhillon, T. Driebe, J. W. T. Hessels, V. M. Kaspi, V. I. Kondratiev, N. Langer, T. R. Marsh, M. A. McLaughlin, T. T. Pennucci, S. M. Ransom, I. H. Stairs, J. van Leeuwen, J. P. W. Verbiest, and D. G. Whelan, "A Massive Pulsar in a Compact Relativistic Binary," *Science*, vol. 340, p. 448, Apr. 2013.

[15] E. Gourgoulhon, P. Grandclément, J.-A. Marck, and J. Novak, "LORENE: Langage Objet pour la RElativité NumériquE." http://www.lorene.obspm.fr, 1997–2014.

[16] "stellarcollapse.org." .

[17] J. M. Lattimer, "The Nuclear Equation of State and Neutron Star Masses," *Annual Review of Nuclear and Particle Science*, vol. 62, pp. 485–515, Nov. 2012.

[18] J. B. Hartle, "Slowly Rotating Relativistic Stars. I. Equations of Structure," *ApJ*, vol. 150, p. 1005, Dec. 1967.

[19] J. B. Hartle and K. S. Thorne, "Slowly Rotating Relativistic Stars. II. Models for Neutron Stars and Supermassive Stars," *ApJ*, vol. 153, p. 807, Sept. 1968.

[20] S. Bonazzola, E. Gourgoulhon, P. Grandclement, and J. Novak, "Constrained scheme for the einstein equations based on the dirac gauge and spherical coordinates," *Phys. Rev. D*, vol. 70, 2004.

[21] L. Lin and J. Novak, "Rotating star initial data for a constrained scheme in numerical relativity," *Class. Quantum Grav.*, vol. 23, pp. 4545–4561, 2006.

[22] H. Dimmelmeier, J. Novak, J. A. Font, J. M. Ibáñez, and E. Müller, "Combining spectral and shock-capturing methods: A new numerical approach for 3D relativistic core collapse simulations," *Phys. Rev. D*, vol. 71, p. 064023, Mar. 2005.

[23] R. Arnowitt, S. Deser, and C. W. Misner, "Republication of: The dynamics of general relativity," *General Relativity and Gravitation*, vol. 40, no. 9, pp. 1997–2027, 2008.

[24] P. Grandclément and J. Novak, "Spectral methods for numerical relativity," *Living Rev. Rel.*, vol. 12, p. 1, 2009.

[25] V. Ferrari, G. Miniutti, and J. Pons, "Gravitational waves from newly born, hot neutron stars," *Mon. Not. R. Astron. Soc.*, vol. 342, pp. 629–638, 2003.

[26] E. Gourgoulhon, *3+1 Formalism in General Relativity*. Springer-Verlag, 2012.

[27] E. Poisson, *A Relativist's Toolkit*. Cambridge University Press, 2004.

[28] A. Komar, "Positive-definite energy density and global consequences for general relativity," *Phys. Rev.*, vol. 129, pp. 1873–1876, Feb 1963.

[29] A. Komar, "Covariant conservation laws in general relativity," *Phys. Rev.*, vol. 113, pp. 934–936, Feb 1959.

[30] R. Beig, "Arnowitt-deser-misner energy and g00," *Physics Letters A*, vol. 69, no. 3, pp. 153 – 155, 1978.

[31] A. Ashtekar and A. MagnonâAshtekar, "On conserved quantities in general relativity," *Journal of Mathematical Physics*, vol. 20, no. 5, 1979.

[32] S. Bonazzola and E. Gourgoulhon, "A virial identity applied to relativistic stellar models," *Class. Quantum Grav.*, vol. 11, pp. 1775–1784, 1994.

[33] E. Gourgoulhon and S. Bonazzola, "A formulation of the virial theorem in general relativity," *Classical and Quantum Gravity*, vol. 11, pp. 443–452, Feb. 1994.

[34] C. Canuto, M. Y. Hussaini, A. Quarteroni, and T. A. Zang, *Spectral Methods in Fluid Dynamics*. Springer-Verlag, 1988.

[35] E. Fermi, *Thermodynamics*. Dover, 1937.

[36] A. Phillips, *The Physics of Stars*. Wiley, 1999.

[37] J. Schaffner and I. N. Mishustin, "Hyperon-rich matter in neutron stars," *Phys. Rev. C*, vol. 53, pp. 1416–1429, Mar. 1996.

[38] T. Nozawa, N. Stergioulas, E. Gourgoulhon, and Y. Eriguchi, "Construction of highly accurate models of rotating neutron stars - comparison of three different numerical schemes," *A&AS*, vol. 132, pp. 431–454, Nov. 1998.

[39] N. Stergioulas, "Rotating stars in relativity," *Living Reviews in Relativity*, vol. 6, no. 3, 2003.

[40] J. P. Ostriker and J. W.-K. Mark, "Rapidly rotating stars. I. The self-consistent-field method," *ApJ*, vol. 151, pp. 1075–1088, Mar. 1968.

[41] B. Carter, "Killing Horizons and Orthogonally Transitive Groups in Space-Time," *Journal of Mathematical Physics*, vol. 10, pp. 70–81, Jan. 1969.

[42] B. Carter, "The commutation property of a stationary, axisymmetric system," *Communications in Mathematical Physics*, vol. 17, no. 3, pp. 233–238, 1970.

[43] J. Walecka, "A theory of highly condensed matter," *Annals of Physics*, vol. 83, no. 2, pp. 491 – 529, 1974.

[44] S. Chin and J. Walecka, "An equation of state for nuclear and higher-density matter based on relativistic mean-field theory," *Physics Letters B*, vol. 52, no. 1, pp. 24 – 28, 1974.

[45] F. D. Swesty, "Thermodynamically Consistent Interpolation for Equation of State Tables," *Journal of Computational Physics*, vol. 127, pp. 118–127, Aug. 1996.

[46] J. R. Wilson, "Models of Differentially Rotating Stars.," *ApJ*, vol. 176, p. 195, Aug. 1972.

[47] S. Bonazzola and J. Schneider, "An Exact Study of Rigidly and Rapidly Rotating Stars in General Relativity with Application to the Crab Pulsar," *ApJ*, vol. 191, pp. 273–290, July 1974.

[48] B. Franzon, V. Dexheimer, and S. Schramm, "Internal composition of proto-neutron stars under strong magnetic fields," *Phys. Rev. D*, vol. 94, p. 044018, Aug. 2016.

[49] G. Camelio, L. Gualtieri, J. A. Pons, and V. Ferrari, "Spin evolution of a proto-neutron star," *Phys. Rev. D*, vol. 94, p. 024008, July 2016.

[50] G. Martinon, A. Maselli, L. Gualtieri, and V. Ferrari, "Rotating protoneutron stars: Spin evolution, maximum mass, and I-Love-Q relations," *Phys. Rev. D*, vol. 90, p. 064026, Sept. 2014.

[51] U. M. Schaudt and H. Pfister, "The boundary value problem for the stationary and axisymmetric einstein equations is generically solvable," *Phys. Rev. Lett.*, vol. 77, pp. 3284–3287, Oct 1996.

[52] E. Berti *et al.*, "Testing General Relativity with Present and Future Astrophysical Observations," *Class. Quant. Grav.*, vol. 32, p. 243001, 2015.

[53] B. P. Abbott *et al.*, "Tests of general relativity with GW150914," *Phys. Rev. Lett.*, vol. 116, no. 22, p. 221101, 2016.

[54] P. C. C. Freire, N. Wex, G. Esposito-Farèse, J. P. W. Verbiest, M. Bailes, B. A. Jacoby, M. Kramer, I. H. Stairs, J. Antoniadis, and G. H. Janssen, "The relativistic pulsar-white dwarf binary PSR J1738+0333 - II. The most stringent test of scalar-tensor gravity," *MNRAS*, vol. 423, pp. 3328–3343, July 2012.

[55] R. C. Tolman, "Static Solutions of Einstein's Field Equations for Spheres of Fluid," *Physical Review*, vol. 55, pp. 364–373, Feb. 1939.

[56] J. R. Oppenheimer and G. M. Volkoff, "On Massive Neutron Cores," *Physical Review*, vol. 55, pp. 374–381, Feb. 1939.

[57] T. Fischer, S. C. Whitehouse, A. Mezzacappa, F.-K. Thielemann, and M. Liebendörfer, "Protoneutron star evolution and the neutrino-driven wind in general relativistic neutrino radiation hydrodynamics simulations," *A&A*, vol. 517, p. A80, July 2010.

[58] M. Prakash, I. Bombaci, M. Prakash, P. J. Ellis, J. M. Lattimer, *et al.*, "Composition and structure of protoneutron stars," *Phys.Rept.*, vol. 280, pp. 1–77, 1997.

[59] J. A. Pons, J. A. Miralles, M. Prakash, and J. M. Lattimer, "Evolution of protoneutron stars with kaon condensates," *Astrophys.J.*, vol. 553, pp. 382–393, 2001.

[60] J. A. Pons, S. Reddy, P. J. Ellis, M. Prakash, and J. M. Lattimer, "Kaon condensation in proto neutron star matter," *Phys.Rev.*, vol. C62, p. 035803, 2000.

[61] J. A. Pons, A. W. Steiner, M. Prakash, and J. M. Lattimer, "Evolution of proto-neutron stars with quarks," *Phys. Rev. Lett.*, vol. 86, pp. 5223–5226, Jun 2001.

[62] O. E. Nicotra, M. Baldo, G. F. Burgio, and H.-J. Schulze, "Hybrid protoneutron stars with the MIT bag model," *Phys. Rev. D*, vol. 74, p. 123001, Dec. 2006.

[63] H. Chen, M. Baldo, G. F. Burgio, and H.-J. Schulze, "Hybrid protoneutron stars with the Dyson-Schwinger quark model," *Phys. Rev. D*, vol. 86, p. 045006, Aug. 2012.

[64] D. P. Menezes and C. Providencia, "Equation of State for supernova explosion simulations," 2007.

[65] V. Dexheimer and S. Schramm, "Proto-Neutron and Neutron Stars in a Chiral SU(3) Model," *Astrophys.J.*, vol. 683, pp. 943–948, 2008.

[66] N. Yasutake and K. Kashiwa, "Lepton effects on the protoneutron stars with the hadron-quark mixed phase in the Nambu Jona-Lasinio model," vol. 79, p. 043012, Feb. 2009.

[67] I. Bombaci, D. Logoteta, C. Providencia, and I. Vidana, "Effects of quark matter nucleation on the evolution of proto-neutron stars," *Astron.Astrophys.*, vol. 462, pp. 1017–1022, 2007.

[68] G. F. Burgio, H.-J. Schulze, and A. Li, "Hyperon stars at finite temperature in the Brueckner theory," *Phys. Rev.*, vol. C83, p. 025804, Feb. 2011.

[69] C. Ishizuka, A. Ohnishi, K. Tsubakihara, K. Sumiyoshi, and S. Yamada, "Tables of Hyperonic Matter Equation of State for Core- Collapse Supernovae," *J. Phys. G*, vol. 35, p. 085201, 2008.

[70] K. Nakazato, K. Sumiyoshi, and S. Yamada, "Astrophysical implications of equation of state for hadron-quark mixed phase: Compact stars and stellar collapses," vol. 77, p. 103006, May 2008.

[71] I. Sagert, T. Fischer, M. Hempel, G. Pagliara, J. Schaffner-Bielich, A. Mezzacappa, F.-K. Thielemann, and M. Liebendörfer, "Signals of the QCD Phase Transition in Core-Collapse Supernovae," *Phys. Rev. Lett.*, vol. 102, p. 081101, Feb. 2009.

[72] M. Oertel, A. Fantina, and J. Novak, "An extended equation of state for core-collapse simulations," *Phys.Rev.*, vol. C85, p. 055806, 2012.

[73] F. Gulminelli, A. Raduta, M. Oertel, and J. Margueron, "Strangeness-driven phase transition in (proto-)neutron star matter," *Phys.Rev.*, vol. C87, no. 5, p. 055809, 2013.

[74] S. Banik, M. Hempel, and D. Bandyopadhyay, "New Hyperon Equations of State for Supernovae and Neutron Stars in Density-dependent Hadron Field Theory," *Astrophys.J.Suppl.*, vol. 214, p. 22, Oct. 2014.

[75] M. Buballa, V. Dexheimer, A. Drago, E. Fraga, P. Haensel, *et al.*, "EMMI rapid reaction task force meeting on quark matter in compact stars," *J.Phys.*, vol. G41, no. 12, p. 123001, 2014.

[76] S. Typel, M. Oertel, and Kl

[77] W. Hillebrandt, K. Nomoto, and R. G. Wolff, "Supernova explosions of massive stars - The mass range 8 to 10 solar masses," *A&A*, vol. 133, pp. 175–184, Apr. 1984.

[78] A. Raduta and F. Gulminelli, "Statistical description of complex nuclear phases in supernovae and proto-neutron stars," *Phys.Rev.*, vol. C82, p. 065801, 2010.

[79] F. Gulminelli and A. R. Raduta, "Unified treatment of subsaturation stellar matter at zero and finite temperature," *Phys. Rev.*, vol. C92, no. 5, p. 055803, 2015.

[80] M. Hempel and J. Schaffner-Bielich, "Statistical Model for a Complete Supernova Equation of State," *Nucl. Phys.*, vol. A837, pp. 210–254, 2010.

[81] S. Typel, G. Röpke, T. Klähn, D. Blaschke, and H. Wolter, "Composition and thermodynamics of nuclear matter with light clusters," *Phys.Rev.*, vol. C81, p. 015803, 2010.

[82] K. Sumiyoshi and G. Röpke, "Appearance of Light Clusters in Post-bounce Evolution of Core-Collapse Supernovae," *Phys. Rev.*, vol. C77, p. 055804, 2008.

[83] N. Buyukcizmeci, A. Botvina, I. Mishustin, R. Ogul, M. Hempel, *et al.*, "A comparative study of statistical models for nuclear equation of state of stellar matter," *Nucl.Phys.*, vol. A907, pp. 13–54, 2013.

[84] N. Buyukcizmeci, A. S. Botvina, and I. N. Mishustin, "Tabulated Equation of State for Supernova Matter Including Full Nuclear Ensemble," *Astrophys.J.*, vol. 789, p. 33, jul 2014.

[85] J. D. Kaplan, C. D. Ott, E. P. O'Connor, K. Kiuchi, L. Roberts, and M. Duez, "The Influence of Thermal Pressure on Equilibrium Models of Hypermassive Neutron Star Merger Remnants," *ApJ*, vol. 790, p. 19, July 2014.

[86] L. Villain, J. A. Pons, P. Cerdá-Durán, and E. Gourgoulhon, "Evolutionary sequences of rotating protoneutron stars," *A&A*, vol. 418, pp. 283–294, Apr. 2004.

[87] S. Heckel, P. P. Schneider, and A. Sedrakian, "Light nuclei in supernova envelopes: a quasiparticle gas model," *Phys. Rev.*, vol. C80, p. 015805, 2009.

[88] F. Gulminelli, P. Chomaz, A. Raduta, and A. Raduta, "The Influence of Coulomb on the liquid gas phase transition and nuclear multifragmentation," *Phys.Rev.Lett.*, vol. 91, p. 202701, 2003.

[89] F. Gulminelli and A. Raduta, "Ensemble in-equivalence in supernova matter within a simple model," *Phys.Rev.*, vol. C85, p. 025803, 2012.

[90] G. Audi, A. H. Wapstra, and C. Thibault, "The Ame2003 atomic mass evaluation (II). Tables, graphs and references," *Nucl. Phys. A*, vol. 729, pp. 337–676, Dec. 2003.

[91] P. Möller, J. R. Nix, W. D. Myers, and W. J. Swiatecki, "Nuclear Ground-State Masses and Deformations," *Atom. Data Nucl. Data*, vol. 59, p. 185, 1995.

[92] M. Dutra, O. LourenÃ§o, S. Avancini, B. Carlson, A. Delfino, *et al.*, "Relativistic Mean-Field Hadronic Models under Nuclear Matter Constraints," *Phys.Rev.*, vol. C90, no. 5, p. 055203, 2014.

[93] S. Weissenborn, D. Chatterjee, and J. Schaffner-Bielich, "Hyperons and massive neutron stars: vector repulsion and SU(3) symmetry," *Phys.Rev.*, vol. C85, p. 065802, 2012.

[94] T. Miyatsu, S. Yamamuro, and K. Nakazato, "A new equation of state for neutron star matter with nuclei in the crust and hyperons in the core," *Astrophys.J.*, vol. 777, p. 4, 2013.

[95] I. Vidaña, A. Polls, A. Ramos, and H. J. Schulze, "Hypernuclear structure with the new Nijmegen potentials," *Phys. Rev.*, vol. C64, p. 044301, 2001.

[96] E. Khan, J. Margueron, F. Gulminelli, and A. R. Raduta, "Microscopic evaluation of the hypernuclear chart with Λ hyperons," *Phys. Rev.*, vol. C92, no. 4, p. 044313, 2015.

[97] M. Oertel, C. Providência, F. Gulminelli, and A. R. Raduta, "Hyperons in neutron star matter within relativistic mean-field models," *J. Phys.*, vol. G42, no. 7, p. 075202, 2015.

[98] M. Oertel, F. Gulminelli, C. ProvidÃªncia, and A. R. Raduta, "Hyperons in neutron stars and supernova cores," *Eur. Phys. J.*, vol. A52, no. 3, p. 50, 2016.

[99] M. Oertel, M. Hempel, T. Klähn, and S. Typel, "Equations of state for supernovæ and compact stars," *in preparation*, 2016.

[100] J. M. Lattimer and Y. Lim, "Constraining the Symmetry Parameters of the Nuclear Interaction," *Astrophys. J.*, vol. 771, p. 51, 2013.

[101] J. M. Lattimer and F. D. Swesty, "A Generalized equation of state for hot, dense matter," *Nucl.Phys.*, vol. A535, pp. 331–376, 1991.

[102] H. Shen, H. Toki, K. Oyamatsu, and K. Sumiyoshi, "Relativistic Equation of State for Core-Collapse Supernova Simulations," *Astrophys.J.Suppl.*, vol. 197, p. 20, 2011.

[103] T. Fischer, M. Hempel, I. Sagert, Y. Suwa, and J. Schaffner-Bielich, "Symmetry energy impact in simulations of core-collapse supernovae," *Eur.Phys.J.*, vol. A50, p. 46, 2014.

[104] K. Hebeler, J. Lattimer, C. Pethick, and A. Schwenk, "Equation of state and neutron star properties constrained by nuclear physics and observation," *Astrophys.J.*, vol. 773, p. 11, 2013.

[105] P. Demorest, T. Pennucci, S. Ransom, M. Roberts, and J. Hessels, "Shapiro Delay Measurement of A Two Solar Mass Neutron Star," *Nature*, vol. 467, pp. 1081–1083, 2010.

[106] E. Fonseca *et al.*, "The NANOGrav Nine-year Data Set: Mass and Geometric Measurements of Binary Millisecond Pulsars," 2016.

[107] J. Antoniadis, P. C. C. Freire, N. Wex, T. M. Tauris, R. S. Lynch, M. H. van Kerkwijk, M. Kramer, C. Bassa, V. S. Dhillon, T. Driebe, J. W. T. Hessels, V. M. Kaspi, V. I. Kondratiev, N. Langer, T. R. Marsh, M. A. McLaughlin, T. T. Pennucci, S. M. Ransom, I. H. Stairs, J. van Leeuwen, J. P. W. Verbiest, and D. G. Whelan, "A Massive Pulsar in a Compact Relativistic Binary," *Science*, vol. 340, p. 448, Apr. 2013.

[108] B. Peres, M. Oertel, and J. Novak, "Influence of pions and hyperons on stellar black hole formation," *Phys.Rev.*, vol. D87, p. 043006, 2013.

[109] Y. Sekiguchi, K. Kiuchi, K. Kyutoku, and M. Shibata, "Gravitational Waves and Neutrino Emission from the Merger of Binary Neutron Stars," *Physical Review Letters*, vol. 107, p. 051102, July 2011.

[110] D. Radice, F. Galeazzi, J. Lippuner, L. F. Roberts, C. D. Ott, and L. Rezzolla, "Dynamical mass ejection from binary neutron star mergers," *MNRAS*, vol. 460, pp. 3255–3271, Aug. 2016.

[111] J. Bretz, K. Yagi, and N. Yunes, "Four-hair relations for differentially rotating neutron stars in the weak-field limit," *Phys. Rev. D*, vol. 92, p. 083009, Oct. 2015.

[112] H. Shen, H. Toki, K. Oyamatsu, and K. Sumiyoshi, "Relativistic equation of state of nuclear matter for supernova explosion," *Prog.Theor.Phys.*, vol. 100, p. 1013, 1998.

[113] K. Yagi and N. Yunes, "I-Love-Q," *Science*, vol. 341, pp. 365–368, 2013.

[114] K. Yagi and N. Yunes, "I-Love-Q Relations in Neutron Stars and their Applications to Astrophysics, Gravitational Waves and Fundamental Physics," *Phys. Rev.*, vol. D88, no. 2, p. 023009, 2013.

[115] A. Maselli, "From macro to micro: universal properties of neutron stars," *Proceeding of the conference: The Modern Physics of Compact Stars 2015, Yerevan*, 2015.

[116] A. Maselli, V. Cardoso, V. Ferrari, L. Gualtieri, and P. Pani, "Equation-of-state-independent relations in neutron stars," *Phys. Rev.*, vol. D88, no. 2, p. 023007, 2013.

[117] D. D. Doneva, S. S. Yazadjiev, N. Stergioulas, and K. D. Kokkotas, "Breakdown of I-Love-Q universality in rapidly rotating relativistic stars," *Astrophys. J.*, vol. 781, p. L6, 2013.

[118] K. Strobel, C. Schaab, and M. K. Weigel, "Properties of non-rotating and rapidly rotating protoneutron stars," *A&A*, vol. 350, pp. 497–512, Oct. 1999.

[119] Y. Yuan and J. S. Heyl, "Rotational Evolution of Protoneutron Stars," May 2003.

[120] Y.-F. Yuan and J. S. Heyl, "Rotational evolution of protoneutron stars with hyperons: spin up or not?," *MNRAS*, vol. 360, pp. 1493–1505, July 2005.

[121] J. V. Romero, J. Diaz Alonso, J. M. Ibanez, J. A. Miralles, and A. Perez, "Field theoretical model for nuclear and neutron matter. V - Slowly rotating warm cores in neutron stars," *ApJ*, vol. 395, pp. 612–621, Aug. 1992.

[122] A. Burrows and J. M. Lattimer, "The birth of neutron stars," *ApJ*, vol. 307, pp. 178–196, Aug. 1986.

[123] J. A. Pons, S. Reddy, M. Prakash, J. M. Lattimer, and J. A. Miralles, "Evolution of protoneutron stars," *Astrophys. J.*, vol. 513, p. 780, 1999.

[124] W. Baade and F. Zwicky, "Cosmic Rays from Super-novae," *Proceedings of the National Academy of Science*, vol. 20, pp. 259–263, May 1934.

Résumé

Les étoiles à neutrons sont parmi les objets les plus extrêmes dans l'univers. Elles sont des étoiles compactes, nées à la suite d'une explosion de supernova gravitationnelle, au point final de l'évolution stellaire. Le champ gravitationnel y est très fort, et la matière à l'intérieur atteint des densités extrêmement élevées. Elles sont donc des "laboratoires" prometteurs, non seulement pour tester le régime de champ fort en relativité générale, mais aussi pour en apprendre davantage sur la physique nucléaire à haute densité, qui actuellement ne peut pas être reproduit avec des expériences terrestres. Ainsi, les étoiles à neutrons nous permettent d'adresser des questions telles que l'existence éventuelle de particules autres que nucléons à haute-densité. À cause de la naissance violente de ces objets, les étoiles à neutrons très jeunes, que l'on appelle proto-étoiles à neutrons, sont également très chaudes, et souvent en rotation différentielle rapide. Dans cette thèse nous avons pour but de développer un modèle stationnaire d'une telle proto-étoile à neutrons. Ainsi, nous présentons une nouvelle méthode pour calculer numériquement les équations d'équilibre d'un fluide parfait relativiste, axisymétrique et stationnaire, en rotation différentielle et à température finie, valable pour une équation d'état réaliste. Nous présentons en détail le code (accessible au public) développé. Nous avons appliqué ce code avec des nouvelles équations d'état réalistes à température finie, basée sur une théorie relativiste du champ moyen, en incluant tous les degrés de liberté hyperoniques. Nous avons calculé des modèles relativistes stationnaires de proto-étoiles à neutrons en rotation différentielle rapide. Nous allons discuter les applications de nos modèles pour explorer plus en détail la physique de ces objets.

Mots Clés

Étoiles relativistes, étoiles à neutrons, temperature finie, supernovae gravitationnelle, hyperons dans les étoiles compact.

Abstract

Neutron stars are among the most extreme objects in the universe. They are compact stars born as the aftermath of a core-collapse supernova explosion, at the endpoint of stellar evolution, with a strong gravitational field, and extremely high densities. They are therefore promising “laboratories”, not only to test the strong-field regime of general relativity, but also to learn about nuclear physics in the high density regime, which presently is not accessible in earth based experiments. This allows to address questions such as the possible existence of particles other than nucleons at high-densities. As a consequence of the violent birth of these objects, new-born (proto-)neutron stars are extremely hot and, in general, rapidly rotating, which raises interesting problems in the task of developing a stationary model of such objects. In this thesis, we present a new self-consistent method to numerically compute the equilibrium equations of stationary axisymmetric relativistic (differentially) rotating perfect fluids at finite temperature, with a realistic equation of state. We introduce in detail the (publicly available) code in which we implemented the described numerical scheme. We use newly developed realistic equations of state with finite temperature, which are based on density dependent relativistic mean field theory, and in which all hyperonic degrees of freedom are included, to compute realistic stationary relativistic models of rapidly differentially rotating proto-neutron stars. We discuss future applications of our code for further exploring the physics of proto-neutron stars.

Keywords

Relativistic stars, neutron stars, finite temperature, core-collapse, hyperon puzzle.